Interplay between information theory and optimization: Applications to multi-user wireless communications

Anne Savard

Interplay between information theory and optimization: Applications to multi-user wireless communications

By

Anne Savard

Enseignante-chercheuse à l'IMT Nord Europe
CERI Systèmes numériques

HABILITATION À DIRIGER DES RECHERCHES
CY CERGY PARIS UNIVERSITÉ
Section CNU 61, génie informatique, automatique et traitement du signal

Defended on the 10$^{\text{th}}$ of July 2023 in front of the jury composed of

Didier Le Ruyet	CNAM, France	President of the jury (Président)
Eduard Jorswieck	TU Braunschweig, Germany	Reviewer (Rapporteur)
Gerhard Kramer	TU Munich, Germany	Reviewer (Rapporteur)
Michèle Wigger	Télécom Paris, France	Reviewer (Rapporteure)
Catherine Douillard	IMT Atlantique, France	Examiner (Examinateur)
Anthony Fleury	IMT Nord Europe, France	Examiner (Examinateur)
Charly Poulliat	ENSEEIHT, France	Examiner (Examinateur)
Inbar Fijalkow	ENSEA, France	HDR Guarantor (Garant HDR)
Iryna Andriyanova	CY Cergy Paris Univ., France	HDR Referent (Référent HDR)

Abstract

The ever increasing number of communicating devices as well as the enormous growth of high data rate applications are driving the transition to future generation of wireless networks. As such, many challenges arise in terms of users' connectivity, energy- and spectral-efficiency as well as managing the interference. To tackle such challenges in multi-user wireless networks, the aim of this HDR thesis is to study the interaction between information theory and optimization.

Many investigations showed that in heterogeneous and multi-user networks, the interference exhibits an impulsive nature, which is not encompassed by the Gaussian model. In the first part of this HDR thesis, we focus on approximating the resulting non-linear log-likelihood ratios (LLR) using an information-theory based criterion. Since sending pilots decreases the useful data rate, we propose an unsupervised LLR estimation in both the asymptotic and the short blocklength regime, without requiring any prior on the input and noise distribution. Our proposed LLR estimation method, numerically evaluated using LDPC codes, was shown to be able to cope with various noise models.

In the second part of this HDR thesis, we focus on resource optimization for cooperative multi-user communications, where we first derive the achievable rate regions of the considered networks. On the one hand, we investigate a backscatter enhanced multi-user downlink non orthogonal multiple access (NOMA) transmission, whose energy-efficiency is maximized under user minimum quality of service (QoS) constraints. For this, we consider both the perfect channel state information (CSI) case and the other extreme case, where no CSI is available at the transmitter side and for which this lack of knowledge is compensated by the use of reinforcement learning. On the other hand, we study a relay-aided cognitive radio network, where the opportunistic achievable rate is maximized under a primary QoS constraint. While under NOMA the optimal resource allocation policy was derived in closed-form in the perfect CSI case, deep learning techniques were used in the cooperative cognitive network because the non-linear relay operations rendered the optimization problem non-convex and difficult to solve.

The HDR thesis is concluded by discussing some open and future research directions.

Résumé

Le nombre toujours croissant de dispositifs communicants ainsi que l'augmentation sans précédent des applications à haut débit entraînent la transition vers la future génération de réseaux sans fil. Ainsi, de nombreux défis se posent en termes de connectivité des utilisateurs, d'efficacité énergétique et spectrale ainsi que de gestion des interférences. Pour relever ces défis dans les réseaux sans fil multi-utilisateurs, l'objectif de cette thèse d'HDR est d'étudier l'interaction entre la théorie de l'information et l'optimisation.

De nombreux travaux de recherche ont montré que, dans des réseaux hétérogènes et multi-utilisateurs, l'interférence présente une nature impulsive qui n'est pas prise en compte par le modèle Gaussien. Dans la première partie de cette thèse d'HDR, nous nous concentrons sur l'approximation des rapports de log-vraisemblance (LLR) non linéaires résultants en utilisant un critère basé sur la théorie de l'information. Puisque l'envoi de pilotes diminue le débit de données utiles, nous proposons une estimation non supervisée des LLRs dans le régime asymptotique et pour des blocs de taille finie, sans hypothèses a priori sur l'entrée du canal et la distribution du bruit. La méthode d'estimation du LLR que nous proposons, évaluée numériquement à l'aide de codes LDPC, est capable de faire face à divers modèles de bruit.

Dans la deuxième partie de cette thèse d'HDR, nous nous concentrons sur l'optimisation des ressources pour les communications multi-utilisateurs coopératives, où nous dérivons d'abord les régions de débit atteignable pour les réseaux considérés. D'une part, nous étudions une transmission multi-utilisateurs descendante à accès multiple non orthogonal (NOMA) améliorée par rétrodiffusion, dont l'efficacité énergétique est maximisée sous des contraintes de qualité de service (QoS) minimales par utilisateur. Pour cela, nous considérons à la fois le cas d'une information parfaite sur l'état du canal (CSI) et l'autre cas extrême, où aucune CSI n'est disponible du côté de l'émetteur et pour lequel ce manque de connaissance est compensé par l'utilisation de l'apprentissage par renforcement. D'autre part, nous étudions un réseau de radio cognitive assisté par un relais, où le débit atteignable opportuniste est maximisé sous une contrainte de qualité de service primaire. Alors que sous NOMA, la politique d'allocation optimale de ressources a été obtenue de façon analytique dans le cas d'une CSI parfaite, des techniques d'apprentissage profond ont été utilisées dans le réseau de radio cognitive coopératif car les opérations non linéaires du relais rendent le problème d'optimisation non convexe et difficile à résoudre.

La thèse d'HDR est conclue en discutant de plusieurs axes de recherche ouverts pour de futures investigations.

Acknowledgments

First of all, I would like to express my deepest gratitude to all my jury members for kindly accepting my invitation and serving on this committee, as well as for the many interesting discussions: Catherine Douillard (IMT Atlantique), Anthony Fleury (IMT Nord Europe), Didier Le Ruyet (CNAM) and Charly Poulliat (ENSEEIHT); my three reviewers Eduard Jorswieck (TU Braunschweig), Gerhard Kramer (TU Munich) and Michèle Wigger (Télécom Paris); as well as my HDR guarantor Inbar Fijalkow (ENSEA) and HDR referent Iryna Andriyanova (CY Cergy Paris University).

Being an associate professor at IMT Nord Europe in Lille and defending my HDR at CY Cergy Paris University was not an easy task. As such, I would like to give a huge thanks to all administrative officers - Annick, Anne, Nathalie and Christine - for all their help and assistance, as well as to Inbar, Iryna and Sylvain for all their support. Although eight years have passed since my PhD defense in Cergy, I was very happy and moved to see many of my former colleagues there. A special thanks to Inbar, who has been mentoring me from the start as one of my professors at ENSEA when I was an undergraduate student; thank you so much for believing in me and always being there when I needed support and guidance.

I would also like to thank all my current colleagues of IMT Nord Europe and IEMN/IRCICA, it has been a real pleasure to work with you since I joined in 2016. A special thanks to Christophe and now Arthur, my office-mates - thank you for sharing the ups and downs; as well as to Christelle, Gilbert, Giulia, Vincent, Manu, Wadih, ... for all the very nice lunches and coffee breaks. Thanks also to Marie, Julie, and everyone taking part to the sport classes, it was so funny to suffer in this all together.

On a more scientific side, I would like to thank Giulia, Arthur, Yahia, Laurent, as well as Eric, Valeria, ... for all our very interesting discussions. A huge thanks to all my collaborators and co-authors, Veronica, Romain, Laurent, Rodrigo, Philippe, Alban, Malcolm, ..., I would not have done all of this without your help and support; thank you all very much for all our interactions and discussions. To my PhD students and Post-docs: Yasser, Hajar, Yacine, Miled, Samet, Sahar, Mariem, ... thank you so much for your dedication and hard work.

I would also like to thank my family and close friends for all their support. Veronica, thank you so much for everything; you are among my closest collaborators and dearest friends, you were there through ups and downs, for any piece of advice and you kindly handled so much, with Romain, for the defense in Cergy. On the same page, a special thanks to Anthony for all his help regarding this HDR preparation, thanks for all the discussions and cooking sessions. On a more personal side, I would like to dedicate this HDR thesis to Sébastien and Clémence. Thank you both very much for all your love, your extreme patience and support through this year.

Contents

List of Figures

List of Tables

Acronyms and notations

$C(x) = \frac{1}{2}\log_2(1+x)$	Gaussian capacity function
$\mathbb{D}_{KL}$	Kullback-Leibler divergence
$\mathbb{E}$	Expectation
$\mathbb{H}$	Entropy
$\mathbb{I}$	Mutual information
$\mathbb{P}$	Probability
AF	Amplify-and-Forward
AI	Artificial intelligence
AmBC	Ambient backscatter communications
AWGN	Additive White Gaussian Noise
BER	Bit error rate
BP	Belief-Propagation
BPSK	Binary Ohase Shift Keying
BS	Base station
CDI	Channel distribution information
CF	Compress-and-Forward
CSI	Channel State Information
DF	Decode-and-Forward
DNN	Deep neural networks
DoS	Denial-of-service
EE	Energy efficiency

EXP3	Exponential weights for exploration and exploitation
FER	Frame error rate
GAD	Genie-aided Decoder
IoT	Internet of Things
IRS	Intelligent reflecting surfaces
KKT	Karush-Kuhn-Tucker
LDPC	Low-Density Parity Check
LLR	Log-Likelihood Ratio
MAB	Multi-armed bandit
NOMA	Non Orthogonal Multiple Access
NUSD	New Unsupervised Decoder
OMA	Orthogonal Multiple Access
pdf	Probability density function
QoS	Quality of Service
RF	Radio frequency
$S\alpha S$	Symmetric α-stable
SIC	Successive interference cancellation
SINR	Signal-to-interference-plus-noise ratio
SNR	Signal-to-noise ratio
SUD	Single user detection
SWIPT	Simultaneous wireless information and power transfer
UCB	Upper Confidence Bound
USD	Unsupervised Decoder

Anne Savard

Associate Professor (Enseignante-chercheuse) at IMT Nord Europe, CERI SN

Address	IMT Nord Europe Rue G. Marconi 59653 Villeneuve d'Ascq	Office Phone Email	+33 3 20 33 55 68 anne.savard@imt-nord-europe.fr
Nationality	French	Webpage	https://sites.google.com/view/anne-savard

Research interests

Optimization, Resource allocation, Multi-user information theory, Cooperative communications, Cognitive radio, Green communications, NOMA, Channel coding

Professional experience

2016 - **Associate Professor** (Enseignante-chercheuse) - IMT Nord Europe, Lille, France

2015 - 2016 **Post-doctoral Researcher** - Georgia Institute of Technology, Atlanta, USA
Collaborators: Matthieu Bloch (Georgia Institute of Technology), Mérouane Debbah (Huawei)

June - Sept. 2014 **Visiting Researcher** - LNT, Technische Universität, Munich, Germany
Prof. Gerhard Kramer's group

2012 - 2015 **Teaching Assistant** (Mission d'enseignement) - ENSEA, Cergy, France
Teaching: Signal processing, Random processes, Digital communications

Education

2012 - 2015 **PhD in Telecommunications** - University of Cergy-Pontoise, France
Research: ETIS, Advisors: David Declercq and Claudio Weidmann
Coding for cooperative communications: Topics in distributed source coding and relay channels
Defense: 22nd September 2015, **Mention:** Très honorable

2011 - 2012 **M. Sc. M2R SIC** - University of Cergy-Pontoise, France
Specialization : Signal and Communication
Mention: Très bien, **Rank: 1/21**

2009 - 2012 **Engineer Diploma** - ENSEA (École Nationale Supérieure de l'Électronique et de ses Applications), Cergy, France
Specialization: Multimedia systems
Rank: 1/16 (3rd year), 1/192 (2nd year), 1/148 (1st year)

2007 - 2009 **Classes préparatoires MPSI/MP*** - Lycée Fabert, Metz, France

2007 **Baccalauréat Franco-Allemand S-MP** - Deutsch-französiches Gymnasium, Saarbrücken, Germany
Mention: Très bien, **N.C.:** 1,0

Advising

PhDs 2 ongoing (40%, 40%); 2 defended (30%, 40%)

Post-docs 1 ongoing; 1 alumni

Publications ∗Related to PhD work

6(1∗) +1 sub. International journal papers

20(4∗) International conference papers

10(4∗) +1 sub. National conference papers

Local responsibilities

2022 - Elected member of the CSAS (former CST) of IMT Nord Europe

2021 - Elected member (Assoc. Prof. representative) of the COPIL of CERI SN, IMT Nord Europe

Oct. 2020 Examiner of the VAE jury of Xavier Foin, IMT Nord Europe

2019 - Validation of the Telecom-oriented internship at IMT Nord Europe

2017 - Elected member of the Commission de Qualification pour Promotion et Changement d'Appellation, IMT Nord Europe

2014 - 2015 Elected member (PhD representative) of ETIS lab board

Research project expert

2022, 2023 French ANR, phase 2

Editorial activities

Jan. 2020 - Feb. 2023 Executive Editor of Transactions on Emerging Telecommunications Technologies (ETT), 20 journal articles handled as Editor

Feb. 2023 - Editor in Area 2: Network Optimization and Resource Management, IEEE Transactions on Machine Learning in Communications and Networking

TPC IEEE EuCNC 2019, 2020, 2021, 2022, 2023;
IEEE WCNC 2019 Workshop MoTION;
IEEE SPAWC 2019, 2022

Conference organization

2023 Workshop RAWNET, WiOPT 2023 - jointly with S. Lasaulce, S. Perlaza, V. Y. F. Tan, C. Zhang

2019 Session chair of the Session 'Machine Learning & Data analytics' at EAI ValueTools 2019

2019 Volunteer in the local organization team (gift bags, welcoming participants, technical support, ...) of GRETSI 2019, Lille, France

Nov. 2017 GdR ISIS meeting 'Méthodes et outils mathématiques pour la modélisation des réseaux IoT' (*Methods and mathematical tools for IoT network modeling*), Paris, France, co-organized with P. Mary and C. Goursaut

Women in Science

Sept. 2022 Invited speaker to the Table ronde 'Quelques conseils pour les jeunes chercheuses en TSI et leurs encadrants' (*Some advice for young female researchers in signal processing*), GRETSI, Nancy, 2022

Chapter 1

Activity review

Following the previous brief Curriculum Vitae, this chapter is dedicated to a detailed review of both the teaching and research activities, as well as the administrative and scientific responsibilities, I have been leading as an Enseignante-Chercheuse in IMT (*Institut Mines Télécom*) Nord Europe since September 2016. My research activities have been performed within IEMN, UMR 8520 and partially supported by IRCICA, CNRS USR 3380 from Sept. 2016 to Feb. 2023, and performed within the Centre for Digital Systems (CERI SN) of IMT Nord Europe since 2019.

1.1 Teaching activities

During my PhD, between October 2012 and September 2015, my teaching activities were given in ENSEA (*Ecole Nationale Supérieure de l'électronique et ses application, Cergy-Pontoise, France*). During these three years, I mainly taught TD (*Travaux dirigés - tutorials*) and TP (*Travaux pratiques - lab sessions*) in digital signal processing, random processes, digital communications and channel coding as well as proposing some new lectures on multimedia compression. I also served as a referee for some internships. The total amount of taught hours reached 192 hours (équivalent TD).

Since September 2016, my teaching activities were first given in the former Department of Communication System of Télécom Lille, and then in the Centre for Digital Systems of IMT Nord Europe.

IMT Nord Europe follows from the fusion of two former engineer schools, namely Télécom Lille and Mines de Douai. Although some classes were given in Télécom Lille, all the material has been updated for IMT Nord Europe since the teaching volume of a module changed radically: all modules in IMT Nord Europe taught at the master level (M1 and M2) are intensive 4 weeks-duration classes, which was not the case in Télécom Lille. Further, some classes, especially in the electronic domain were removed from the training tracks proposed in Télécom Lille.

IMT Nord Europe, and previously Télécom Lille, proposes two main training tracks: one for apprentices, termed as *FISA*; and one for post-bac and post-CPGE students, termed

as *FISE*. Even if the names of some modules are the same in the two training tracks, the contents are rather different: more practical interpretations and lab sessions are provided to the apprentices students, at the price of a slightly lighter mathematical content.

Table 1.1 offers a concise summary of my teaching activities in terms of amount of hours, student level and type: CM (*Cours magistral - lecture*), TD, TP. The students projects are added to the TP of the corresponding course. The hours listed under 'Other' correspond to various modules and administrative responsibilities as well as internships and apprentices supervision. Table 1.2 provides an overview of the taught subjects from 2020 to present: 2020 was the first year where only the new training tracks of IMT Nord Europe were taught, whereas the training tracks of both Télécom Lille and IMT Nord Europe were taught simultaneously from 2017 to 2020. The corresponding module names are given in Table 1.3.

Year	CM	TD	TP	Other	Total
2016 - 2017	61	66	44.5	25	196.5
2017 - 2018	67.5	42	48.5	25	183
2018 - 2019	94.5	35.5	31.5	70	231.5
2019 - 2020	110	14.5	55.5	88	268
2020 - 2021	117	27.5	47	93	284.5
2021 - 2022 ‡	49.5	1.5	25	74	150
2022 - 2023	35.5	18	36.5	75	173
Total	535	205	288.5	450	1478.5

Table 1.1: Teaching at IMT Nord Europe from 2016 to present in nb hours (équivalent TD), ‡: maternity leave from August 2021 to January 2022

Subject	Level	Type	Nb hours	Percentage
Signal processing	L3 FISE	TD	4	1.2
Intro. to Telecommunications	L3, FISE, FISA	CM, TD, TP	97	29.2
Digital communication	M1, FISE, FISA	CM, TD, TP	101	30.4
Information theory	M1 FISE	CM, TP	112	33.8
Mobile communications	M1, M2, FISE, FISA	CM	18	5.4

Table 1.2: Subjects taught at IMT Nord Europe from 2020 to present in nb hours (équivalent TD) under both the FISE and FISA status.

Subject	Module Name	Level
Signal processing	Signal	L3 FISE
Intro. to Telecommunications	I-CNUM	L3 FISE, FISA
Digital communication	CNUM	M1 FISE
Digital communication	CNUM-A	M1 FISA
Information theory	CODES	M1 FISE
Mobile communications	MOBIL	M1, M2, FISE FISA

Table 1.3: Classes names of the taught subjects at IMT Nord Europe from 2020 to present under both the FISE and FISA status.

Tables 1.4 and 1.5 summarize my teaching activities in terms of modules in the former

Télécom Lille and current IMT Nord Europe training tracks for the different levels under FISE and FISA status respectively. Both tables also highlight the modules I am currently coordinating (or coordinated for Télécom Lille), marked as (*), as well as the modules I have created from scratch (in bold) or entirely changed (in italic). Note that after the fusion, my teaching activities focused mainly on telecommunication (signal processing, digital and mobile communications), whereas my implication in the electronics domain vanished, following the suppression of the VHDL module.

Télécom Lille		IMT Nord Europe	
Analog Electronics	L2		
Signal and Communication	L3	Signal **I-CNUM (*)**	L3 L3
Digital Communication VHDL	M1 M1	*CNUM* **CODES (*)**	M1 M1
MOBIL			M1, M2

Table 1.4: Taught classes in the former Télécom Lille and current IMT Nord Europe training track for post-bac and post-CPGE (FISE) students. Courses marked as (*) correspond to classes I am currently coordinating (or coordinated for Télécom Lille); courses in italic are courses I have changed and entirely prepared; bold courses correspond to courses I have created from scratch.

Télécom Lille		IMT Nord Europe	
		I-CNUM (*)	L3
CNUM-A (*)	M1	CNUM-A	M1
MOBIL			M1, M2

Table 1.5: Taught classes in the former Télécom Lille and current IMT Nord Europe training track for apprentice (FISA) students. Courses marked as (*) correspond to classes I am currently coordinating (or coordinated for Télécom Lille); courses in italic are courses I have changed and entirely prepared; bold courses correspond to courses I have created from scratch.

In the following, I briefly present the content of the taught classes within the IMT Nord Europe training tracks.

MOBIL

Level: M1 FISE and M2 FISA

Content: Mobile communications, GSM, GPRS, EDGE, 3G, 4G, Application with NEMO

Implication: I taught mainly the basis of GSM and GPRS (network equipment, mobility, identities, physical layer).

Signal

Level: L3 FISE

Content: Digital signal processing, Fourier transform, random processes

Implication: I taught some TD (tutorials).

1.1.1 Proposed Modules

Since September 2016, **I have proposed and prepared from scratch the two following modules (which did not exist):**

I-CNUM

Level: L3 FISE and FISA

Content: Information theory (entropy, mutual information, channel capacity), Digital communication (baseband transmission, eye diagram and ISI, modulation), Mobile communication (network equipment, security and mobility management)

Type:
FISE - CM (12 hours);
FISA - CM (12 hours), TD (3 hours), TP (9 hours)

Implication: I created this module from scratch. I am in charge of all lecture slides and TDs, as well as the coordination (exam sheets and planning) since 2018. This class is also taught to the apprentices since 2021 with additional TPs on image compression.

CODES

Level: M1 FISE

Content: Information theory (entropy, mutual information, channel capacity computation), Source coding (rate distortion theory, scalar and vector quantization, Lloyd Max algorithm), Application to image and speech compression (JPEG, Haar wavelet), Modern channel coding (convolutional codes, polar codes and LDPC), Application to image transmission, Resource allocation (Water-filling, Reinforcement learning)

Type: CM (33 hours), TP (22.5 hours), Project (28.5 hours)

Implication: I created this module from scratch. I am in charge of all lecture slides, TDs, and TPs, as well as project subjects. I am coordinating this module since 2019 (exam sheets and planning).

Further, **I have also entirely changed and prepared the following, although existed, two modules:**

CNUM

Level: M1 FISE

Content: Signal processing recap, Baseband communication, Digital modulations, ISI, Error probability, Bandwidth, Bennett formula, Physical layer of GSM

Type: CM (33 hours), TD (10,5 hours), TP (6 hours), Project (13.5 hours)

Implication: Although existing in a former version within the Télécom Lille training track, I have entirely changed, jointly with C. Séguinot (IMT Nord Europe, France), this class for IMT Nord Europe. We proposed new class slides, new TDs and new TPs, as well as student projects. The coordination (exam sheets and planning) of this module was shared with C. Séguinot from 2019 to 2022.

CNUM-A

Level: M1 FISA

Content: Baseband transmission (Gray labeling, eye diagram and ISI, error probability), Analog modulation, Digital modulation (modulations, bandwidth, error probability)

Type: CM (10,5 hours), TD (4.5 hours)

Implication: Although existing in a former version, I have entirely changed and prepared this class when I arrived in 2016. I proposed new class slides and new TDs. I have been coordinating (exam sheets and planning) this module from 2016 to 2022 (until its new version due to a major apprentices classes update).

1.1.2 Module responsibilities

I have been in charge of organizing (exam sheets, grading, updating or creating the contents, plannings) of the following modules:

- CNUM (jointly with C. Seguinot from 2020 to 2022)
- CODES (2019 to present)
- I-CNUM (2019 to present)
- CNUM-A (2016 to 2022)

I also coordinated (exam sheets, planning, inviting all external lecturers) the module PMS (Models and Principles of security) in 2022 - 2023 after the leave of the Cybersecurity professor previously in charge of this class.

1.2 Research activities

1.2.1 Summary and main research interests

My research activities as an Associate Professor (Enseignante-chercheuse) have been performed at IEMN, UMR 8520 (Sept. 2016 to Feb. 2023) and IMT Nord Europe, CERI SN (from 2019 to present), and partially supported by IRCICA, CNRS USR 3380, Lille, France from Sept. 2016 to Feb. 2023. My research interests focus on information theory and multi-user information theory and more precisely on channel coding aspects, resource optimization in cooperative multi-user networks and physical layer security.

During my PhD, which was performed at ETIS lab (*Equipes Traitement de l'Information et Systèmes*), UMR 8051, Cergy-Pontoise, France, under the direction of David Declercq and the co-supervision of Claudio Weidmann, my research has focused on both source coding with coded side information and deriving achievable rate regions for cooperative communications. Regarding the source coding part, my main contribution was to characterize the fundamental Hamming-space Voronoi region of a convolutional code by the help of a finite state machine and then to exploit the later to improve the decoding algorithm as well as to

optimize the Low Density Parity Check (LDPC) code used [C1], [C2]. Regarding the cooperative communication part, I focused on the Gaussian full-duplex relay channel with correlated noises, the Gaussian full-duplex two-way relay channel with correlated noises and the Gaussian multiway relay channel with direct link for which I derived both upper-bounds on the capacity and lower-bounds achieved by Decode-and-Forward (DF), Compress-and-Forward (CF), Amplify-and-Forward (AF), Compute-and-Forward or Compress/Decode-and-Forward [C3], [C4], [J1].

Since my PhD, both the range of applications and exploited tools have diversified. Although related to information theory, the main focus of my current research activity lies in optimization, with tools ranging from convex optimization to machine learning techniques. Here optimization can be either related to resource optimization in multi-user and cooperative network, where the cooperation can be achieved with the help of a relay node or an ambient backscatter node; or to information theory-based Log-Likelihood Ratio (LLR) estimation optimization when the additive noise exhibits an impulsive nature. Nonetheless, a non-negligible part of my research activities remains related to channel coding, especially polar or LDPC codes, and deriving achievable rate regions.

More precisely, since my PhD, I have been interested in the following issues and applications:

Channel coding and information theory

Under impulsive noise

- Publications: 1 journal [J3] and 5 international conferences [C5], [C7], [C9], [C10], [C15]
- Collaborations: A. Goupil (Univ Reims, France), L. Clavier (IMT Nord Europe, France), P. Mary (INSA Lyon, France), M. Egan (INSA Lyon, France), JM. Gorce (INSA Lyon, France)
- Students: Y. Mestrah (PhD, 30% supervision), D. Anade (PhD), M. de Freitas (PhD)
- Supported by: ANR Arburst

Polar codes

- Publications: Publications: 1 journal [J7 sub] and 2 international conferences [C17], [C18]
- Collaborations: P. Mary (INSA Rennes), JY. Baudais (INSA Rennes),
- Students: S. Gelincik (Post-doc)
- Supported by: ANR Arburst

Physical layer security

- Publications: 1 journal [J2]
- Collaborations: M. Bloch (Georgia Institute of Technology, Atlanta, USA), G. Cervia (IMT Nord Europe, France)
- Students: M. Tahmasbi (PhD), M. Alam (PhD, 40% supervision)
- Supported by: ANR Wise-Phy, Beyond5G

Resource optimization for cooperative networks

NOMA and ambient backscattering via convex optimization and online learning

- Publications: 2 journals [J5], [J6] and 4 international conferences [C11], [C13], [C14], [C20]
- Collaborations: E. V. Belmega (ESIEE, France), R. de Lamare (PUC, Rio, Brazil)
- Students: H. El Hassani (PhD, 40% supervision)
- Supported by: ANR PRCI ELIOT

Cooperative cognitive networks via convex optimization and deep learning

- Publications: 1 journal [J4] and 5 international conferences [C16], [C19], [C12], [C8], [C6]
- Collaborations: E. V. Belmega (ESIEE, France), R. Negrel (ESIEE, France), M. Bennis (Univ. Oulu, Finland)
- Students: Y. Benatia (PhD, 40% supervision)
- Supported by: POTIONS, student mobility grant

1.2.2 Advising

Since 2016, my overall student advising activities (including the official advising percentages) can be summarized as follows:

- Post-docs: 1 ongoing, 1 alumni
- PhD students: 2 ongoing (40%, 40%) and 2 defended (30%, 40%)
- M1 students: 4
- M2 students: 2

Ongoing PhD students

1) Miled Alam
   Title: *Secrecy energy efficient power allocation for multi-user NOMA transmissions*

Period: April 2022 - April 2025
Advising: **40%** with G. Cervia (IMT Nord Europe, France, 50%), L. Clavier (IMT Nord Europe, France, 5%, co-director) and S. Lecomte (IMT Nord Europe, France, 5%, co-director)
Funding: 1/2 IMT Nord Europe, 1/2 Beyond 5G

2) Yacine Benatia
Title: *Cooperation, optimization and AI for future communications: interplay between model-based and data-driven approaches*
Period: Oct. 2020 - Sept. 2023
Defense date: **Expected in Sept./Oct. 2023**
Advising: **40%** with R. Negrel (ESIEE, France, 30%) and E. V. Belmega (ESIEE, France, 30%, official director)
Funding: 1/2 IMT Nord Europe, 1/2 ED EM2PSI
Publications: [C16], [C19]

Defended PhD students

1) Hajar El Hassani
Title: *Energy-efficient solutions for non-orthogonal multiple access systems aided by ambient backscattering*
Period: Oct. 2019 - Sept. 2022 + 6 months (COVID)
Defense date: 2nd December 2022
Jury: M. Wigger (Rewiever - Telecom Paris, France), R. Schober (Rewiever - FAU, Germany), M. di Renzo (L2S, France), M. G. Di Benedetto (Univ Rome, Italy), P. Mary (INSA Rennes, France), JM. Gorce (INSA Lyon, France), R. de Lamare (PUC, Brazil)
Advising: **40%** with E. V. Belmega (ESIEE, France, 60%, official director)
Funding: ANR PRCI ELIOT
Publications: [J5], [J6], [C11], [C13], [C14], [C20]
Current position: Post-doctoral researcher, L2S, France

2) Yasser Mestrah
Title: *Robust communication systems with unknown noise distribution*
Period: Oct. 2016 - Sept. 2019
Defense date: 16th December 2019
Jury: C. Poulliat (Reviewer - ENSEEIHT, France), P. Mary (Reviewer - INSA Rennes, France), V. Vrabie (Univ Reims, France), E. Boutillon (UBS, France), M. Egan (INSA Lyon, France)
Advising: **30%** with A. Goupil (Univ. Reims, France, 50%) and L. Clavier (IMT Nord Europe, France 20%, official director)
Funding: 1/2 Univ. Reim, 1/2 Télécom Lille
Publications: [J3], [C7], [C9], [C15]

Current position: R&D engineer, Mitsubishi Eletric, Rennes, France

Ongoing Post-doc

1) Mariem Belhor
   Title: *Wireless attack localization*
   Period: July 2023 - August 2024
   Collaborators: A. Fleury (IMT Nord Europe), V. Loscri (INRIA Lille), V. Deniau (UGE Lille)
   Funding: ANR ASTRID DEPOSIA
2) Sahar Masmoudi
   Title: *Characterization of sensor networks data*
   Period: October 2022 - December 2023
   Collaborators: C. Garnier, V. Itier, S. Sauvage (IMT Nord Europe, France), P. Kaluzny (TERA, Marseille, France)
   Funding: Plan de relance

Alumni Post-doc

1) Samet Gelincik
   Title: *Channel coding for finite block-length*
   Period: March 2020 - March 2022
   Collaborators: P. Mary and JY. Baudais (INSA Rennes, France)
   Funding: ANR Arburst
   Publications: [J7 sub], [C17], [C18]
   Current position: Post-doctoral researcher, Eurecom, France

M1 students:

1) Mohammed Achbouk, Summer 2023 - *Processing of data measured by pollution sensors using deep learning*
2) Stephen Somsack, Summer 2020 - *Machine learning for communications*
3) Mengxuan Li, Summer 2017 - *Spiking neuron - Performance of an IF detector*
4) Haoyang Zheng, Summer 2017 - *Spiking neuron - Sequence recognition*

M2 students:

1) Birhanu Samuel, Nov. 2018-Feb. 2019 - *Spiking neuron - LIF*
2) Ashenafi Fekede Haile, Nov. 2018-Feb. 2019 - *Spiking neuron - LIF*

1.2.3 Research projects

Since 2016, I have participated to the following research projects:

- PEPR 5G: 2022 - 2027 (Member)
  Consortium: CNRS, CEA, IMT
  Co-PI of PC7 WP1.4 *Backscattering communications*;
  Member of PC6 WP3.2 *AI for energy-efficient resource management in highly mobile and non-stochastic IoT networks*
  Funding: 2 PhD students to be hired (expected start: Oct. 2023, Oct. 2024)

- Plan de relance: Oct. 2022 - Dec. 2023 (Member)
  Consortium: IMT Nord Europe, TERA environement
  Characterization of sensor networks data
  Funding: Post-doctoral researcher S. Masmoudi

- ANR ASTRID DEPOSIA: Dec. 2021 - Dec. 2024 (Member)
  Consortium: UGE, IMT Nord Europe, INRIA, INODESIGN Group, MC2 Technologies
  Member of WP5 *Data analysis and AI for detection and geolocation of outdoor attacks*
  Funding: Post-doctoral researcher M. Belhor

- France Relance Beyond 5G: 2021 - 2024 (Member)
  Consortium: Thalès, Ericson, IMT, Eurecom
  Member of WP2 *Access layer and physical layer techniques for massive access in B5G networks*
  Funding: PhD M. Alam (1/2 Beyond 5G, 1/2 IMT Nord Europe)

- ANR U-Wake: 2021 - 2024 (Member)
  PI: L. Clavier (IMT Nord Europe, France)
  Member of WP1 *Prerequisites: Energy harvesting and signal detection*
  Consortium: IEMN, INSA Lyon, IRISA

- ANR Arburst: 2016 - 2020 (Member)
  PI: JM. Gorce (INSA Lyon, France)
  Consortium: INSA Lyon, INSA Rennes, IMT Nord Europe
  Funding: Post-doctoral researcher S. Gelincik

Since 2016, I also lead as **Principal investigator** several projects.

2020 - 2023	POTIONS - *Cooperation, optimization and artificial intelligence for future communications: interplay between model-based and data-driven approaches* Funding: PhD Y. Benatia (1/2 IMT Nord Europe, 1/2 ED EM2PSI, Cergy-Pontoise)
2016 - 2018	IRCICA internal call Funding: B. Samuel, A. Fekede Haile, M. Li and H. Zheng (M.Sc.)
2019 - 2020	IMT Nord Europe internal call Funding: S. Somsack (M.Sc.)

1.2.4 Collaborations

International collaborations

Rodrigo de Lamare, PUC-Rio, Brazil
Supported by: ANR PRCI ELIOT
Publications: [J6], [C14], [C20]

Matthieu Bloch, Georgia Institute of Technology, Atlanta, USA
Supported by: ANR Wise-Phy
Publications: [J2]

Mehdi Bennis, Univ. Oulu, Finland
Supported by: mobility grant CY and GdR ISIS for Y. Benatia

National collaborations

Jean-Yves Baudais, INSA Rennes
Supported by: ANR Arburst
Publications: [J7 sub], [C17], [C18]

E. Veronica Belmega, ESIEE
Supported by: POTIONS, ANR PRCI ELIOT
Publications: [J5], [J6], [J4], [C11], [C13], [C14], [C20], [C16], [C19], [C12], [C8], [NC10]

Virginie Deniau, UGE Lille
Supported by: ANR ASTRID DEPOSIA

Malcolm Egan, INSA Lyon
Supported by: ANR Arburst
Publications: [C5], [C10], [C15]

Jean-Marie Gorce, INSA Lyon
Supported by: ANR Arburst
Publications: [C5], [C10], [C15]

Alban Goupil, Univ. Reims
Publications: [J3],[C7], [C9], [C15]

Valeria Loscri, INRIA Lille
Supported by: ANR ASTRID DEPOSIA

Philippe Mary, INSA Rennes
Supported by: ANR Arburst
Publications: [J7 sub], [C15], [C17], [C18]

Romain Negrel, ESIEE
Supported by: POTIONS
Publications: [C16], [C19]

Local collaborations

Giulia Cervia
Supported by: B5G

Laurent Clavier
Supported by: ANR Arburst, ANR U-wake
Publications: [J3],[C7], [C9], [C15], [C6]

Anthony Fleury
Supported by: ANR ASTRID DEPOSIA

Christelle Garnier
Supported by: Plan de relance

Vincent Itier
Supported by: Plan de relance

Stéphane Sauvage
Supported by: Plan de relance

1.2.5 International stays

- Georgia Institute of Technologies, Atlanta, USA
  Duration: Post-doc in 2015-2016
- TUM, Munich, Germany
  Duration: 3 months in 2014

1.3 Scientific and collective responsibilities

1.3.1 Scientific responsibilities

Editorial activity

From January 2020 to February 2023, I served as Executive Editor for the Transactions on Emerging Telecommunications Technologies (ETT), for which I handled 20 papers as an Editor.

Since February 2023, I serve as Editor in Area 2: Network Optimization and Resource Management for the IEEE Transactions on Machine Learning in Communications and Networking.

Conference and seminar organization, session chairing

- Workshop RAWNET, WiOPT 2023 - jointly with S. Lasaulce, S. Perlaza, V. Y. F. Tan, C. Zhang

- Session chair of the Session 'Machine Learning & Data analytics' at EAI ValueTools 2019
- Volunteer in the local organization team (gift bags, welcoming participants, technical support, ...) of GRETSI 2019, Lille, France
- GdR ISIS meeting 'Methods and mathematical tools for IoT network modeling', jointly organized with P. Mary (INSA Lyon, France) and C. Goursaud (INSA Lyon, France), France, Nov. 2017
- Organization of 5 seminars at IRCICA, CNRS USR 3380, Lille, France

Research project expert

French ANR - phase 2: 2023, 2022

National responsibilities

- Invited speaker to the Table ronde 'Some advice for young female researchers in signal processing', GRETSI, Nancy, France, Sep. 2022
- Invited talks: *ETIS, Cergy-Pontoise, France (4); IMS Bordeaux, France (1); INSA Lyon, France (1); Cristal, Lille, France (1); Télécom Lille, France (1); Télécom Paris, France (1); Télécom Bretagne, France (1); LNT Munich, Germany (1); Workshop IWITC, IEMN, Lille, France (1); Webinar IMT, online (1)*

Local responsibilities

- Since Dec. 2022, I am an elected member of the CSAS (former CST) of IMT Nord Europe.
- Since 2021, I am an elected member (Associated Professor representative) of the Comité de Pilotage (COPIL) of the Centre for Digital System, IMT Nord Europe. This committee addresses all the strategical and budget aspects of the Centre of Digital System of IMT Nord Europe.
- Since 2017, I am an elected member of the Commission de Qualification pour Promotion et Changement d'Appellation of IMT Nord Europe. This committee is in charge of studying the possibility of an internal promotion at IMT Nord Europe.

Technical Program Committees (TPC)

- IEEE EuCNC 2023, 2022, 2021, 2020, 2019
- IEEE SPAWC 2023, 2022, 2019
- WiOpt 2023 Workshop Rawnet

- IEEE WCNC 2019 Workshop MoTION

Reviewing

- International journals: *IEEE Internet of Things Magazine, IEEE Transactions on Information Forensics and Security, IEEE Communications letters, IEEE Signal Processing Letters, IEEE Transactions on Communications, Transactions on Emerging Telecommunications Technologies, EURASIP Journal on Wireless Communications & Networking, International Journal of Communication Systems, Computers & Security*

- International conferences: *IEEE ISIT 2023; IEEE SSP 2021; IEEE EuCNC 2023, 2022, 2021, 2020, 2019; IEEE SPAWC 2022, 2019; IEEE ITW 2019; IEEE ISTC 2018; IEEE PIMRC 2021, 2018; IEEE WCNC 2018, 2017; IEEE Globecom 2016; IEEE ICC 2016; IEEE VTC-Fall 2015; NCC 2021*

1.3.2 Collective and pedagogical responsibilities at IMT Nord Europe

- Since 2019, I have been in charge Telecom-oriented internship content validation.

- Oct. 13rd, 2020 - Examiner of the VAE (Validation des acquis de l'expérience - accreditation of prior experiential learning) jury of Xavier Foin, IMT Nord Europe, France.

- Since 2016, I have been the referee of several engineer internships as well as apprentices.

- Since 2016, I have participated to various apprentices and AST (*Admis sur titre*) selection jury.

- Participation to the Open Door Days.

1.4 Personal bibliography

1.4.1 Bibliometry

Since the beginning of my PhD in 2012, my research activities lead to the following publications:

- Peer-reviewed international journals: 6 + 1 submitted

- Peer-reviewed international conferences: 20

- National conferences: 10 + 1 submitted

In the following, all PhD students and Post-doc researchers are underlined.

1.4.2 Peer-reviewed international journal papers

Post-PhD: 5 + 1 submitted

[J8 prep] Y. Benatia, **A. Savard**, R. Negrel, E. V. Belmega, "Robust DNN for power allocation problems in cognitive relay networks", in preparation, Feb. 2023

[J7 sub] S. Gelincik, P. Mary, **A. Savard**, J-Y. Baudais, "A Pre-Transformation Method to Increase the Minimum Distance of Polar-Like Codes", submitted to IEEE Transactions on Communications, **major revision**

[J6] H. El Hassani, **A. Savard**, E. V. Belmega, R. de Lamare, "Multi-user downlink NOMA systems aided by an ambient backscatter device: achievable rate region and energy-efficiency maximization", IEEE Transactions on Green Communications and Networking, **accepted, March 2023**

[J5] H. El Hassani, **A. Savard**, E. V. Belmega, "Adaptive NOMA in time-varying wireless networks with no CSIT/CDIT relying on a 1-bit feedback", IEEE Wireless Communications Letters, Vol. 10, No. 4, April 2021, pp. 750-754

[J4] **A. Savard**, E. V. Belmega, "Full-duplex Relaying for Opportunistic Spectrum Access under an Overall Power Constraint ", IEEE Access, Vol. 8, 2020, pp. 168262 - 168272

[J3] Y. Mestrah, **A. Savard**, A. Goupil, G. Gellé, L. Clavier, "An Unsupervised LLR Estimation with unknown Noise Distribution", EURASIP Journal on Wireless Communications and Networking, Springer Open, 2020, 26, pp. 1 - 11.

[J2] M. Tahmasbi, **A. Savard**, M. R. Bloch, "Covert Capacity of Non-Coherent Rayleigh-Fading Channels", IEEE Transactions on Information Theory, Vol. 66, No. 4, April 2020, pp. 1979-2005

PhD: 1

[J1] **A. Savard**, C. Weidmann, "On the Gaussian multiway relay channel with intra-cluster links", EURASIP Journal on Wireless Communications and Networking, Springer Open, 2016, 52, pp. 1 - 17.

1.4.3 Peer-reviewed international conference papers

Post-PhD: 16

[C20] H. El Hassani, **A. Savard**, E. V. Belmega, R. de Lamare, "Energy-Efficient Solutions in Two-user Downlink NOMA Systems Aided by Ambient Backscattering", IEEE Globecom, Rio de Janeiro, Brazil, 2022

[C19] Y. Benatia, R. Negrel, **A. Savard**, E. V. Belmega, "Robustness to imperfect CSI of power allocation policies in cognitive relay networks", IEEE SPAWC, Oulu, Finland, 2022

[C18] S. Gelincik, P. Mary, **A. Savard**, J-Y. Baudais, "Preserving the Minimum Distance of Polar-Like Codes While Increasing the Information Length", IEEE ISIT, Espoo, Finland, 2022

[C17] S. Gelincik, P. Mary, J-Y. Baudais, **A. Savard**, "Achieving PAC Code Performance with SCL Decoding without Extra Computational Complexity", IEEE ICC, Seoul, South Korea, 2022

[C16] Y. Benatia, **A. Savard**, R. Negrel, E. V. Belmega, "Unsupervised deep learning to solve power allocation problems in cognitive relay networks", IEEE ICC Wokshop, Seoul, South Korea, 2022

[C15] Y. Mestrah, D. Anade, **A. Savard**, A. Goupil, M. Egan, P. Mary, JM. Gorce, L. Clavier, "Unsupervised Log-Likelihood Ratio Parameter Estimation for Short LDPC Packets in Impulsive Noise", IEEE WCNC, Austin, USA, 2022

[C14] H. El Hassani, **A. Savard**, E. V. Belmega, R. de Lamare, "Energy-efficient Cooperative Backscattering Closed-Form Solution for NOMA", IEEE Globecom, Madrid, Spain, 2021

[C13] H. El Hassani, **A. Savard**, E. V. Belmega, "Energy-efficient 1-bit feedback NOMA in wireless networks with no CSIT/CDIT", IEEE SSP workshop, Rio de Janeiro, Brazil, 2021

[C12] **A. Savard**, E. V. Belmega, "Optimal power allocation policies in multi-hop cognitive radio networks", IEEE PIMRC, London, UK, 2020

[C11] H. El Hassani, **A. Savard**, E. V. Belmega, "A closed-form solution for energy-efficiency optimization in multi-user downlink NOMA", IEEE PIMRC, London, UK, 2020

[C10] M. de Freitas, M. Egan, L. Clavier, **A. Savard**, JM. Gorce, "Power Control in Parallel Symmetric α-Stable Noise Channels", IEEE SPAWC, Cannes, France, 2019

[C9] Y. Mestrah, **A. Savard**, A. Goupil, G. Gellé, L. Clavier, "Robust and Simple Log-Likelihood Approximation for Receiver Design", IEEE WCNC, Marrakech, Morocco, 2019

[C8] **A. Savard**, E. V. Belmega, "Optimal Power Allocation in a Relay-aided Cognitive Network", ACM EAI ValueTools, Palma de Mallorca, Spain, 2019

[C7] Y. Mestrah, **A. Savard**, A. Goupil, L. Clavier, G. Gellé, "Blind Estimation of an Approximated Likelihood Ratio in Impulsive Environment", IEEE PIMRC, Bologna, Italy, 2018

[C6] **A. Savard**, L. Clavier, "On the two-way diamond relay channel with lattice-based Compress-and-Forward", IEEE WCNC, Barcelona, Spain, 2018

[C5] M. Egan, L. Clavier, M. de Freitas, L. Dorville, JM. Gorce, **A. Savard**, "Wireless Communication in Dynamic Interference", IEEE Globecom, Singapour, 2017

PhD: 4

[C4] **A. Savard**, C. Weidmann, "Lattice coding for the Gaussian one- and two-way relay channels with correlated noises", IEEE ISIT, Hong-Kong, Jun. 2015

[C3] **A. Savard**, C. Weidmann, “On the multiway relay channel with direct links”, IEEE ITW, Hobart, Australia, Nov. 2014

[C2] **A. Savard**, C. Weidmann, “Optimized codes for the binary coded side-information problem”, IEEE ISTC, Bremen, Germany, Aug. 2014

[C1] **A. Savard**, C. Weidmann, “Improved decoding for binary source coding with coded side information”, IEEE ITW, Sevilla, Spain, Sep. 2013

1.4.4 Peer-reviewed national conference papers

Post-PhD: 6 + 1 submitted

[NC11] R. Negrel, Y. Benatia, **A. Savard**, E. V. Belmega, “Sélection de relais robuste aux canaux imparfaits pour la radio cognitive coopérative exploitant des réseaux profonds”, GRETSI 2023, Grenoble, France

[NC10] **A. Savard**, E. V. Belmega, “Achievable rate regions for cooperative cognitive radio networks with complex channels and circular normal additive noises”, GRETSI 2022, Nancy, France

[NC9] H. El Hassani, **A. Savard**, E. V. Belmega, R. de Lamare, “Rétrodiffusion coopérative efficace en énergie pour un système multi-utilisateurs à accès multiple NOMA”, GRETSI 2022, Nancy, France

[NC8] Y. Mestrah, **A. Savard**, A. Goupil, G. Gellé, L. Clavier, “Mesure indirecte des performances de LLR approché”, GRETSI 2019, Lille, France

[NC7] **A. Savard**, L. Clavier, F. Danneville, C. Loyez, “Performance théorique d’un neurone à spikes Integrate-and-Fire”, GRETSI 2019, Lille, France

[NC6] **A. Savard**, L. Clavier, “Canal à deux relais utilisant Compress-and-Forward”, GRETSI 2019, Lille, France

[NC5] **A. Savard**, E. V. Belmega, “Allocation de puissance pour les réseaux radio cognitifs à relais”, GRETSI 2019, Lille, France

PhD: 4

[NC4] **A. Savard**, C. Weidmann, “Codage basé sur les réseaux de points pour le canal à relais Gaussien mono- et bidirectionnel avec bruits corrélés”, GRETSI 2017, Juan les Pins, France

[NC3] **A. Savard**, C. Weidmann, “Canal à relais multidirectionnel avec liens directs”, GRETSI 2015, Lyon, France

[NC2] **A. Savard**, C. Weidmann, “Décodeur amélioré pour le codage de source avec information adjacente compressée”, GRETSI 2013, Brest, France

[NC1] **A. Savard**, C. Weidmann, “Codes LDPC non-binaires pour le codage de source”,

Journées Codage et Cryptographie 2012, Dinard, France

1.4.5 PhD Thesis

[PhD] **A. Savard**, "Coding for cooperative communications: Topics in distributed source coding and relay channels", Ph.D. Dissertation, Université de Cergy-Pontoise, France, Advisors: C. Weidmann and D. Declercq

Part I

Channel coding

Chapter 2

LLR approximation in Symmetric α-stable noise

In this chapter, we overview the most relevant contributions [J3], [C9] of the work performed by the PhD student Yasser Mestrah, whom I have co-advised (at 30%) jointly with Laurent Clavier (IMT Nord Europe, 20%, official director) and Alban Goupil (Université de Reims, 50%).

Main contributions

Many decoding schemes rely on log-likelihood ratios (LLRs), whose derivation depends on the knowledge of the noise distribution which can be difficult to obtain, especially in dense and heterogeneous network settings. For example, when the interference exhibits an impulsive nature, LLRs become highly non linear and consequently computationally prohibitive. We thus propose to directly estimate the LLRs without relying on the noise knowledge by carefully selecting and tuning the LLR estimation in a parametric family of functions. Our main contributions are the following:

- Deriving an information-theory-based Genie-aided LLR estimation in the asymptotic regime, where the receiver has access to a long sequence of pilot samples.
- Deriving an information-theory-based unsupervised LLR estimation in the asymptotic regime in order to avoid the need of a training sequence.
- Deriving an information-theory-based unsupervised LLR estimation in the short block length regime, where we first analyze the reasons leading to poor LLR approximation in such a regime and then proposing two mechanisms to improve the later.

2.1 Preliminaries

2.1.1 Impulsive noises

5G and future network generations have to deal with denser and heterogeneous networks for which interference may exhibit an impulsive behavior as suggested by theoretical analysis [C5], [1], [2], which is not encompassed by the Gaussian model.

Several models have been proposed to handle the impulsive nature of the interference, ranging from Middleton model to the α-stable one. Middleton first proposed to tackle the impulsive nature by considering a Gaussian mixture with an infinite number of components [3]–[6]. Its model has been shown to accurately model electromagnetic interference and background noise in power line communication [7], [8]. Nonetheless, handling an infinite number of components is not practical, hence various approximation models have been proposed, such as Gaussian mixture or ϵ-contaminated which only consider a limited number of components. On the other hand, α-stable distributions, introduced by Paul Lévy in the 1920s, form a rich class of probability distributions capable of representing skewness and heavy tails. The later were also shown to accurately model the interference in wireless communication systems [C5], [1], [9]–[11] and encompass the widely used Gaussian model as a special case.

In the remaining of this chapter, we assume that the additive impulsive noise Z received over the channel follows a symmetric α-stable ($S\alpha S$) distribution. Its characteristic function is expressed as $\Phi_Z(t) = \exp\left(-\gamma^\alpha |t|^\alpha\right)$, where $0 < \alpha \leq 2$ denotes the characteristic exponent and $\gamma \geq 0$ the scale parameter. The characteristic exponent α sets the degree of impulsiveness: the smaller α, the heavier the tail of the probability density function (pdf), and hence, the more likely to observe large values. The scale parameter γ plays a similar role to the variance in the Gaussian case.

The main drawback of $S\alpha S$ distributions is the lack of closed-form expression of their pdf, except for the following special cases: $\alpha = 0.5$ (Lévy), $\alpha = 1$ (Cauchy) and $\alpha = 2$ (Gaussian). Nevertheless, the later can be numerically computed as

$$g_\alpha(x, \gamma) = \frac{1}{2\pi} \int_{-\infty}^{\infty} \exp(-\gamma^\alpha |t|^\alpha) \exp(-jtx) dt, \tag{2.1}$$

which however induces a generally prohibitive computational burden as well as requiring the knowledge of the noise parameters.

Let us now briefly introduce modern channel coding, and more specifically low density parity check (LDPC) codes that will be used later on for numerical simulations.

2.1.2 Modern channel coding: LDPC codes

Low-density parity check (LDPC) codes are block codes first proposed by Gallager in the 60s [12], but mostly ignored due to the computational limitation of the hardware, until their rediscovery by MacKay in the 90s [13], [14].

In block coding, an information sequence is segmented into message blocks each of length K. At the transmitter side, each input message $\underline{u} = [u_1, \ldots, u_K]$ is encoded into a longer binary sequence $\underline{x} = [x_1, \ldots, x_N]$, with $N > K$. The sequence $\underline{x}$ is called the *codeword* associated to the message $\underline{u}$. The $N - K$ added bits, called *redundancy*, do not carry any new information but provide the capacity of detecting and/or correcting errors at the receiver side. The ratio K/N, called the *code rate*, represents the average number of information bits carried by each code bit.

A binary LDPC code is usually represented by its sparse parity check matrix H of size

$(N-K)\times N$, where all non-zeros entries are ones. The codewords are then defined as the set of binary sequences $\underline{X}\in\{0,1\}^N$ such that $H\underline{X}=\underline{0}$.

At the receiver side, a decoder is used to recover the sent codeword $\widehat{\underline{X}}$ from the received signal $\underline{Y}=\underline{X}+\underline{Z}$, where $\underline{Z}$ is the additive noise sequence.

Since maximum likelihood decoding of a LDPC code is a NP-hard problem, sub-optimal decoders based on iterative belief propagation (BP) have been proposed [12], [13], [15], [16]. The later achieve near-capacity performance while exhibiting a complexity linear in the code length. The main ingredient of BP decoding is the iterative update of LLRs given the received one, defined as $L_i=\log\frac{\mathbb{P}(Y_i=y_i|X_i=0)}{\mathbb{P}(Y_i=y_i|X_i=1)}$, where Y_i denotes the i-th component of the received signal $\underline{Y}$.

Thanks to near-capacity performance as well as to their powerful decoding implementation, LDPC codes are nowadays widely used in wireless communication [13], [17]–[20].

2.2 System model and Information theoretical-based LLR optimization

2.2.1 System model

In the remaining, we consider the transmission between a single device and a receiver and further assume that the considered channel is memoryless. The information source is first encoded using a binary LDPC code and then mapped onto a binary phase shift keying (BPSK) constellation. Hence, the channel input $\underline{X}$ takes its value in $\in\{-1,+1\}^N$ with equal probability. The channel output $\underline{Y}$ is given as $\underline{Y}=\underline{X}+\underline{Z}$, where the additive noise $\underline{Z}$, independent of the message $\underline{X}$, is an independent sequence of $S\alpha S$ random variables. At the receiver side, the sequence $\underline{Y}$ is decoded using the BP algorithm, requiring hence the computation of the LLRs $L_i=\log\frac{\mathbb{P}(Y_i=y|X_i=+1)}{\mathbb{P}(Y_i=y|X_i=-1)}=\log\frac{g_\alpha(y-1,\gamma)}{g_\alpha(y+1,\gamma)}$, where $g_\alpha(x,\gamma)$ denotes the pdf of the noise given in (2.1). Since $g_\alpha(x,\gamma)$ cannot be obtained in closed-form, efficient computation of the LLR is not straightforward. We hence propose to instead focus on LLR approximations that will be fed to the BP decoder.

2.2.2 LLR approximations

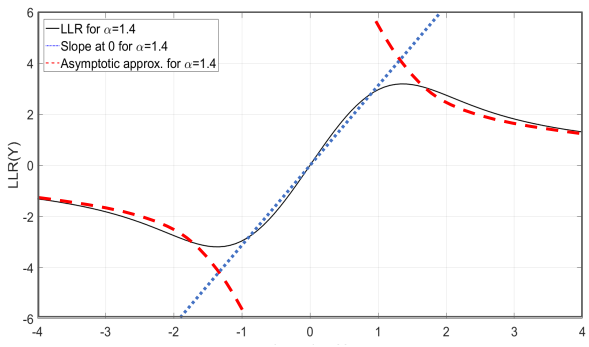

Figure 2.1: LLR under $S\alpha S$ noise with parameters $\alpha=1.4$, $\gamma=0.5$

The LLR under an additive $S\alpha S$ noise of parameters $\alpha = 1.4$ and $\gamma = 0.5$, which is highly non linear, is depicted in Figure 2.1. Except for $\alpha = 2$, which corresponds to the Gaussian case for which the LLR is linear and given as $L(y) = \frac{2}{\sigma^2}y$, the obtained shape in Figure 2.1 is similar for other choices of α and γ. As the channel output increases, the LLR decreases, meaning that the received sample becomes less reliable (as it likely follows from a high amplitude noise sample). Moreover, two specific parts can be observed:

- when the channel output y is close to 0, the LLR is almost a linear function of the channel output;
- whereas when the channel output y is larger, the LLR presents a power-law decrease.

This observation is the starting point of many parametric LLR approximations in impulsive noise depicted in Figure 2.2. At first, only piece-wise linear LLR parametric approximations have been proposed in the 90s, such as the hole puncturer [21] given in (2.2) or the soft limiter [21] (also termed clipping [22]) given in (2.3).

$$L_{\text{hp}}(y) = \begin{cases} ay & \text{if } |y| < \sqrt{b/a} \\ 0 & \text{otherwise} \end{cases} \tag{2.2}$$

$$L_{\text{clip}}(y) = \begin{cases} ay & \text{if } |y| < \sqrt{b/a} \\ \text{sign}(y)\sqrt{ab} & \text{otherwise} \end{cases} \tag{2.3}$$

The first proposed LLR approximation exhibiting a non linear part was proposed in [23] for $S\alpha S$ noise and is given as $L(y) = \text{sign}(y)\min\left\{\frac{\sqrt{2}}{\gamma}|y|, \frac{2(\alpha+1)}{|y|}\right\}$. The later nonetheless requires the knowledge of the noise parameters.

The main contribution of Yasser Mestrah PhD thesis was to consider a parametric non-linear LLR approximation $L_\theta(.)$ and to optimize the vector of parameters θ. Neither the noise model, nor the noise parameters are required at the receiver side while optimizing the LLR approximation. In the remaining, and based on the two specific regions observed in Figure 2.1, we focus on a two terms-based LLR approximation given as

$$L_\theta(y) = L_{ab}(y) = \text{sign}(y)\min\left(a|y|, \frac{b}{|y|}\right), \text{ with } \theta = (a, b) \in \mathbb{R}_+^2. \tag{2.4}$$

In [C9], we also proposed a three terms-based LLR approximation that slightly improves the performance in terms of bit error rate (BER), but at the price of estimating one more optimization parameter.

2.2.3 Information theory based LLR approximation optimization

Once a LLR approximation has been chosen, the question of estimating the parameters vector remains. While various methods, such as direct estimation of the noise model parameters [24], [25] or noise distribution estimation [26], have been proposed in the literature, it was shown in [26] that the one based on maximizing the mutual information between the channel input and output [27] yields the best performance.

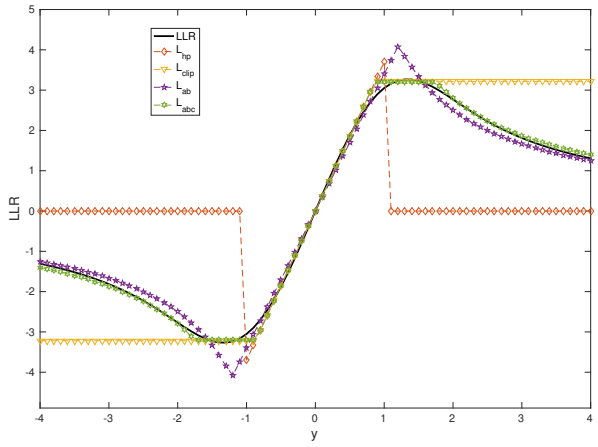

Figure 2.2: Parametric approximations of the LLR in $S\alpha S$ noise with $\alpha = 1.4$, $\gamma = 0.4$

Recall that the capacity of any memoryless, binary input, and symmetric output channel can be expressed as a function of the LLRs L as [27], [28]

$$C_L = 1 - \mathbb{E}_{X,Y}[\log_2(1 + e^{-XL(Y)})] = 1 - \mathbb{E}_{X,Y}[\log_2(1 + e^{-L(XY)})], \tag{2.5}$$

where the last equality follows since LLRs are odd functions and $X = \pm 1$. This expression comes from the decomposition $\mathbb{I}(X;Y) = \mathbb{H}(X) - \mathbb{H}(X|Y)$, where

$$\mathbb{H}(X|Y) = \mathbb{E}_{X,Y}[-\log_2 p(X|Y)] = \mathbb{E}_{X,Y}[\log_2(1 + e^{-XL(Y)})].$$

Following the idea of [27], under approximated LLRs L_θ, one does not have access to the capacity given in (2.5) but to a lower bound expressed as

$$C_{L_\theta} = 1 - \mathbb{E}_{X,Y}[\log_2(1 + e^{-XL_\theta(Y)})] = 1 - \mathbb{E}_{X,Y}[\log_2(1 + e^{-L_\theta(XY)})]. \tag{2.6}$$

Further, approximating the LLRs is equivalent to approximate the conditional probability $p(x|y) = \frac{1}{1+\exp(-xL(y))}$ by $q(x|y) = \frac{1}{1+\exp(-xL_\theta(y))}$, and thus to approximate the conditional entropy $\mathbb{H}(X|Y)$ by $\widehat{\mathbb{H}}(X|Y) = \mathbb{E}_{X,Y}[\log_2(1+e^{-XL_\theta(Y)})]$. The difference between the channel capacity given in (2.5) and its lower bound (2.6) is directly related to the Kullback-Leibler divergence between the conditional densities $p(x|y)$ and $q(x|y)$ as $C_L - C_{L_\theta} = \mathbb{D}_{KL}(p||q)$. Hence, the channel capacity lower bound C_{L_θ} achieves the capacity if the approximated density $q(x|y)$ equals the true distribution $p(x|y)$.

Our goal is thus to derive the optimal LLR estimations parameters as

$$\theta^* = \arg\min_\theta \mathbb{E}_{X,Y}\left[\log_2\left(1 + e^{-L_\theta(XY)}\right)\right]. \tag{2.7}$$

As a stochastic optimization problem, assuming that input samples X_i can be obtained, θ^* can be estimated via sample average approximation as

$$\hat{\theta}^* = \arg\min_\theta \frac{1}{n}\widehat{\mathbb{H}}_n(\theta, \{\Psi_i\}_{i=1}^n) \tag{2.8}$$

where n denotes the number of available samples, $\Psi_i = X_i Y_i$ and

$$\widehat{\mathbb{H}}_n(\theta, \{\Psi_i\}_{i=1}^n) = \sum_{i=1}^{n} \log_2\left(1 + e^{-L_\theta(\Psi_i)}\right). \tag{2.9}$$

Recall that the chosen LLR approximation is given as $L_\theta(\Psi_i) = \text{sign}(\Psi_i)\min\left(a|\Psi_i|, \frac{b}{|\Psi_i|}\right)$.

$$\begin{aligned}
\widehat{\mathbb{H}}_n(\theta, \{\Psi_i\}_{i=1}^n) &= \sum_{i=1}^{n} \log_2\left(1 + e^{-\text{sign}(\Psi_i)\min\left(a|\Psi_i|, \frac{b}{|\Psi_i|}\right)}\right) \\
&= \sum_{i,\Psi_i \geq 0} \log_2\left(1 + e^{-\min\left(a\Psi_i, \frac{b}{\Psi_i}\right)}\right) + \sum_{i,\Psi_i < 0} \log_2\left(1 + e^{\min\left(-a\Psi_i, -\frac{b}{\Psi_i}\right)}\right) \\
&= \sum_{i,\Psi_i \geq 0} \max\left\{\log_2\left(1 + e^{-a\Psi_i}\right); \log_2\left(1 + e^{-\frac{b}{\Psi_i}}\right)\right\} \\
&+ \sum_{i,\Psi_i < 0} \min\left\{\log_2\left(1 + e^{-a\Psi_i}\right); \log_2\left(1 + e^{-\frac{b}{\Psi_i}}\right)\right\}
\end{aligned} \tag{2.10}$$

In order to minimize $\widehat{\mathbb{H}}_n(\theta, \{\Psi_i\}_{i=1}^n)$, one has to increase the estimation parameters a, b whenever the samples $\Psi_i = x_i y_i$ are positive and decrease the estimation parameters whenever the samples $\Psi_i = x_i y_i$ are strictly negative. Minimizing the objective function is hence a compromise between minimizing each of the two sums in (2.10), one of which tends to increase the value of the optimization parameters while the other tends to decrease it. Despite the considered problem being non-convex, we use a simplex method based algorithm to obtain at least a local minimum.

Let us now focus on the LLR estimation when the blocklength N is large enough. We first consider a supervised approach, in which some pilots samples are available at the receiver side, and then consider an unsupervised one. In both cases, neither the noise model, nor its parameters are known at the receiver side, and the proposed method can be applied to a large set of noise models, from impulsive ones to the Gaussian one as will be shown in Section 2.3.3.

2.3 LLR estimation in the asymptotic regime

2.3.1 Baseline approach: genie-aided approximation

In order to estimate the performance of our proposed LLR estimation approach, we start by considering a genie-aided approach, in which a pilot sequence $\{X_i\}$ of n samples is available at the receiver side. The optimization parameter θ^* is triggered after receiving the corresponding channel outputs $\{Y_i\}$ as shown in Figure 2.3, and once obtained, it is used to compute the approximated LLRs $L_{\theta^*}(\underline{Y})$ fed to the BP decoder. All these steps are thereafter denoted as Genie-aided Decoder (GAD) and were presented in [J3], [C7].

In the above, the number of available pilots n can either be N, the length of the send codeword, or only a fraction of it. Of course, the larger the number of available pilots, the

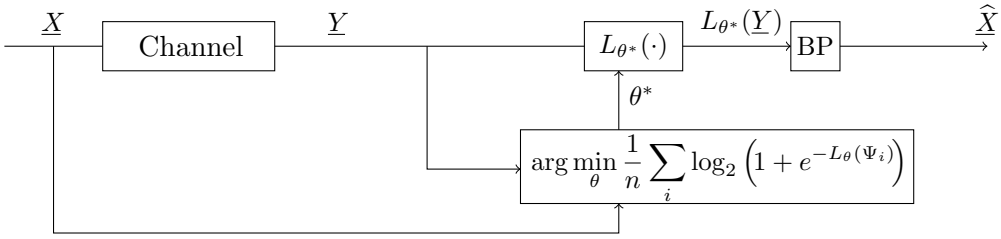

Figure 2.3: Principle of the genie-aided decoder (GAD)

closer the approximated LLRs to the true LLRs, as can be seen in Figure 2.4. The impact of the number of available pilots will be evaluated in terms of BER curves in Section 2.3.3. Intuitively, to obtain good performance in terms of BER, the estimated LLRs need to be as close as possible to the true LLRs.

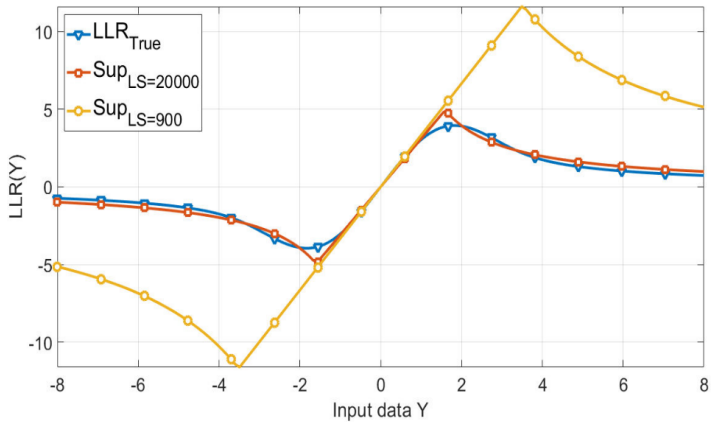

Figure 2.4: Comparison between true LLRs and approximated LLRs when the noise follows a $S\alpha S$ distribution of parameter $\alpha = 1.8$, $\gamma = 0.55$ for $n = 20000$ and $n = 900$ available pilot samples. The more available pilot samples, the closer the approximated LLR to the true one.

A major drawback of this supervised approach is the necessity of the pilots, as it induces an increase in signaling and a decrease of the useful rate. Further, the number of available pilots needs to be large enough to obtain an accurate LLR estimation. We hence propose to move to unsupervised LLR approximation, which directly operates on the channel outputs, without any prior on the input or noise distribution.

2.3.2 Proposed unsupervised approximation

Since our information-theory-based LLR estimation method requires both the channel outputs and inputs, which are no longer available under unsupervised estimation, we proposed in [J3], [C7] to extract a noise sequence $\widetilde{\underline{Z}}$ from the received channel outputs, which is used to simulate a transmission with the all-one codeword at the receiver side. More precisely, the extracted noise sequence is obtained with the help of a sign-detector as $\widetilde{\underline{Z}} = \underline{Y} - \text{sign}(\underline{Y})$. The simulated input symbols are $\widetilde{X}_i = 1$ and the corresponding channel outputs are $\widetilde{Y}_i = \widetilde{X}_i + \widetilde{Z}_i = 1 + \widetilde{Z}_i$. Hence, θ^* is obtained using the samples $(1, \widetilde{Y}_i)$ instead of (X_i, Y_i) when computing (2.8). The principle of such an unsupervised decoder, denoted as USD, is depicted

in Figure 2.5.

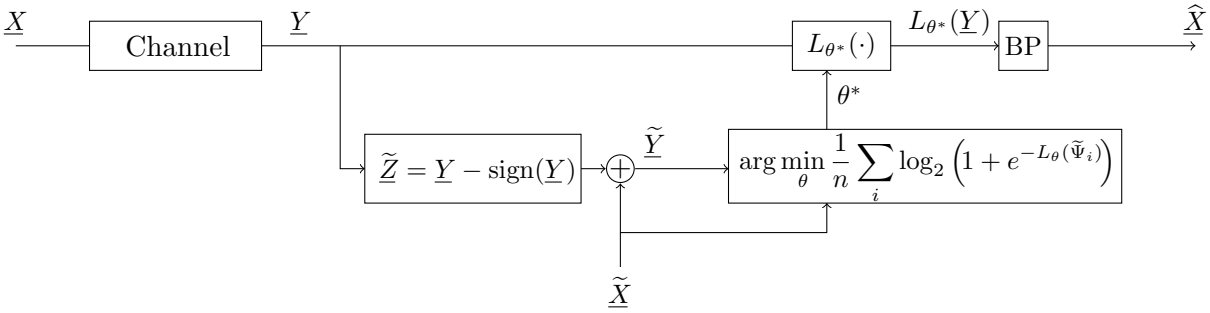

Figure 2.5: Unsupervised decoder (USD)

Figure 2.6 compares the evolution of the mean and standard deviation of the estimated LLR parameters a and b as a function of the γ parameter of a $S\alpha S$ noise with $\alpha = 1.4$. One can note that the gap between the supervised and unsupervised estimation of the parameter a of the approximation L_{ab} keeps very close, whereas the one for the parameter b is significantly larger. The later follows from the fact that b depends on large noise samples which are rare events; consequently its estimation is more difficult. Figure 2.7 compares the LLR shapes obtained under supervised and unsupervised estimations to the true one. Despite the aforementioned gap for the parameter b, the unsupervised approximated LLR keeps rather close to the true one.

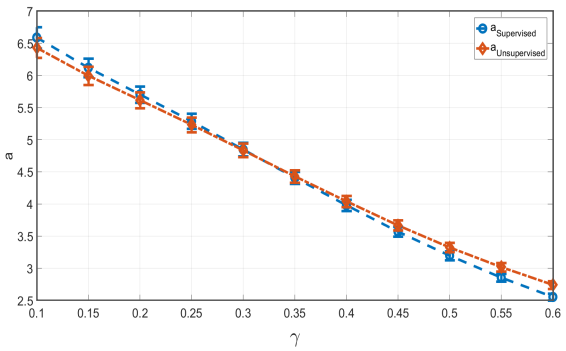

(a) Mean and standard deviation in the estimation of the parameter a of the approximated LLRs

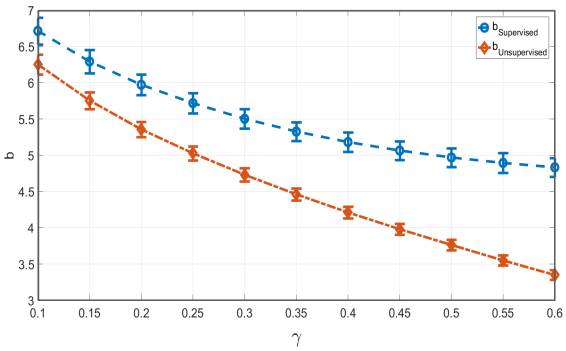

(b) Mean and standard deviation in the estimation of the parameter b of the approximated LLRs

Figure 2.6: Comparison in the approximation parameters under the supervised and unsupervised optimization for a $S\alpha S$ noise with $\alpha = 1.4$.

2.3.3 Numerical simulations

Let us now investigate the impact of our proposed LLR approximation in terms of BER when the source sequence is encoded using a regular (3,6) LDPC code of length $N = 20000$.

In a first step, we investigate the link between the objective function minimized for the LLR approximation given in (2.8) and the obtained BER performance. In Figure 2.8(a) we represent a 3D plot of the objective function under supervised estimation with $n = 20000$ available pilot samples. The white contour delineates the area where the objective function

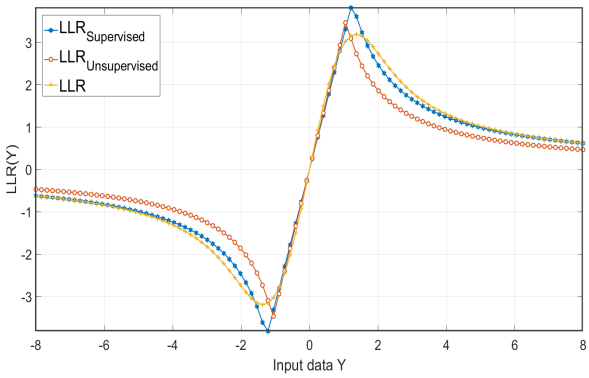

Figure 2.7: Comparison of the supervised, unsupervised estimated LLRs to the true LLR under $S\alpha S$ noise of parameter $\alpha = 1.4, \gamma = 0.5$.

reaches values very close to its minimal value. Note that the objective function is rather flat around its minimal value, leading to an estimation very sensitive to noise and to the number of available pilots. In Figure 2.8(b), we illustrate the link between the objective function and the BER. The white contour is the same as in Figure 2.8(a). Note that the area of small BER and the one corresponding to the minimal value of the objective function overlap and the optimal θ^* values under both the supervised and unsupervised estimation allows the BP decoder to achieve a BER below 10^{-5}.

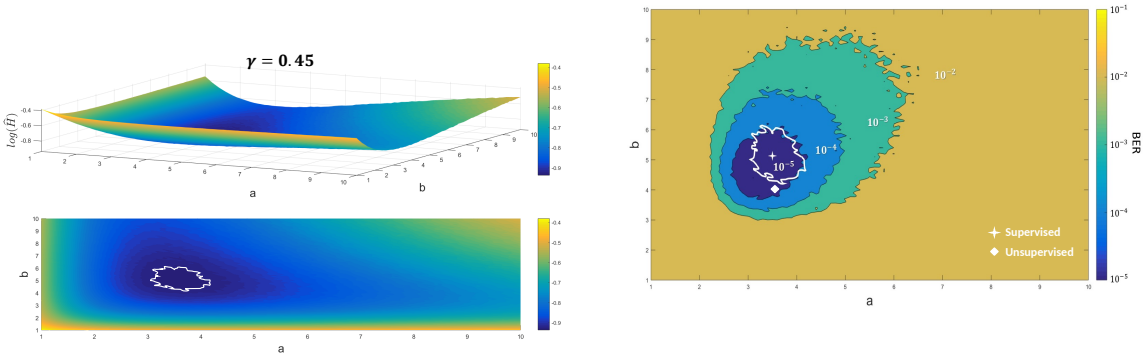

(a) Objective function

(b) BER of the (3,6) regular LDPC code

Figure 2.8: Empirical link between the objective function under study $\widehat{\mathbb{H}}_n(\theta, \{\psi_i\}_{i=1}^n)$ and BER for a $S\alpha S$ noise with $\alpha = 1.4$, $\gamma = 0.45$ for $N = 20000$

Figure 2.9 compares the obtained BER under the supervised and unsupervised LLR estimation, as well as the one obtained with the true LLR for a $S\alpha S$ noise of parameter $\alpha = 1.8$ and $\alpha = 1.4$ respectively. The curve labeled LLR_{La} corresponds to a linear LLR estimation with only the parameter a. Regarding supervised estimation, we use either $n = 1200$ or $n = 20000$ pilots. The longer pilot sequence allows to assess the performance of the LLR estimation, whereas the shorter one allows to evaluate the performance loss due to estimation with a more realistic number of pilots. The proposed supervised estimation under large pilot samples performs very close to the true LLR, which validates the good performance of

our approach. Further, even if the unsupervised approach exhibits a gap compared to the supervised one with long pilot sequence, it performs significantly better than the supervised approach under a realistic pilot amount as well as the linear LLR approximation.

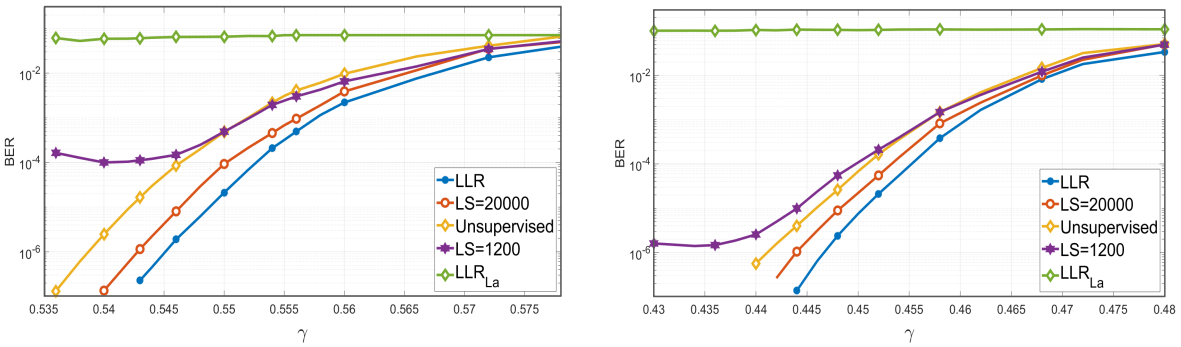

(a) Low impulsive noise ($\alpha = 1.8$)

(b) Highly impulsive noise ($\alpha = 1.4$)

Figure 2.9: BER comparison in impulsive SαS noise

Figure 2.10 compares the BER performance of our supervised and unsupervised approach in other impulsive noises (Middleton and the special Gaussian one). We can note that our proposed approach is able cope with various noise models without requiring its knowledge at the receiver side.

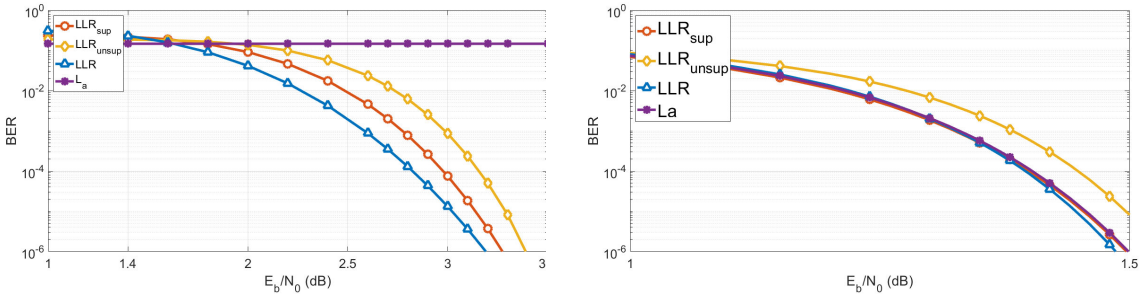

(a) Highly impulsive Middleton Class A noise ($A = 0.1$ and $\Gamma = 0.1$)

(b) Gaussian noise

Figure 2.10: BER comparison in other noises

2.4 Shortening the block length

The Internet of Things (IoT) has driven the emergence of Low Power Wide Area Networks, in which devices with limited transmit power communicate with an access point. Furthermore, these devices are only allowed to transmit very small quantities of data, leading to the use of short channel codes.

Although our proposed USD performs well for large blocklength N, its performance degrades as the blocklength decreases, as will be illustrated in Figure 2.13.

In this Section, we propose a new unsupervised LLR estimation, termed NUSD [C15], which overcomes the performance degradation when the blocklength is small (of the order of

$N = 500$). The later is achieved by first analyzing when poor estimation occurs, and then introducing a combination of sampling and regularization techniques.

2.4.1 Quantifying the risk of poor estimation

First note that based on the LLR approximation form given in Figure 2.11, the domain of the LLR approximation in (2.4) can be partitioned into four regions:

$$B^- = \left[-\infty, -\sqrt{b/a}\right], A^- = \left[-\sqrt{b/a}, 0\right], A^+ = \left[0, \sqrt{b/a}\right], B^+ = \left[\sqrt{b/a}, +\infty\right].$$

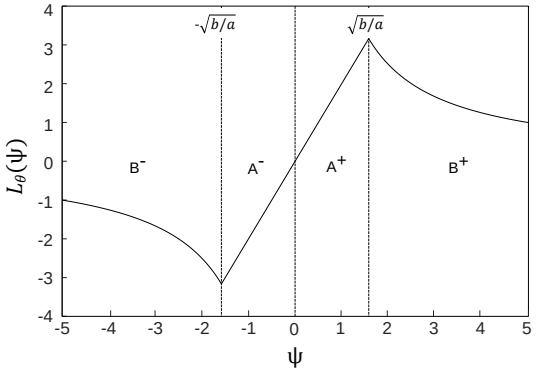

Figure 2.11: The four regions defined in the LLR under L_{ab}

The objective in (2.9) can therefore be written as

$$\widehat{\mathbb{H}}_n(\theta, \{\tilde{\Psi}_i\}_{i=1}^n) = \sum_{i:\tilde{\Psi}_i \in B^- \cup B^+} \log_2(1 + e^{-\frac{b}{\tilde{\Psi}_i}}) + \sum_{i:\tilde{\Psi}_i \in A^- \cup A^+} \log_2(1 + e^{-a\tilde{\Psi}_i}). \tag{2.11}$$

Observe that when $\tilde{\Psi}_i$ is in A^+ or B^+, the exponent inside the logarithm is negative. On the other hand, when $\tilde{\Psi}_i$ is in A^- or B^-, the exponent is positive. As a consequence, samples $\tilde{\Psi}_i$ in B^+ tend to increase the optimized values of b, while samples in B^- tend to decrease the optimized values of b. A similar observation also holds for the a parameter. As a consequence, if only a small number of samples falls in any of these regions, the resulting LLR approximation in (2.4) may be poor.

It is therefore important to understand for which regions the GAD algorithm produces very few samples. Recall that the noise sample estimates are obtained via $\tilde{Z}_i = Y_i - \text{sign}(Y_i)$ with $\tilde{Y}_i = 1 + \tilde{Z}_i$ and $\tilde{X}_i = 1$. As a consequence, $\tilde{\Psi}_i = \tilde{X}_i\tilde{Y}_i < 0$ when $Y_i < -2$. Hence, samples $\tilde{\Psi}_i \in A^+ \cup B^+$ will occur with very high probability. However, samples $\tilde{\Psi}_i \in A^- \cup B^-$ will occur more rarely. While this is less problematic for long packets, it greatly impacts the estimation of L_θ for short packets. In particular:

1. No samples $\tilde{\Psi}_i$ in B^- results in $b^* \to \infty$ and consequently the threshold $\sqrt{b/a}$ tends to infinity. This is not problematic for Gaussian noise where the optimal receiver is linear (i.e., $b^* = \infty$), but causes a problem if the noise is impulsive.

2. No samples $\tilde{\Psi}_i$ in A^- results in $a^* \to \infty$, leading to $\sqrt{b/a} \to 0$. The LLR approximation

around $\tilde{\Psi}_i \approx 0$ is therefore poor. As a consequence, an error floor can occur for small values of γ.

Due to the importance of obtaining samples $\tilde{\Psi}_i$ in $A^- \cup B^-$, it is desirable for the LLR parameter estimation to yield samples in these regions. To quantify the probability such samples do indeed arise, we introduced in [C15] the notion of degeneration risk.

Proposition 2.4.1. *[C15] The degeneration risk of the GAD and USD is the probability that the sequence Ψ_i or $\tilde{\Psi}_i$, $i = 1, \ldots, n$ respectively has only positive elements. That is,*

$$\eta_n^{GAD} = \mathbb{P}(\Psi_i > 0,\ \forall i \in \{1, \ldots, n\}) \text{ and } \eta_n^{USD} = \mathbb{P}(\tilde{\Psi}_i > 0,\ \forall i \in \{1, \ldots, n\}). \tag{2.12}$$

The later are given as

$$\eta_n^{GAD} = \left[1 - Q_\alpha\left(\frac{1}{\gamma}\right)\right]^n \text{ and } \eta_n^{USD} = \left[1 - \frac{1}{2}Q_\alpha\left(\frac{3}{\gamma}\right) - \frac{1}{2}Q_\alpha\left(\frac{1}{\gamma}\right)\right]^n, \tag{2.13}$$

where $Q_\alpha(x) = \int_x^{+\infty} g_\alpha(u; 1)\, \mathrm{d}u$, with $g_\alpha(\cdot; 1)$ denoting the probability density function of a standard $S\alpha S$ random variable.

Figure 2.12 compares the degeneration risk for the GAD and USD as a function of the noise scale parameter γ for $n = 1$ and $\alpha = (1.4; 1.8)$. Observe that there is a significant increase in the degeneration risk for the USD, which suggests that the lack of samples $\tilde{\Psi}_i \in A^- \cup B^-$ may be a key factor leading to performance losses when packets are short.

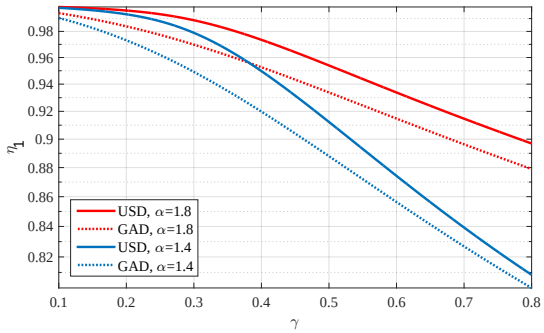

Figure 2.12: Degeneration risk

2.4.2 New unsupervised LLR approximation

Motivated by the aforementioned observations, we proposed in [C15] a new unsupervised LLR estimation (NUSD). In particular, we introduced two techniques to reduce the degeneration risk: a regularization term to limit the growth of a; and an improved sampling method to obtain a better estimate of b.

Estimation of a Our first goal is to improve the estimation of the parameter a when no samples $\tilde{\Psi}_i$ lie in A^-, which leads to a very large value of a^*. To avoid this problem, we incorporated the effect of a small negative sample into the objective in (2.9), now given as

$$\widetilde{\widehat{\mathbb{H}}}_n(\theta, \{\tilde{\Psi}_i\}_{i=1}^n) = \widehat{\mathbb{H}}_n(\theta, \{\tilde{\Psi}_i\}_{i=1}^n) + \log_2(1 + e^{a\epsilon}).$$

Estimation of b The optimization parameter b impacts the way large amplitude samples are treated. Improving its convergence is trickier than improving the one of parameter a, since under Gaussian noise, the optimal value is $b^* = \infty$ leading to a fully linear receiver; whereas under $S\alpha S$ noise with $\alpha < 2$, a too large value of b can lead to a poorly estimated LLR. Hence, adding a regularization term in the objective function is not efficient as it would cause severe performance loss under Gaussian noise. Instead, we propose to increase the spread in the extracted noise sequence, which in turn increases the spread in $\underline{\widetilde{Y}}$ and, as a consequence, reduces the degeneration risk. The proposed solution is described in Algorithm 1.

First, we double the learning sequence length by concatenating the extracted noise $\underline{\widetilde{Z}}$ with its opposite version $(-\underline{\widetilde{Z}})$, yielding a symmetric sequence $\underline{\widetilde{\mathbb{Z}}}$ which length c is twice the one of the original noise sequence N, i.e. $c = 2N$. Then we generate the training sequence $\underline{\widetilde{\Psi}} = \underline{\widetilde{Y}}$ of length c. Since poor LLR approximation arises when the region B^- is empty, we ensure to populate this region by creating a negative sample when $\widetilde{\mathbb{Z}}_i > 1$. Indeed, in order for a sample to belong to B^-, the noise sample must be of opposite sign than $\widetilde{X}_i = 1$ and such that $|\widetilde{\mathbb{Z}}_i| \geq \sqrt{b/a} + 1$.

Algorithm 1 Generating the training sequence $\underline{\widetilde{\Psi}}$

Compute $\underline{\widetilde{Z}} = \underline{Y} - \text{sign}(\underline{Y})$.
Concatenate $\underline{\widetilde{Z}}$ and $-\underline{\widetilde{Z}}$ into $\underline{\widetilde{\mathbb{Z}}}$.
for i=1 to c **do**
  if $\widetilde{\mathbb{Z}}_i \geq 1$ **then**
    $\widetilde{\Psi}_i = 1 - \widetilde{\mathbb{Z}}_i$.
  else
    $\widetilde{\Psi}_i = 1 + \widetilde{\mathbb{Z}}_i$.
  end if
end for

2.4.3 Numerical simulations

Figure 2.13(a) plots the frame error rate (FER) as a function of γ for a $S\alpha S$ noise with $\alpha = 1.8$ for a regular $(3, 6)$ LDPC code of size $N = 408$. The curve labeled 'Optimal' is achieved with the true numerically computed LLRs, whereas the one labeled 'USD' is achieved with the previously proposed unsupervised LLR approximation of [J3], [C7]. Since GAD almost achieves the FER obtained with the true LLRs, the performance loss of the USD is solely due to the unsupervised optimization and not to the LLR approximation itself.

The FER curve obtained with our proposed training sequence design and the adding of the regularization term with $\epsilon = 0.1$ is also provided in Figure 2.13(a) under the label 'NUSD'. First, observe that the FER achieved by the NUSD is monotonic and does not exhibit any bump as the one obtained under the USD of [J3], which appears to be due to the lack of samples $\tilde{\Psi}_i$ lying in A^-. Furthermore, the performance of NUSD is close to that of GAD. Hence, our proposed method improves the performance of LLR parameter estimation for short packets without requiring the noise model knowledge at the receiver.

The 'UB saddlepoint' curve in Figure 2.13(b) is an achievable FER. This bound follows from an upper-bound based on the dependence testing bound [29, Theorem 17], which is

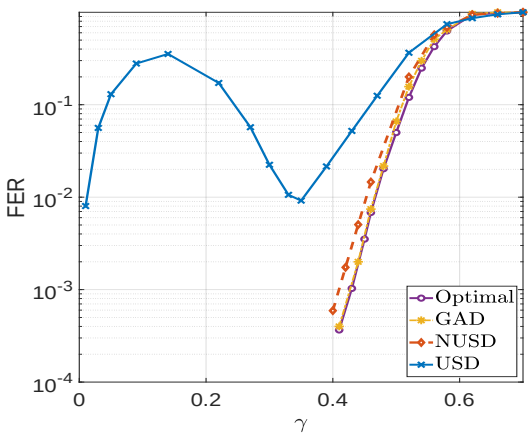

(a) FER comparison obtained with the supervised genie-aided, the unsupervised and the new unsupervised estimation to the one obtained with the true LLRs

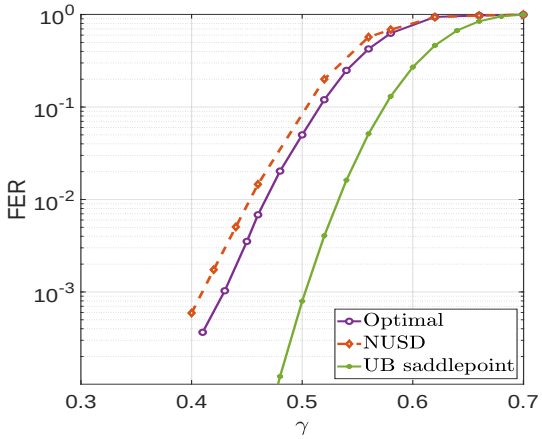

(b) FER comparison obtained with the true LLR, the new unsupervised estimation and the upper bound of the dependence testing bound

Figure 2.13: FER comparison under a $S\alpha S$ noise of parameter $\alpha = 1.8$ for the regular (3,6) LDPC code with $N = 408$

computed using the recently proposed method of [30, Theorem 5]. Since the FER achieved by our NUSD (and indeed the 'Optimal' decoder with perfect knowledge of LLR parameters) and the one achieved by the saddlepoint technique do not match, we can conclude that there is still room for efficient LDPC code design under impulsive noise and short blocklength.

2.5 Conclusions and perspectives

In this chapter, we proposed a receiver design that can adapt to various noise models, ranging from Gaussian ones to impulsive ones by approximating by a parametric function the LLRs fed to the BP decoder. The estimation parameters are tuned by minimizing an approximated conditional entropy. We further proposed an unsupervised estimation to avoid the use of a learning sequence that, as shown by the numerical simulations needs to be long enough to obtain good performance. We further studied the robustness of our proposed unsupervised estimation in the short blocklength regime. Whereas adding an extracted noise sequence to the all-zero codeword performed well in the asymptotic regime, the later exhibits severe performance loss in the short blocklength regime. As such we proposed a new design for the simulated transmission required by our unsupervised approach and added a regularization term in the considered optimization problem. These two mechanisms allowed to perform close to a genie-aided decoder in a wide range of noise types.

Nonetheless, a non-negligible gap remains between our proposed approach and a theoretical achievable error rate, showing that there is still room for LDPC code design under impulsive noise. LDPC codes can be optimized by the mean of differential evolution and density evolution, the later requiring the pdf of the received LLR. Whereas this pdf is given in closed-form and hence easy to implement under Gaussian noise, it is not the case in impulsive noise. The almost vanishing gap between the results obtained with the true numerically

computed LLR and with our proposed approximated ones could hence be used to provide the pdf of the estimated LLRs as the input of the density evolution step, allowing to design better performing codes in impulsive noise than the ones designed for Gaussian ones.

The next part will focus on resource allocation for cooperative multi-user communications.

Part II

Resource allocation for cooperative multi-user communications

Chapter 3

Preliminaries

The ever increasing number of communicating devices, along with the enormous growth of bandwidth-hungry and high speed applications are challenging the existing wireless networks and driving the transition to future generations of mobile networks. Future communications target highly ambitious objectives, among which, a 1000 times increase in network capacity and throughput, an explosion of the number of users and devices, as well as a large number of use cases while saving 90% of energy [31], [32]. In order to reach these goals, various candidate technologies are envisioned, such as Non-Orthogonal Multiple Access (NOMA), ambient backscattering, cognitive radio, cooperative or full-duplex communications, that each focus on specific targets. Further, the resulting network optimization problems are complex and usually non-convex, as such their solution requires tools beyond classical optimization, like data-driven tools, deep networks and machine learning techniques, emerging as promising and necessary for the design of future networks.

This chapter first presents the technologies considered in this HDR manuscript, namely NOMA, ambient backscattering, full-duplex cooperative communications and cognitive radio, and then briefly introduces the considered optimization metrics as well as the used machine learning tools.

3.1 Candidate technologies envisioned for future wireless networks

3.1.1 Power domain downlink NOMA

In previous generations of wireless systems, orthogonal multiple access (OMA) techniques, allowing several users to share the communication resources, were designed such that only one user was served on each resource block. While these techniques prevent any interference between users, they are limited by the number of available orthogonal resources and hence cannot efficiently deal with the ever increasing number of communicating devices and users. Recently, *Non-Orthogonal Multiple Access* (NOMA) has been proposed as a promising technique to support the expected massive connectivity of future wireless networks by superposing the messages of an arbitrary number of users on the same resource block [33]–[36],

where at the receiver side, the resulting interference is managed via successive interference cancellation (SIC) [37], [38].

Let us introduce the principle of power-domain NOMA by the considering a two users downlink transmission as a toy example. In such a case, each user $i \in \{1, 2\}$ is intended a message X_i such that $\mathbb{E}[X_i^2] = 1$. The transmitter, e.g. a base station (BS), employs superposition coding and broadcasts the message $X = \sqrt{p_1}X_1 + \sqrt{p_2}X_2$, where p_i denotes the power allocated to user i that is constrained by the BS available power budget as $p_1 + p_2 \leq \overline{P}$.

At the receiver side, each user receives the signal $Y_i = h_i X + Z_i$, where the additive noise $Z_i, i \in \{1, 2\}$ follows a Gaussian distribution $Z_i \sim \mathcal{N}(0, 1)$. Let us without loss of generality assume that the channel gains are ordered as $h_1^2 \geq h_2^2$. Each user then recovers its intended message by applying SIC based on the ordering of the channel gains: it decodes the messages of users with weaker channel gains to cancel out their interference but suffers the interference of users with better channel gains. In our considered toy example, the strongest user, here user 1, first decodes the message X_2 intended to user 2, cancels it out from its received signal and finally decodes its message X_1; whereas the weakest user, here user 2, directly decodes its message X_2 by treating the message intended to user 1 as additional noise, as depicted in Figure 3.1.

Note that under NOMA, more power is usually allocated to users with poor channel links to ensure some minimum Quality of Service (QoS) at each user or to to enhance user fairness, which in our toy example would result in $p_2 \geq p_1$.

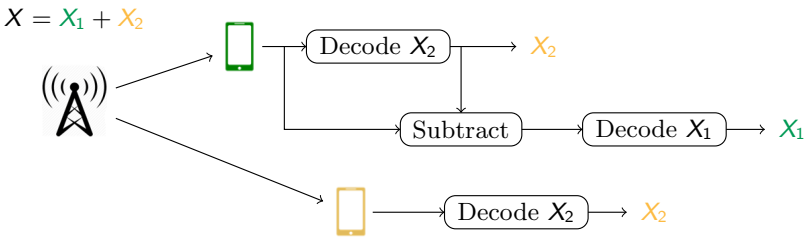

Figure 3.1: Principle of power-domain downlink NOMA

From an information point of view, NOMA is a special case of superposition coding and SIC over the degraded broadcast channel, in which the strong and weak users are considered as least and most degraded respectively, i.e. $\mathbb{I}(X_2; Y_2) \leq \mathbb{I}(X_2; Y_1)$. As such, its capacity region is known [39], [40].

Building on our example, the capacity region of the considered 2 users downlink NOMA setup is given as

$$R_1 \leq \mathbb{I}(X_1; Y_1 | X_2) \qquad \text{decoding of } X_1 \text{ knowing } X_2 \text{ at user 1} \tag{3.1}$$

$$R_{2\to1} \leq \mathbb{I}(X_2; Y_1) \qquad \text{decoding of } X_2 \text{ at user 1} \tag{3.2}$$

$$R_{2\to2} \leq \mathbb{I}(X_2; Y_2) \qquad \text{decoding of } X_2 \text{ at user 2,} \tag{3.3}$$

where R_1 denotes the data rate of the message X_1 and $R_{2\to i}, i \in \{1, 2\}$ denotes the required data rate when decoding the message X_2 at user i. Since the message X_2 is decoded at both users, the achievable data rate of the message X_2 must satisfy $R_2 \leq \min\{\mathbb{I}(X_2; Y_1), \mathbb{I}(X_2; Y_2)\}$.

However, since the channel is degraded, R_2 reduces to $R_2 \leq \mathbb{I}(X_2; Y_2)$ and the capacity region writes as

$$R_1 \leq \mathbb{I}(X_1; Y_1|X_2),\ R_2 \leq \mathbb{I}(X_2; Y_2), \tag{3.4}$$

leading to the following capacity region in the Gaussian case:

$$R_1 \leq C\left(h_1^2 p_1\right),\ R_2 \leq C\left(\frac{h_2^2 p_2}{h_2^2 p_1 + 1}\right),$$

where $C(x) = \frac{1}{2}\log_2(1+x)$ denotes the capacity of the point-to-point additive white Gaussian noise (AWGN) channel.

3.1.2 Ambient backscattering

Recently, *ambient backscatter communications* (AmBC) has emerged as a very promising low-energy technology [41], [42] able to transmit data in a passive way by recycling radio frequency (RF) waves in the vicinity of the backscatter device while harvesting energy. As such, backscatter devices do not require local oscillators to generate carrier frequencies, and hence, consume much less power than conventional devices [43], [44]. In its simplest implementation, the backscatter device, consisting of a dipole antenna being in either a short or open circuit, switches between two states: a backscattering one, in which the ambient signal coming from a RF source is reflected; and a transparent one, in which no signal is reflected. These two states encode its own binary message that can be decoded via a simple energy detector [41], [45], [46]. The principle of ambient backscatter communications is depicted in Figure 3.2.

More formally, let h denote the channel between the RF source and the backscatter device and X the message sent by the RF source. The signal sent by the backscatter device is given as

$$X_b = \sqrt{\rho} h X B, \tag{3.5}$$

where ρ denotes the reflection coefficient of the backscatter device, representing the percentage of the backscattered signal, and B denotes the backscatter device binary message. The other portion $(1-\rho)$ of the signal is used for energy harvesting. The binary message B is encoded by modulating the amplitude of the received RF signal with two distinct scattering states: the backscattering one, in which $B = 1$; and the transparent one, in which $B = 0$. Note that, in the transparent state where $B = 0$, the backscatter device does not reflect the ambient signal, which is hence fully harvested for energy.

3.1.3 Full-duplex cooperative communications

Traditionally, mobile networks rely either on frequency or time division duplexing, requiring thus two separate modes in order to achieve an orthogonal reception and transmission. This leads to a waste of half of the available resources. To counter this waste, *full-duplexing* is an emerging technology that enables full-duplex nodes to transmit and receive data simultane-

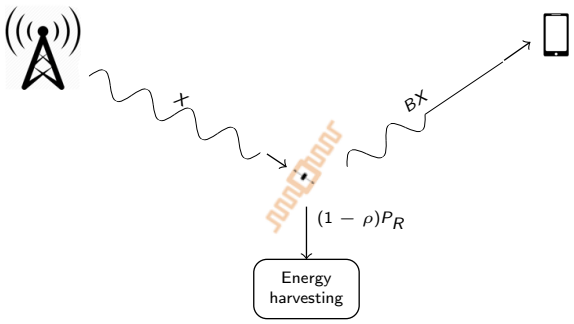

Figure 3.2: Ambient backscatter communication

ously in the same frequency band and to double the spectral efficiency [47]. In the remaining, we assume that the full-duplex operating node can perfectly cancel out any self-interference. Even if the assumption of perfect self-interference cancellation may not be realistic in practical settings, it allows us to simplify the expressions of the achievable rates, and hence the considered optimization problems, leading to low-complexity optimal power allocation policies. In order to provide insights or closed-form expressions of the outage probabilities when the relay cannot perfectly cancel the self-interference, other assumptions such as: a high signal-to-noise regime, an interference-limited environment, or neglecting some links in the network, etc. are necessary [48]–[52].

Cooperative communications aim at increasing the network capacity and throughput by taking advantage of the wireless medium, which allows any node within range to access and potentially relay the transmitted message, enhancing thus the communication between the source and its destination. The easiest model of such a cooperative communication is the well-known relay channel composed of three nodes: a source, its associated destination and an extra helping node, called relay [53], as depicted in Figure 3.3. The relay does not have any message on its own to transmit but assists the transmission between the source and the destination.

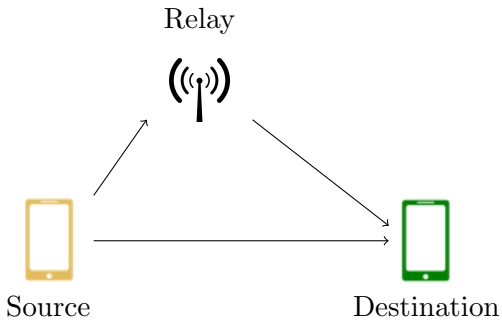

Figure 3.3: Relay channel

Three main relaying schemes have been proposed in the literature: Amplify-and-Forward (AF), where the relay amplifies its observed signal [54]; Decode-and-Forward (DF), where the relay decodes the sent message; and Compress-and-Forward (CF), where the relay quantizes the received signal [55].

None of the above is optimal in all settings; nevertheless, they have been shown to perform

well over various extensions of the basic relay channel [53], such as the two-way relay channel [56], the diamond relay channel [C6], the multiway relay channel [C3], [C4], [J1], and the interference relay channel [57], [58]. Moreover, DF usually performs well when the relay is close to the source, whereas CF performs well when the user is close the destination. AF, on the other side, is easy to implement but is usually outperformed by CF and DF.

Ambient backscattering communication vs. AF At a first glance, AmBC seems to operate similarly to AF relaying. Indeed, under AF, the relay receives the signal $Y = hX + Z$, where X is the message sent by the source, h is the channel between the source and the relay and Z is the AWGN at the relay; which is then amplified by a factor G before forwarding

$$X_R = G(hX + Z). \tag{3.6}$$

The amplification gain G, which depends on the power budget at the relay, seems hence to play a similar role as the reflection coefficient ρ of the ambient backscatter device.

Nonetheless, there are major differences between the two technologies:
i) AmBC are more efficient in terms of energy and in hardware complexity since relays require dedicated power source and active electronic components [59], leading to an increase of the cost and the power consumption in the system;
ii) thanks to the absence of active components in AmBC, no noise is reflected at the receiver side as shown in (3.5), as opposed to AF as shown in (3.6);
iii) the relay only improves the communication between one source and its destination without sending any message of its own; whereas the ambient backscatter device exploits the signal sent by the source to send its own information.

3.1.4 Cognitive radio

Cognitive radio is another candidate technology to tackle the spectrum scarcity by allowing an opportunistic access to underutilized licensed bands. Three paradigms of cognitive radio can be found in the literature: interweave, overlay and underlay [60], [61]. On the one hand, under the interweave mode, secondary transmission is only allowed over non-occupied primary frequency bands, requiring hence spectrum sensing. On the other hand, under both overlay and underlay mode, the secondary and the primary transmissions coexist: in the overlay mode, the secondary users cooperate with the primary ones to enhance the primary transmissions and hence be granted access, whereas in the underlay mode, the secondary transmissions are allowed provided that the primary transmissions are not degraded below a given threshold [47], [62]. In the following, underlay cognitive radio will be considered.

3.2 Resource allocation in wireless communications networks

3.2.1 Performance metrics

The exponential growth of the number of connected devices, alongside with the development of high speed applications, raises serious sustainability concerns. On the one hand, ever

increasing network throughput is required but on the other hand, the power consumption must be reduced: trading off between these two aspects becomes hence ineluctable for future wireless networks.

In the remaining of this manuscript, we will focus on two different performance metrics trading off between maximizing the network throughput and limiting the power consumption for two distinct considered networks:
i) ***Opportunistic rate maximization*** in the context of cooperative cognitive radio, where the opportunistic user and the relay powers need to be kept as low as possible to protect the primary transmission and as large as possible to enhance the opportunistic data rate. The resulting optimization problems, detailed in Chapter 5, which are not convex, are solved by the use of deep learning that is briefly presented later on in Section 3.2.3.
ii) ***Energy efficiency maximization*** defined as either the tradeoff between the achievable sum rate vs. power consumption or the ratio of the two in the context of multi-user downlink NOMA transmission enhanced by the presence of a backscatter device in static or dynamic environments. The resulting optimization problems, detailed in Chapter 4, are not convex but are either solved by introducing some relaxation leading to convex optimization problems solved via the Karush-Kuhn-Tucker (KKT) conditions, or by turning to online learning, which will be briefly explained in Section 3.2.2.

Before presenting the machine learning tools used in our studies, let us present the two energy efficiency metrics defined as either the tradeoff or the ratio of the sum rate vs. power consumption.

Sum rate vs. power consumption tradeoff Energy efficiency, which captures the tradeoff between the sum rate and the power consumption of a system, can be formulated as a bi-criterion optimization problem [63], [64], in which the objectives are the sum rate R_{sum} on the one hand and the negative overall power consumption on the other hand:

$$\max_{x\in\mathcal{X}} \left(R_{\text{sum}}(x); -P_{\text{sum}}(x) - P_c\right) \tag{3.7}$$

where x denotes the optimization variables, for instance the power allocation policy, $\mathcal{X}$ is the feasible set and P_{sum} and P_c are respectively the total transmit power and the circuit power consumption taking into account the power dissipated in all transmitter and receivers circuit blocks. The two above objectives are obviously contradictory: maximizing the sum rate requires the transmission to take place at full power, which is not energy-efficient; whereas no transmission should take place to minimize the power consumption, which is neither rate- nor QoS-efficient. Solving such a bi-criterion optimization problem requires to find the Pareto-boundary of the feasible set, which contains all feasible rate-power pairs that cannot be improved in both objectives simultaneously while remaining in the feasible set. If both objectives are convex, and if the feasible set $\mathcal{X}$ is convex, finding the Pareto boundary reduces

to maximize a weighted sum of the two contradictory objectives [65] given as

$$\max_{x\in\mathcal{X}} R_{\text{sum}}(x) - \alpha(P_{\text{sum}}(x) + P_c), \tag{3.8}$$

where $\alpha \geq 0$ is the parameter that trades off between the sum rate and the power consumption: Setting large values of α turns the optimization problem into a power-consumption driven one; whereas choosing small values of α turns the optimization problem into a rate-driven one.

Sum rate vs. power consumption ratio Let us now consider another popular energy efficiency metric defined as the ratio between the sum rate and the overall power consumption $\xi_{EE}(x) = \frac{R_{sum}(x)}{P_{sum}(x)+P_c}$ [63], [64], [66], whose solution lies on the Pareto boundary of the bi-criterion optimization problem (3.7) [67].

Assuming that the sum rate is concave and since the overall power consumption is affine, the maximization of the ratio ξ_{EE} is a concave-convex fractional problem whose solution is equivalent to find the unique zero of the scalarized trade-off between the sum-rate and the total power consumption of (3.8) with respect to α [66], which can be obtained with Dinkelbach's iterative algorithm [66], [68], [69] given in Algorithm 2.

Algorithm 2 Dinkelbach's algorithm

1: Initialize $\epsilon > 0$, $n = 0$, $\alpha_0 = 0$
2: **repeat**
3: Compute $x_n^* = \arg\max_{x\in\mathcal{X}} R_{sum}(x) - \alpha_n(P_{sum}(x) + P_c)$
4: Update $F(\alpha_n) = R_{sum}(x_n^*) - \alpha_n(P_{sum}(x_n^*) + P_c)$
5: Update $\alpha_{n+1} \leftarrow \frac{R_{sum}(x_n^*)}{P_{sum}(x_n^*)+P_c}$
6: $n \leftarrow n + 1$
7: **until** $F(\alpha_n) \leq \epsilon$

3.2.2 Online learning

Reinforcement learning is a branch of machine learning that learns through trial and error by receiving a positive or negative feedback from the environment for taking certain decisions or actions [70].

Later on in Chapter 4, we exploit the so-called Multi-Armed Bandits (MAB) framework, a class of reinforcement learning. At each iteration t of a repeated decision process, an agent or decision maker selects an arm or action $a^{(t)}$ among a given and known set of actions $\mathcal{A}$ and receives the corresponding reward $u^{(t)}(a^{(t)})$ generated by the environment. Given this reward, the agent chooses the next action or arm, the goal being to maximize the expected reward which is unknown. As such, the agent faces an exploration-exploitation tradeoff: On the one hand, exploring more arms allows the agent to obtain more information about actions that have no been played so far, leading to possible better choices in the future; but on the other hand, by doing so, the agent fails to exploit arms which have already lead to good payoff [71].

Regret as a performance metric: The performance of a MAB algorithm is usually measured in terms of pseudo-regret [72] defined as

$$\mathbb{E}[\mathrm{Reg}_T] = \mu^* - \frac{1}{T}\sum_{t=1}^{T}\mathbb{E}[u^{(t)}(a^{(t)})], \tag{3.9}$$

where μ^* represents the maximal expected reward given as $\mu^* = \max_{a\in\mathcal{A}}\mu(a)$, with $\mu(a) = \mathbb{E}[u^{(t)}(a)]$ being the unknown expected reward of an arbitrary action $a \in \mathcal{A}$. In other words, the pseudo-regret measures the gap between the agent's online policy $a^{(t)}, \forall t \in \{1, ..., T\}$ and the best fixed action that maximizes the expected reward over the given horizon of play $a^* = \arg\max_{a\in\mathcal{A}}\mu(a)$.

The figure of merit of an online optimization problem, and hence of MABs, is to design an online policy that achieves no regret, i.e. is such that $\limsup_{T\to\infty}\mathrm{Reg}_T \leq 0$. Intuitively, the later means that the designed online policy needs to perform at least as good as the fixed policy which maximizes the expected reward when the time horizon T grows large. Further, among all policies exhibiting the no-regret property, one should also choose the one with the best possible regret decay rate, which of course is not straightforward since unknown and arbitrary variations in the environment lead to a reward function not known in advance [71].

Below, we briefly provide an overview of two of the most popular no-regret MAB algorithms, namely UCB and EXP3. The former is based on a deterministic arm selection update rule, whereas in the latter, the next arm to be selected is drawn from a random iteratively updated probability distribution.

Upper Confidence Bound (UCB): UCB is a deterministic no-regret algorithm designed specifically for stochastic environments. Its pseudo-regret decay rate is optimal in the sense that it achieves the best possible one, i.e. $\mathbb{E}[\mathrm{Reg}_T] = \mathcal{O}(\log T/T)$ [73], where the expectation is taken over the stochastic environment [72]. Its deterministic updating rule is given as

$$a^{(t+1)} = \arg\max_{a\in\mathcal{A}}\left(\hat{\mu}_a^{(t)} + \sqrt{\frac{\delta\log t}{2n_a^{(t)}}}\right), \tag{3.10}$$

where $n_a^{(t)}$ is the number of times arm a has been played so far, $\hat{\mu}_a^{(t)}$ denotes the empirical mean reward of arm a up to time t and δ is the learning parameter that trades off between data exploitation and exploration. Intuitively, the first term of the updating rule tends to exploit the arm with the highest empirical mean, whereas the second term allows to explore arms that have not be played much so far, especially in the first iterations of the algorithm.

Having a deterministic updating rule, UCB can easily be brought to a fault when the environment is adversarial. Hence, other updating rules such as EXP3, based on random arm selection drawn from some given probability, have been proposed.

Exponential weights for exploration and exploitation (EXP3): EXP3 is a random no-regret algorithm designed for more general environments going beyond the stochastic case, e.g. adversarial one [74]. Its pseudo-regret decay rate is such that $\mathbb{E}[\mathrm{Reg}_T] = \mathcal{O}(1/\sqrt{T})$, hence

slower than the one of UCB, but having the advantage of accounting for arbitrary dynamics that may even be adversary (some simulations in adversarial environments were presented in [J5]). The expectation in the regret decay rate is here taken with respect to the randomness within the EXP3 algorithm and any randomization employed by the adversary.

Under EXP3, the arm $a^{(t+1)} \in \mathcal{A}$ is randomly drawn following the updated probability distribution

$$q^{(t+1)}(a) = \frac{q^{(t)}(a)\exp(\eta\ \hat{u}^{(t)}(a))}{\sum_{b=1}^{|\mathcal{A}|} q^{(t)}(b)\exp(\eta\ \hat{u}^{(t)}(b))}, \forall a \in \mathcal{A}, \tag{3.11}$$

where $\hat{u}^{(t)}(b) = u^{(t)}(a^{(t)})\mathbb{1}[b = a^{(t)}]/q^{(t)}(b)$ is the estimated reward of arm b and η is the learning parameter. In the above, $\mathbb{1}[x]$ denotes the indicator function which equals 1 when x is true and 0 otherwise.

3.2.3 Deep learning

Deep learning is a branch of machine learning field that exploits deep neural networks (DNNs) composed of multiple hidden layers to predict an output from relevant training data [75]. Whereas deep learning has already been widely used in many fields, such as image processing, computer vision, language processing, etc., its use in wireless communication networks is rather new. Indeed, up to very recently, various mathematical models were available in the field of wireless communications, making the use of data-driven approaches not necessary [76]. Nonetheless, future wireless networks are expected to be very heterogeneous and dense ones, as such the lack of explicit mathematical models could be compensated by the use of data-driven approaches, the most promising one being deep learning. As such, deep learning techniques have been widely considered to solve non-convex and complex optimization problems, thanks to their universal approximation capability, i.e. their ability to learn any input-output relationship when properly trained [76].

Deep learning can be performed either in a supervised or unsupervised manner. Under the supervised approach, the DNN is trained with the help of labeled data to either classify them into some given categories or to predict a continuous outcome. In this case, each training sample is composed of both the input and its associated ground-truth label or variable to be predicted. During the training process, the DNN identifies relationships between the input and the corresponding desired output to then generalize over new unseen data for which of course no labels are provided. On the other hand, under the unsupervised approach, the DNN is trained with only raw data without any associated ground-truth output. The DNN hence identifies patterns and relationships based only on the inputs.

In the remaining of this section, we briefly present some DNN-based works related to resource allocation in cooperative cognitive relay networks, the framework under study in Chapter 5.

In the context of cognitive radio networks, various resource allocation problems have been tackled via deep learning [77]–[80]. In [77], the authors have proposed a deep learning approach for resource allocation problems in cognitive radio networks maximizing the spectrum and energy efficiency. Further, the opportunistic spectral efficiency of such a system was

maximized using DNN-based techniques while regulating the interference caused to the primary user, either in a centralized [79], or in a distributed manner [80]. In [78], a DNN is used to determine the power allocation over multiple channels of the opportunistic users.

On the other hand, regarding cooperative communications, various optimization problems, such as maximizing the energy efficiency, selecting the best relay within a set of candidates as well as selecting the best relaying scheme to be performed, can also be solved via deep learning. In [81], the authors studied the power allocation and relay selection problem maximizing the energy efficiency of an AF relay channel with the help of a DNN. Many works can be found regarding DNN-based relay selection, in which one searches for the best relay node among multiple relay candidates [82]–[84], as well as on relaying scheme selection [85], [86], in which the relaying scheme yielding the best signal-to-noise ratio or the lowest outage were respectively selected in [85] and [86].

The following two chapters present some of our main results on resource allocation for cooperative multi-user networks.

More precisely, Chapter 4 focuses on energy-efficiency maximization in cooperative backscattering downlink NOMA networks under two extreme cases regarding the available channel state information (CSI), namely perfect CSI knowledge and no CSI at the transmitter side. Under perfect CSI, the optimal resource allocation policy is obtained in closed-form (up to a line search) thanks to some constraints relaxation leading to a convex optimization problem; whereas in the extreme case of no CSI, online learning is used to compensate the lack of CSI.

Chapter 5 then presents our results on opportunistic rate maximization in cooperative cognitive radio networks where we first assume that perfect CSI is available, leading to a closed-form solution under CF but already requires the use of deep learning techniques under DF as the non-linear operations performed at the relay render the optimization problem non-convex and hence difficult to solve. We then study the impact of imperfect CSI, leading to a deep learning based solution under both CF and DF, and finally extend our DNN-based solutions to jointly optimize the power allocation policy and select the best relaying scheme to be performed.

Chapter 4

Energy-efficient cooperative backscattering NOMA

In this chapter, we overview the most relevant contributions [J6], [C14] of the work performed by the PhD student Hajar El Hassani, whom I have co-advised (at 40%) jointly with E. Veronica Belmega (ETIS lab, 60%, official director).

Main contributions

Let us consider a multi-user downlink Non-Orthogonal Multiple Access (NOMA) system aided by an ambient backscatter device that modulates its own information by reflecting the incident signal coming from the NOMA transmitter. We propose a joint optimization framework for maximizing the system energy efficiency (EE) under user minimum rate constraints and perfect channel state information (CSI). We further investigate the robustness of our solution to imperfect CSI. We then move to the 2-users case with no CSI nor channel distribution information (CDI) when the basckscatter is only in the harvesting mode and propose an online learning method that is energy efficient and relies only on a 1-bit feedback.
Our main contributions are the following:

- Deriving the information-theoretic achievable rate region of a multi-user downlink NOMA system aided by an ambient backscatter device that reflects the signal coming from a source employing NOMA while sending its own binary information.
- Proposing a joint optimization framework to maximize the system EE given as the tradeoff and ratio between the overall sum rate and the power consumption. We jointly optimize the reflection coefficient and the power allocation under power budget, QoS, SIC decoding order and reflection coefficient constraints, which is not convex.
- Introducing a modification on the constraints enabling to decouple the problem which can then be solved analytically.
- Proposing an adaptive MAB-based NOMA scheme maximizing the EE for the 2-users case when no CSI nor CDI is available at the transmitter's side.

4.1 System model

Consider the ambient backscatter multiple access downlink NOMA communication system depicted in Figure 4.1. The later is composed of one transmitter or source (e.g., BS, femtocell,

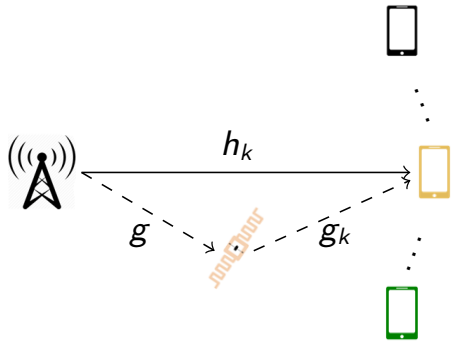

Figure 4.1: Multi-user downlink NOMA system aided by an ambient backscatter device

Wi-Fi hotspot, etc.), $K \geq 2$ receivers or users (e.g., mobile phones, IoT devices, etc.) and one ambient backscatter device. The source sends the message M_i encoded as X_i intended for each receiver $i \in \{1, \ldots, K\}$ with power p_i via superposition coding and broadcasts $X = \sum_{i=1}^{K} X_i$. We further denote by $\overline{P}$ the power budget of the BS, such that $\sum_i p_i \leq \overline{P}$. Also, each user k is required to meet a QoS constraint expressed in terms of a minimum achievable rate of $R_{\min,k}$. We moreover assume that the backscatter device sends a common binary information B to all receivers.

The received signal Y_k at user k is composed of the direct signal coming from the source and the backscattered signal, which is given by

$$Y_k = \underbrace{h_k X}_{\text{direct signal}} + \underbrace{\sqrt{\rho}\, g\, g_k B X}_{\text{backscattered signal}} + Z_k, \tag{4.1}$$

where h_k, g and g_k are the channel gains between the source and receiver k, the source and the backscatter device and the backscatter device and receiver k, respectively, $Z_k \sim \mathcal{N}(0, \sigma^2)$ is AWGN, and the parameter ρ is the reflection coefficient of the backscatter device.

Let us first assume that perfect CSI is available at the source and that without loss of generality, the channel gains $h_k,\ k \in \{1, \ldots, K\}$ are arranged in a decreasing order such that $\frac{h_k^2}{\sigma_k^2} \geq \frac{h_{k+1}^2}{\sigma_{k+1}^2}, \forall k$ [87], [88]. Following the superposition coding principle adopted in NOMA, each receiver i performs SIC [87], [89] by first decoding the messages $X_j,\ j \in \{K, K-1, \ldots, i+1\}$, while treating other messages $X_s,\ s \in \{i-1, \ldots, 1\}$ as noise, before decoding its own message X_i. Note that the source decides the SIC ordering only based on the direct link to the users without accounting for the backscattered link. Indeed, since the backscatter device is inherently opportunistic when sending its own message, the source has no control over its backscattering state.

Most of the existing works [90]–[97] consider either the simple backscattering state $B = 1$, or that the backscattered signal composed of the product BX follows a Gaussian distribution in order to approximate the achievable rate region with the help of Shannon's capacity function $C(\cdot)$. These assumptions may not be realistic in practice, since the backscatter device usually has its own information to transmit besides harvesting energy for its circuit operation and when both X and B are random variables, the received signal is no longer Gaussian.

As such, we first derive an achievable rate region by explicitly taking into account the message of the backscatter device, which clearly sets our work apart from the existing literature.

4.2 Achievable rate region

4.2.1 Discrete case

Let us start with the discrete memoryless channel case of the joint multiple access and broadcast communication system depicted in Figure 4.2, and then derive an achievable rate region for the Gaussian channel described in our predefined model.

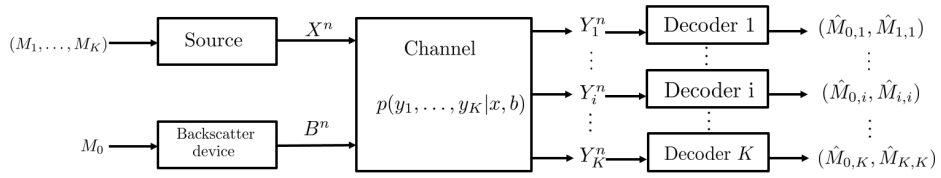

Figure 4.2: Source-backscatter device to K-receivers discrete channel model

Both the source and the backscatter device wish to send independent messages reliably to K receivers. The backscatter device encodes its common message M_0 into a codeword B^n and transmits it over the shared channel. The source uses a superposition coding technique to encode each private message M_i destined to receiver i in a layered manner and broadcasts the codeword X^n consisting of all merged encoded messages $M_1, \ldots, M_K$. Upon receiving the sequence Y_i^n, receiver $i \in \{1, \ldots, K\}$ computes an estimate $\hat{M}_{0\to i}$ of the message M_0 and uses SIC to obtain an estimate $\hat{M}_{i\to i}$ of the message M_i, by first computing the estimates $\hat{M}_{j\to i}$ of the messages M_j, for all $j \in \{K, K-1, \ldots i+1\}$ following this precise successive order.

Theorem 4.2.1. *[J6] An achievable rate region of the discrete memoryless source-backscatter device to K receivers channel is given by the set of rate tuples $(R_0, R_1, \ldots, R_K)$ defined below:*

$$R_0 \leq \min_{1\leq i\leq K} \mathbb{I}(B; Y_i|U_K), \tag{4.2}$$

$$R_K \leq \min_{1\leq i\leq K} \mathbb{I}(U_K; Y_i|B), \tag{4.3}$$

$$R_0 + R_K \leq \min_{1\leq i\leq K} \mathbb{I}(U_K, B; Y_i), \tag{4.4}$$

$$R_j \leq \min_{i\leq j} \mathbb{I}(U_j; Y_i|B, U_K, \ldots, U_{j+1}),\ \forall\ 1 \leq j \leq K-1, \tag{4.5}$$

where U_i are auxiliary randoms variables accounting for X_i for all $2 \leq i \leq K$.

Proof. The proof follows from standard information-theoretic techniques [39], [40]. Superposition coding, with auxiliary random variables $U_j,\ j \in \{2, \ldots, K\}$ serving as "cloud centers" representing the messages M_j that can be distinguished by receivers $i \leq j$, is used at the

source side. The achievable rates are then obtained by defining the error events of unsuccessful decoding of X and B and by using typicality arguments. The detailed proof can be found in [J6]. □

In practice, the data rate of the backscatter device is significantly lower than that of the source because of its design simplicity and power limitations as argued in [41], [43], [92], [98]–[101]. Assuming that $R_0 \ll R_K$ in particular, the expressions (4.3) and (4.4) in Theorem 4.2.1 reduce to

$$R_K \leq \min\left(\min_{1\leq i\leq K} \mathbb{I}(U_K;Y_i|B), \min_{1\leq i\leq K} \mathbb{I}(U_K,B;Y_i)\right) \overset{(a)}{=} \min_{1\leq i\leq K} \mathbb{I}(U_K;Y_i|B), \tag{4.6}$$

where (a) follows from the chain rule and the positivity of the mutual information. This yields the achievable rate region given in the following Lemma.

Lemma 4.2.1. *[J6] Assuming that the backscatter device has a very low data rate compared to that of the source, $R_0 \ll R_K$, the achievable rate region in Theorem. 4.2.1 simplifies to*

$$R_0 \leq \min_{1\leq i\leq K} \mathbb{I}(B;Y_i|U_K), \tag{4.7}$$

$$R_K \leq \min_{1\leq i\leq K} \mathbb{I}(U_K;Y_i|B), \tag{4.8}$$

$$R_j \leq \min_{i\leq j} \mathbb{I}(U_j;Y_i|B,U_K,\ldots,U_{j+1}),\ \forall\ 1\leq j\leq K-1. \tag{4.9}$$

4.2.2 Gaussian case

Let us now move to the AWGN case described in 4.1 and more specifically for the received signal Y_k given in (4.1).

The message of the backscatter device B follows the Bernoulli distribution $B \sim \text{Bern}(q)$, where $q = \mathbb{P}[B=1]$ is the probability of the backscattering state and $(1-q) = \mathbb{P}[B=0]$ is the probability of the transparent state. By assuming, as commonly used in the literature when describing the codeword $X = \sum_{k=i}^{K} X_i$ sent using NOMA, that $X_1 = V \sim \mathcal{N}(0,p_1)$ and $X_i = U_i \sim \mathcal{N}(0,p_i), \forall i \in \{2,\ldots,K\}$, we can compute an achievable rate region for the Gaussian case which is given in the following theorem.

Theorem 4.2.2. *[J6] An achievable rate region of the AWGN source-backscatter device to K-receiver channel is the set of rate tuples $(R_0,R_1,\ldots,R_K)$, such that*

$$R_0 \leq \min_{1\leq i\leq K} \mathbb{H}(Y_i|U_K) - \frac{q}{2}\log_2\left(2\pi e\sigma_i^2\left(H_{i|1}(\rho)\sum_{k=1}^{K-1}p_k+1\right)\right) - \frac{1-q}{2}\log_2\left(2\pi e\sigma_i^2\left(H_{i|0}\sum_{k=1}^{K-1}p_k+1\right)\right)$$

$$R_k \leq qC\left(\min_{i\leq k}(\gamma_{k\to i|1})\right) + (1-q)C\left(\min_{i\leq k}(\gamma_{k\to i|0})\right),\ \forall\ 1\leq k\leq K,$$

where $H_{i|0} = h_i^2/\sigma_i^2$, $H_{i|1}(\rho) = (h_i+\sqrt{\rho}gg_i)^2/\sigma_i^2$ represent the channel gains when the backscatter device is in the transparent state ($B=0$) and in the backscattering state ($B=1$),

respectively, and $\gamma_{k\to i|0} = \frac{H_{i|0}p_k}{1+H_{i|0}(p_1+\ldots+p_{k-1})}$ *and* $\gamma_{k\to i|1} = \frac{H_{i|1}(\rho)p_k}{1+H_{i|1}(\rho)(p_1+\ldots+p_{k-1})}$ *are the corresponding signal-to-interference-plus-noise ratio (SINR) values when receiver* i *decodes the message intended for receiver* k*.*

Note that the expression of R_0 cannot be obtained in closed form because the term $\mathbb{H}(Y_i|U_K)$ is very difficult to compute due to the non trivial sum of two independent variables X and BX in the received signal Y_k, where $B \sim \text{Bern(p)}$ and $X \sim \mathcal{N}(0, \sum_{i=1}^{K} p_i)$, which is left open for future investigation. Also, the achievable rate of receiver k can be seen as an expected value of the Shannon capacity over the message $B \in \{0, 1\}$ (i.e., the ergodic rate over the fading channel $h_k + \sqrt{\rho} g g_k B$).

Let us now investigate the system energy-efficiency maximization defined as the tradeoff between the sum of the achievable data rates and the consumed power. Since by assumption we have $R_0 \ll R_K$ and knowing that the backscatter device is a low-power device which performs energy harvesting for its own circuit operations, we only focus on maximizing the energy efficiency (EE) of the downlink NOMA system (enhanced by ambient backscattering).

4.3 Resource allocation for energy-efficient NOMA in static environments

4.3.1 Optimization problem under study

The energy efficiency maximization problem under study writes as [63], [66]

$$(\mathbf{EE0}) \quad \max_{(\rho,\mathbf{p})\in\mathcal{P}} \sum_{k=1}^{K} R_k(\rho, \mathbf{p}) - \alpha \left(\sum_{k=1}^{K} p_k + P_c \right), \tag{4.10}$$

where $R_k(\rho, \mathbf{p})$ denotes the achievable rate of receiver k and follows from Theorem 4.2.2

$$R_k(\rho, \mathbf{p}) = qC\left(\min_{i\leq k}(\gamma_{k\to i|1}) \right) + (1-q)C\left(\min_{i\leq k}(\gamma_{k\to i|0}) \right), \ \forall\ 1 \leq k \leq K. \tag{4.11}$$

The set $\mathcal{P}$ contains all admissible reflection coefficients ρ and transmit power allocation policies $\mathbf{p} = (p_1, \ldots, p_K)$. This feasible set accounts for all the constraints: the maximum power budget of the source, the receivers targeted QoS, the successful SIC process expressed as $qC\left(\gamma_{k\to i|1}\right)+(1-q)C\left(\gamma_{k\to i|0}\right) \geq qC\left(\gamma_{k\to k|1}\right)+(1-q)C\left(\gamma_{k\to k|0}\right)$ to avoid error propagation when receiver i, $\forall i \leq k-1$, performs SIC and decodes the message destined to receiver k and the range of the reflection coefficient, respectively.

Special case $q = 0$**:** When $q = 0$, the optimization problem (**EE0**) is equivalent to the optimization problem solved in [C11], in which the system model was only composed by one BS and K users, served with downlink NOMA, for which we derived the optimal power allocation policy in closed form.

Special case $q = 1$**:** On the other hand, when $q = 1$, the optimization problem (**EE0**) is equivalent to the optimization problem solved in [C14], in which the system model was

composed by one BS, K users served with downlink NOMA and one backscatter which was always in the backscattering state with $B = 1$. The optimal power and reflection coefficient allocation policy was derived in closed form. The later was extended to the two-users multiple backscatter devices case, where the optimal power and reflection coefficient allocation policy was derived in closed form for the special case of 2 backscatter devices and numerically derived for more than 2 backscatter devices in [C20].

General case: Since SIC decoding is a key component for NOMA [87], [89], [102]–[105], it has to be performed successfully and independently from the backscatter device state (backscattering or transparent) in order to avoid error propagation that may affect the performance of the system (e.g., the targeted quality of service). To ensure successful SIC, we impose a minimum QoS constraint for each state of the backscatter device: $\gamma_{k\to i|1} \geq \gamma_{k\to k|1}$ and $\gamma_{k\to i|0} \geq \gamma_{k\to k|0}$, $\forall k \in \{1,\dots,K\}$ and $i \leq k$. All the above leads to the feasible set:

$$\mathcal{P} \triangleq \Bigg\{ (\rho,\mathbf{p}) \in [0,1]\times\mathbb{R}_+^K \;\Bigg|\; 0\leq\rho\leq 1, \sum_{j=1}^{K} p_j \leq \overline{P}, R_k(\rho,\mathbf{p}) \geq R_{\min,k}, \\ \gamma_{k\to i|0} \geq \gamma_{k\to k|0}, \gamma_{k\to i|1} \geq \gamma_{k\to k|1},\ \forall 1\leq k\leq K, \forall i\leq k \Big\}. \tag{4.12}$$

Note that the successful SIC decoding constraint in the transparent state $\gamma_{k\to i|0} \geq \gamma_{k\to k|0}$ is readily satisfied due to the assumed channels ordering. By ensuring that $\gamma_{k\to i|1} \geq \gamma_{k\to k|1}$ is met in the optimization problem (**EE0**), the achievable rate of receiver k in (4.11) reduces to

$$R_k(\rho,\mathbf{p}) = qC(\gamma_{k\to k|1}) + (1-q)C(\gamma_{k\to k|0}),\ \forall\ 1\leq k\leq K. \tag{4.13}$$

To simplify the presentation, we introduce the notations $\theta_k(\mathbf{p}) = \sum_{i=1}^{k} p_i$, $\forall 1 \leq k \leq K$ with $\theta_0(\mathbf{p}) = 0$ and $A_k = 2^{2R_{\min,k}}$. The optimization problem hence writes as

$$\begin{aligned}
(\mathbf{EE0}) \quad & \max_{\rho,\mathbf{p}} \sum_{k=1}^{K} R_k(\rho,\mathbf{p}) - \alpha(\theta_K(\mathbf{p}) + P_{\mathrm{c}}) \\
& \text{s.t. } \theta_K(\mathbf{p}) \leq \overline{P}, && (C1)\\
& \quad R_k(\rho,\mathbf{p}) \geq R_{\min,k}, \forall 1\leq k\leq K && (C2)\\
& \quad \gamma_{k\to i|1}(\rho,\mathbf{p}) \geq \gamma_{k\to k|1}(\rho,\mathbf{p}), \forall 2\leq k\leq K, \forall i\leq k-1 && (C3)\\
& \quad 0\leq\rho\leq 1. && (C4)
\end{aligned}$$

Unfortunately, (**EE0**) is not convex due to the joint optimization of the reflection coefficient and the vector of allocated powers $\mathbf{p}$ as well as to the constraint $(C2)$ in which the rate $R_k(\rho,\mathbf{p})$ is not concave w.r.t. $\mathbf{p}$.

To overcome this challenge, we introduce a modification to this constraint as follows: instead of having $R_k(\rho,\mathbf{p}) \geq R_{\min,k}$, we require each of the averaged terms in (4.13) to be bounded: $C(\gamma_{k\to k|0}) \geq R_{\min,k}$ and $C(\gamma_{k\to k|1}) \geq R_{\min,k}$. This means that the QoS constraint needs to be satisfied in the transparent state and in the backscattering state individually.

This modification restricts in fact the original feasible set, leading to a potential optimality loss in case the optimal solution of (**EE0**) lies outside of the restricted constraints. In our setting, we believe that any incurred optimality loss will be limited. This intuition, validated through numerical results in Section V, is based on the the fact that the rate of the backscatter device is much lower than that of the source in practice. This implies that the message of the backscatter remains fixed for a relatively long period of time from the source's perspective and, hence, imposing the minimum source rate constraint for each individual backscatter state is relevant.

By imposing the QoS constraints on each state separately, and after some mathematical manipulations, the constraint $(C2)$ can be expressed as

$$\theta_k(\mathbf{p}) \geq \ A_k\theta_{k-1}(\mathbf{p}) + \frac{A_k - 1}{H_{k|0}}, \quad \forall\ 2 \leq k \leq K, \forall i \leq k-1, \tag{4.14}$$

$$\theta_k(\mathbf{p}) \geq \ A_k\theta_{k-1}(\mathbf{p}) + \frac{A_k - 1}{H_{k|1}(\rho)}, \quad \forall\ 2 \leq k \leq K, \forall i \leq k-1, \tag{4.15}$$

where $A_k = 2^{2R_{\min,k}}$. The main advantage of this modification is that it leads to the following simpler non-convex optimization problem, which we show can be solved analytically.

$$\begin{aligned}
(\mathbf{EE1}) \quad & \max_{\rho,\mathbf{p}} \ \sum_{k=1}^{K} R_k(\rho,\mathbf{p}) - \alpha(\theta_K(\mathbf{p}) + P_{\mathrm{c}}) \\
& \text{s.t. } \theta_K(\mathbf{p}) \leq P_{\max}, && (C1) \\
& \quad \theta_k(\mathbf{p}) \geq \ A_k\theta_{k-1}(\mathbf{p}) + \frac{A_k - 1}{H_{k|0}}, \quad \forall 2 \leq k \leq K, \forall i \leq k-1 && (C2a) \\
& \quad \theta_k(\mathbf{p}) \geq \ A_k\theta_{k-1}(\mathbf{p}) + \frac{A_k - 1}{H_{k|1}(\rho)}, \quad \forall 2 \leq k \leq K, \forall i \leq k-1 && (C2b) \\
& \quad \frac{p_k}{\frac{1}{H_{i|1}(\rho)} + \theta_{k-1}(\mathbf{p})} \geq \frac{p_k}{\frac{1}{H_{k|1}(\rho)} + \theta_{k-1}(\mathbf{p})}, \quad \forall 2 \leq k \leq K, \forall i \leq k-1 && (C3) \\
& \quad 0 \leq \rho \leq 1, && (C4)
\end{aligned}$$

where $(C2a)$ and $(C2b)$ are the modified QoS constraints for the transparent and backscattering states, respectively, and all other constraints remain unchanged. Note that since $H_{k|1}(\rho) \geq H_{k|0}$ ($H_{k|1}(\rho)$ is a composition of the direct and backscattered channels), the constraint $(C2b)$ will be omitted since satisfying $(C2a)$ is sufficient.

Even though we restricted $(C2)$ to simplify the problem (**EE0**), the resulting optimization problem (**EE1**) remains non-convex due to the joint optimization of the reflection coefficient ρ and the vector of allocated powers $\mathbf{p}$. Nevertheless, following a similar approach to [C14] (in which the backscatter device did not transmit any information and operated always in a backscattering state), we show here that (**EE1**) can be solved by decoupling it into two sub-problems without loss of optimality:
i) we first optimize ρ for an arbitrary power allocation $\mathbf{p}$;
ii) then optimize $\mathbf{p}$ with the fixed optimal reflection coefficient ρ^*.

4.3.2 Optimal resource allocation policy

Let us first consider a fixed arbitrary power allocation $\mathbf{p} \in \mathcal{P}$ and solve the optimization problem (**EE1**) w.r.t to the reflection coefficient ρ.

Proposition 4.3.1. *[J6] The optimal reflection coefficient is independent of* $\mathbf{p}$ *and can be obtained in closed form as*

$$\rho^* = \begin{cases} \min\left(1, \min \xi\right), & \text{if } \xi \neq \emptyset \\ 1, & \text{otherwise,} \end{cases} \tag{4.16}$$

where $\xi \triangleq \left\{ \left(\frac{h_k}{\sigma_k} - \frac{h_{k+1}}{\sigma_{k+1}}\right)^2 \Big/ \left(g\left(\frac{g_{k+1}}{\sigma_{k+1}} - \frac{g_k}{\sigma_k}\right)\right)^2 \mid 2 \leq k \leq K \text{ s.t. } g_{k+1} > g_k \right\}$. *When the reflection coefficient is set to* ρ^*, *the constraints* $(C3)$ *and* $(C4)$ *of the optimization problem* (**EE1**) *are readily satisfied.*

Proof. For a fixed arbitrary power allocation $\mathbf{p}$, one can show that the objective function is increasing w.r.t. ρ. Hence, the reflection coefficient must be chosen as large as possible within the feasible range given by the constraints $(C3)$ and $(C4)$. A detailed proof can be found in [C14]. □

Because the optimal reflection coefficient ρ^* in (4.16) is independent of $\mathbf{p}$ and since the remaining constraints $(C1)$ and $(C2')$ are independent of ρ, decoupling the optimization problem by first optimizing over the reflection coefficient and then over the power allocation policy does not induce any optimality loss.

We can thus fix $\rho = \rho^*$ and solve the remaining convex problem in terms of the power allocation policy $\mathbf{p}$ with no optimality loss.

$$\begin{aligned} (\mathbf{EE2}) \quad & \max_{\mathbf{p}} \ \eta_{EE}(\mathbf{p}) \triangleq \sum_{k=1}^{K} R_k(\rho^*, \mathbf{p}) - \alpha(\theta_K(\mathbf{p}) + P_{\mathrm{c}}) \\ & \text{s.t. } \theta_K(\mathbf{p}) \leq \overline{P}, && (C1) \\ & \qquad \theta_k(\mathbf{p}) \geq A_k \theta_{k-1}(\mathbf{p}) + \frac{A_k - 1}{H_{k|0}}, \ \forall\ 1 \leq k \leq K. && (C2a) \end{aligned}$$

The next theorem states both the feasibility condition as well as the optimal power allocation policy.

Theorem 4.3.1. *[J6] The optimization problem* (**EE2**) *is feasible if and only if the following condition holds:*

$$P_{\min} \triangleq \sum_{i=1}^{K} \frac{(A_i - 1)}{H_{i|0}} \prod_{j=i+1}^{K} A_j \leq \overline{P}. \tag{4.17}$$

If the optimization problem (**EE2**) *is feasible, the optimal power allocation* $\mathbf{p}$ *is given analyt-*

ically as follows:

$$\begin{aligned} p_k^* &= (A_k-1)\left(\frac{1}{H_{k|0}} + p_1^* \prod_{i=2}^{k-1} A_i + \sum_{i=2}^{k-1} \frac{(A_i-1)}{H_{i|0}} \prod_{j=i+1}^{k-1} A_j\right), \quad \forall\ k \geq 2, \\ p_1^* &= \max\left(\min\left(\overline{p_1}; u\right); \ell\right), \end{aligned}$$

where $\ell = \frac{(A_1-1)}{H_{1|0}}$, $u = \left(\overline{P} - P_{\min} + \ell \prod_{j=2}^{K} A_j\right) \Big/ \prod_{i=2}^{K} A_i$ *and* $\overline{p_1}$ *represents the unique critical point of the single variable function* $f_1(p_1) \triangleq \eta_{EE}(p_1, p_2^*, \ldots, p_K^*)$ *w.r.t* p_1.

Proof. Provided that the feasibility condition is met, and given that (**EE2**) is convex, we can apply the Lagrange multipliers to obtain the optimal expressions of p_k^*, $\forall k \geq 2$ as functions of p_1 by solving the KKT optimality conditions, which are necessary and sufficient [65]. Hence, the multi-variable problem (**EE2**) is turned into a single variable optimization problem w.r.t. p_1 which is proved to be a convex optimization problem in [J6]. □

Ratio between the achievable sum rate and the overall consumed power Let us now consider the EE metric defined as the ratio between the achievable sum rate and the overall consumed power $\xi_{EE}(\rho, \mathbf{p}) = \frac{\sum_{k=1}^{K} R_k(\rho,\mathbf{p})}{\sum_{k=1}^{K} p_k + P_c}$. Since only the numerator depends on the reflection coefficient ρ, the optimal ρ^* given in (4.16) also maximizes $\xi_{EE}(\rho, \mathbf{p})$ for all feasible $\mathbf{p}$. Once ρ^* obtained, since the numerator is is concave w.r.t. $\mathbf{p}$ and the denominator is affine, $\xi_{EE}(\rho^*, \mathbf{p})$ is a fractional program that can be solved using Dinkelbach's method, which reduces to finding the solution to the following equation w.r.t. α:

$$F(\alpha) \triangleq \sum_{k=1}^{K} R_k(\rho^*, \mathbf{p}^*) - \alpha \left(\sum_{k=1}^{K} p_k^* + P_c\right) = 0. \tag{4.18}$$

4.3.3 Numerical simulations

In the following, the positions of the users are uniformly drawn in a disk of radius 20m around the source, whereas the backscatter device position is drawn in a disk of radius 4m surrounding the source. Since the coverage area of ambient backscatter communication systems is relatively small, we assume that the communication links have a strong line-of-sight (LOS) and fading-free pathloss channels of the type $h = d^{-\frac{\gamma}{2}}$ [106]–[109], where d is the distance between different nodes and $\gamma = 2.5$ is the path loss exponent. The other system parameters are: $\sigma^2 = -20$ dBm, $R_{\min,k} = R_{\min} = 1$ bpcu, $\forall k$, $\overline{P} = 30$ dBm, unless stated otherwise, and $P_c = 30$ dBm. The simulation results are averaged over 10^3 random draws of the nodes positions satisfying the feasibility condition in Theorem 4.17.

Impact of our modified constraints In Figure 4.3, we compare the EE of the optimal solution to the original problem (**EE0**), obtained via exhaustive search, and our analytical solution to the modified problem (**EE1**) as a function of $q \in [0, 1]$ and for $R_{\min} \in \{1, 2\}$ bpcu. We see that the sub-optimality gap becomes smaller when q decreases. Indeed, the case $q = 0$

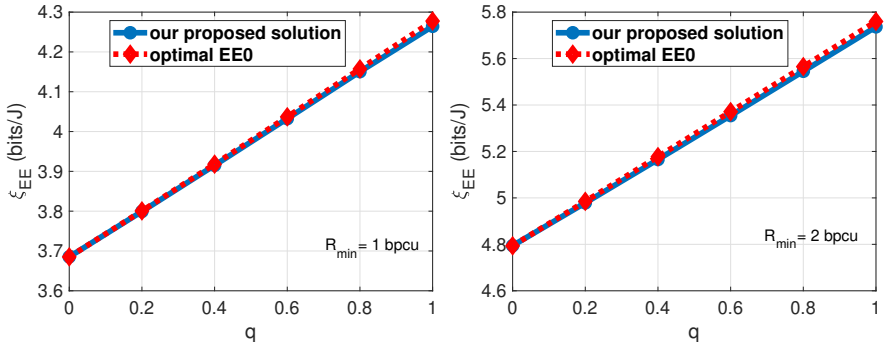

Figure 4.3: Energy efficiency (ξ_{EE}) sub-optimality comparison for different values of q and $R_{\min}$.

corresponds to conventional NOMA, without backscattering, for which the two solutions are identical (as (**EE0**) becomes equivalent to (**EE1**)). The sub-optimality gap increases with $R_{\min}$, but remains negligible, which validates our intuition and highlights the interest of our analytical solution.

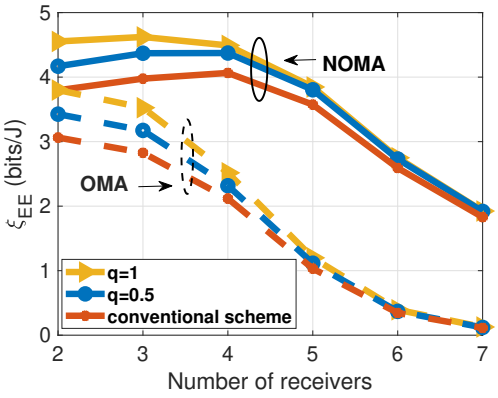

Figure 4.4: Energy efficiency (ξ_{EE}) as a function of the number of receivers K for different values of q.

NOMA vs. OMA evaluation In Figure 4.4, we plot the EE, defined as the ratio ξ_{EE}, of ambient backscatter-aided NOMA and OMA (as benchmark), as a function of the number of receivers for different values of $q \in \{0, 0.5, 1\}$ with $\overline{P} = 60$ dBm and $R_{\min} = 1$ bpcu. First, we see that NOMA with backscattering always outperforms its OMA counterpart irrespective from q. Moreover, we observe that the EE decreases with the number of receivers. The intuition comes from the expression of the optimal reflection coefficient in (4.16) that depends on the smallest difference between the channel gains. The larger the number of receivers K, the smaller the channel gap. When K increases, ρ^* tends to zero, vanishing the backscattering effect and leading to the conventional scheme without backscattering ($q = 0$).

In Figure 4.5 we plot the achievable sum rate and overall power consumption as functions of the tradeoff parameter α where $q = 0.5$ and $R_{\min} = 1$bpcu. We see that NOMA achieves higher sum rate while consuming as much power as OMA, irrespective from α. Moreover, both the sum rate and the power consumption decrease as α increases. Indeed, for larger

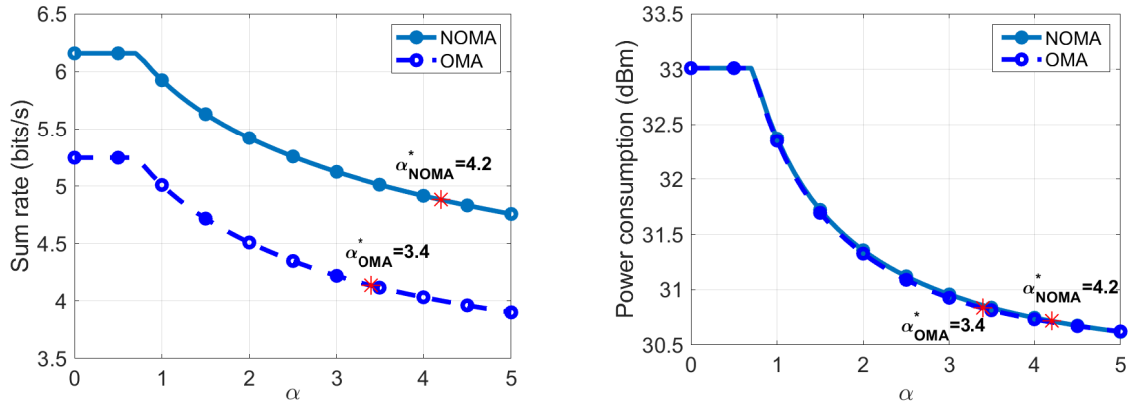

(a) Achievable sum rate (b) Overall power consumption

Figure 4.5: Achievable sum rate and overall power consumption as functions of the tradeoff parameter α for an ambient backscatter-aided NOMA system with $K = 2$ and $q = 0.5$

values of α, the power minimization is given more weight when maximizing the sum rate vs. power consumption tradeoff. We also highlight the two points α^*_{NOMA} and α^*_{OMA} referring to the respective solutions of $F(\alpha) = 0$ in (4.18) providing the achievable sum rate and overall power consumption that are optimal in the sense of the EE ratio ξ_{EE}.

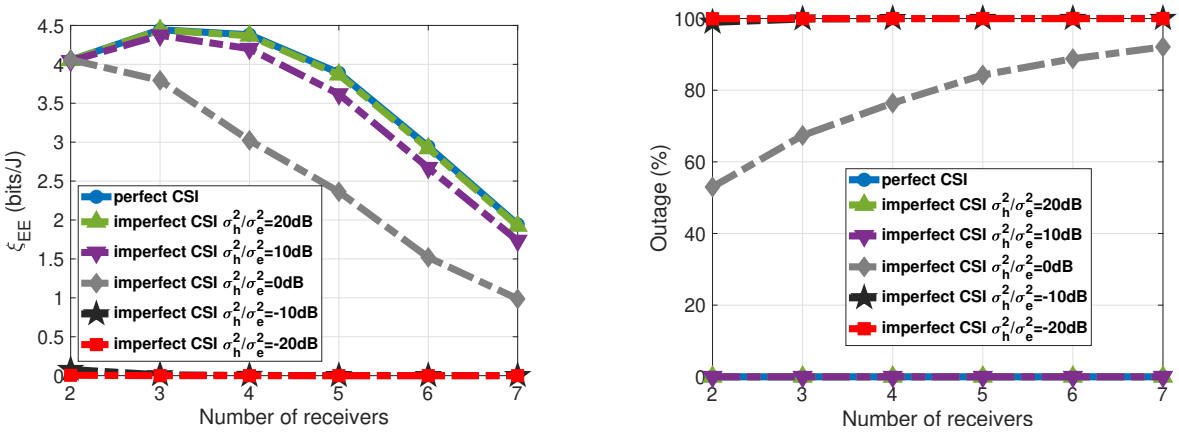

(a) Energy efficiency (ξ_{EE}) for different values of σ_e^2 (b) Outage performance for different values of σ_e^2

Figure 4.6: Impact of imperfect CSI on the energy efficiency (ξ_{EE}) and outage performance of NOMA as a function of the number of receivers K for different values of the error variance σ_e^2.

Impact of imperfect CSI At last, we investigate the impact of imperfect CSI on our solution. We assume that only channel gain estimates $\hat{h}$ are available at the transmitter side such that $\hat{h} = h - e$, where $e \sim \mathcal{N}(0, \sigma_e^2)$ represents the estimation error of variance σ_e^2 for any link h. The power allocation policy is computed based on the estimated channel gains $\hat{h}$ and the system performance is obtained with the true channel gains h. Imperfect CSI may result in violating the user QoS or the SIC constraints in (4.12), leading to an outage event.

Hence, we plot both the EE when the system is not in outage and the outage probability in Figure 4.6 for $q = 0.5$.

As expected, the performance is impacted by the quality of the channel estimation. For $\sigma_h^2/\sigma_e^2 \in \{-10, -20\}$ dB (poor estimation), the system is almost always in outage. For $\sigma_h^2/\sigma_e^2 = 20$ dB (excellent estimation), the imperfect CSI curves are superposed to the perfect CSI ones. When $\sigma_h^2/\sigma_e^2 = 10$ dB (good estimation), the outage is negligible and the EE is impacted but not critically (the loss is below 11% for any K). When the error variance is as high as the channel variance ($\sigma_h^2/\sigma_e^2 = 0$ dB), the outage is very high: above 50% for $K = 2$ and reaches up to 90% for $K = 7$. Except for $K = 2$, the EE is also highly impacted in this case, the loss reaching up to 49% for $K = 7$ users. Hence, our solution relies on high quality CSI estimation.

In the next Section, we move toward an extreme case, where neither perfect or imperfect CSI nor channel distribution information (CDI) is available at the transmitter side.

4.4 Resource allocation for energy-efficient NOMA in dynamic environments

4.4.1 System model

Throughout this Section, we restrict the system model under study to the case of $K = 2$ users and the backscatter being in the transparent mode ($B = 0,\ q = 0$). The received signal at each user k writes as $y_k^{(t)} = h_k^{(t)} x^{(t)} + z_k^{(t)}$, where $h_k^{(t)}$ represents the instantaneous channel gain which is assumed to follow a stochastic time-varying small-scale fading model as in [110]. The later are unknown to the transmitter; and only the receivers know their own channels.

When the channels are known by the transmitter, the user with the best channel conditions carries out SIC and the other performs single user detection (SUD). Under unknown channels, the decoding techniques of the users have to be chosen differently. One solution is to consider it as an optimization variable: let $i \in \{1, 2\}$ and $j \in \{1, 2\} \setminus \{i\}$ denote the user performing SIC and the one performing SUD respectively. The discrete variable $i \in \{1, 2\}$ assigning the users' decoding techniques is a control variable that has to be optimized at the transmitter alongside the power allocation vector $\mathbf{p} = (p_i, p_j)$. User i first decodes the message of user j with the data rate $R_{j\to i}^{(t)} = \log\left(1 + \Gamma_{j\to i}^{(t)}\right)$, where $\Gamma_{j\to i}^{(t)} = \frac{|h_i^{(t)}|^2 p_j}{|h_i^{(t)}|^2 p_i + \sigma^2}$ denotes the SINR at user i when decoding user j's message. User i then removes this message and decodes its own message with the data rate $R_i^{(t)} = \log(1 + \Gamma_i^{(t)})$, where $\Gamma_i^{(t)} = \frac{|h_i^{(t)}|^2 p_i}{\sigma^2}$ denotes the SNR at user i. User j treats user i's message as additional noise, with the data rate $R_{j\to j}^{(t)} = \log(1 + \Gamma_{j\to j}^{(t)})$, where $\Gamma_{j\to j}^{(t)} = \frac{|h_j^{(t)}|^2 p_j}{|h_j^{(t)}|^2 p_i + \sigma^2}$ is the SINR at user j.

An EE measure well suited to stochastic small-scale fading channels, as its numerator represents the long-term average sum rate of the system, is defined as [111], [112]

$$GEE(i, \mathbf{p}) = \frac{(R_{\min,1} + R_{\min,2})(1 - \mathbb{P}_{\text{out}}(i, \mathbf{p}))}{p_i + p_j + P_c}, \tag{4.19}$$

where $(1 - \mathbb{P}_{\text{out}}(i, \mathbf{p}))$ is the probability that the QoS constraints are met. The outage probabil-

ity, on the other hand, is given as $\mathbb{P}_{\text{out}}(i,\mathbf{p}) = \mathbb{P}\left[\Gamma_i^{(t)} \leq \Gamma_{\min,i} \ \cup \ \min(\Gamma_{j\to j}^{(t)}, \Gamma_{j\to i}^{(t)}) \leq \Gamma_{\min,j}\right]$, with $\Gamma_{\min,i} \triangleq 2^{R_{\min,i}} - 1$ and $\Gamma_{\min,j} \triangleq 2^{R_{\min,j}} - 1$. Since the QoS constraints are incorporated into the objective, the feasible set simplifies to

$$\mathcal{P} = \left\{(i,\mathbf{p}) \mid i,j \in \{1,2\}, j \neq i, p_i, p_j \geq 0, p_i + p_j \leq \overline{P}\right\}.$$

When CDI is available, the closed-form expressions of the outage probability are known [34] for Rayleigh distributed channels. Hence finding the optimal policy maximizing $GEE(i,\mathbf{p})$ reduces to solving two continuous optimization problems (one for each value of i) with respect to $\mathbf{p}$ and then choosing the best value of i.

The absence of CSI and CDI leads to an unknown objective function which cannot be minimized via classical optimization techniques. Instead, we propose to exploit reinforcement learning and Multi-Armed Bandits (MABs) to propose iterative and adaptive schemes that exploit past transmissions and do not rely on CSI/CDI. We first introduced this tool to minimize the outage probability of the same system model in the absence of CDI and CSI at the transmitter side in [J5]. Here, MABs are used to maximize an EE metric based on the outage probability. While transmitting at full power is optimal when minimizing the outage probability, the later is no longer optimal when maximizing the energy-efficiency leading to a different feasible set [C13] compared to [J5].

4.4.2 Multi-Armed Bandits for adaptive NOMA with no CSIT/CDIT

In order to exploit the MAB framework, we first need to quantize the feasible set $\mathcal{P}$. Given that transmitting at full power as in [J5] is not energy-efficient in general, we consider that only a fraction of the maximum budget $\overline{P}$ is exploited with $\beta \in \mathcal{B} \subset [0,1]$ such that $\mathcal{B} = \{\beta_1, \beta_2, \ldots, \beta_B\}$ is discrete. In order to maintain fairness among users, user i carrying out SIC is allocated less power than user j; and focus on the special choice of power allocation policy $\mathbf{p}_\beta = (0.25\beta\overline{P}, 0.75\beta\overline{P})$. Of course, the quantization set $\mathcal{B}$ and the $0.25 - 0.75$ power split between the two users will both incur an optimality loss which will be evaluated and analyzed thoroughly via numerical simulations.

A possible action or arm at the BS is defined by the pair $\mathbf{a} \triangleq (i,\beta) \in \mathcal{A} = \{1,2\} \times \mathcal{B}$ which will dictate both the decoding schemes of the two users via i and the discrete transmit power allocation policy $\mathbf{p}_\beta$ via β as described above.

A generic dynamic policy for adaptive NOMA in this framework can be described as follows. At each iteration t, the BS selects an arm $a^{(t)} \in \mathcal{A}$, informs the users of their decoding schemes $i^{(t)}$, which can be conveyed via 1-bit and transmits the superimposed signal using $\mathbf{p}_\beta^{(t)}$. Then, both users perform their respective decoding schemes and determine if they met their QoS requirements and send a one-bit ACK feedback. Based on this feedback, the BS computes the reward $u^{(t)}(a^{(t)})$ defined in (4.20) and updates the arm selection process.

$$u^{(t)}(\mathbf{a}) = \begin{cases} \frac{R_{\min,1}+R_{\min,2}}{p_{i,\beta}+p_{j,\beta}+P_c}, & \text{if } \Gamma_i^{(t)} \geq \Gamma_{\min,i} \text{ and } \min(\Gamma_{j\to j}^{(t)}, \Gamma_{j\to i}^{(t)}) \geq \Gamma_{\min,j}, \\ 0, & \text{otherwise.} \end{cases} \tag{4.20}$$

Note that here, maximizing the expected reward is equivalent to minimizing the outage probability since $\mu(a) = \mathbb{E}[u^{(t)}(a)] = (1 - \mathbb{P}_{\text{out}}^{\text{NOMA}})\frac{R_{\min,1}+R_{\min,2}}{p_{i,\beta}+p_{j,\beta}+P_c} = GEE$.

4.4.3 Simulation results

Let us now investigate the EE of our proposed adaptive NOMA scheme with no CSI/CDI. Three cases based on the quantization set $\mathcal{B}$ are considered:
a) 5-element $\mathcal{B}_1 = \{0.2, 0.4, \dots 1\}$;
b) 10-element $\mathcal{B}_2 = \{0.1, 0.2, \dots, 1\}$;
c) 20-element $\mathcal{B}_3 = \{0.05, 0.1, \dots, 1\}$ such that $\mathcal{B}_1 \subset \mathcal{B}_2 \subset \mathcal{B}_3$.
The considered arm sets are thus given as $\mathcal{A}_i = \{1, 2\} \times \mathcal{B}_i$ of 10, 20 and 40 arms respectively.

We further assume Rayleigh fading channels, i.e, $h_k^{(t)} \sim \mathcal{CN}(0, 1)$, and consider the following system parameters: $\sigma^2 = 0.1$, $\Gamma_{\min,1} = 1$ ($R_{\min,1} = 1$ bpcu), $\Gamma_{\min,2} = 10$ ($R_{\min,2} \simeq 3.5$ bpcu), $P_c = 1$ W and $\overline{P} = 100$ W (unless stated otherwise). The time horizon is set to $T = 5000$ for both UCB and EXP3 algorithms and the illustrated curves are averaged over 10^3 horizon realizations. The learning parameters were carefully tuned in order to provide the best performance and were set as $\delta = 0.1$ and $\eta = 0.08$.

To benchmark the performance of our proposed adaptive NOMA scheme, we consider OMA where each of the two users is served in a time-sharing manner.

In Figure 4.7, we compare the EE of our NOMA scheme with UCB and EXP3 using $\mathcal{A}_3$ (40 arms), with the fixed optimal arm a^* computed offline with the use of CDI. Note that both algorithms reach the EE of a^*, the best fixed offline policy, by requiring only one bit of feedback and no CSI/CDI. Further, our proposed NOMA scheme significantly outperforms OMA after a few iterations. UCB outperforms EXP3, as expected in the stochastic case [113].

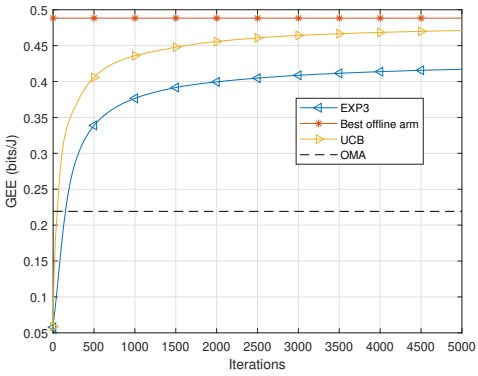

Figure 4.7: Energy efficiency of our adaptive NOMA (via UCB or EXP3) compared to the best offline arm and OMA.

In Figure 4.8(a) and Figure 4.8(b), we investigate the impact of the number of arms and the sub-optimality caused by the discretization $\mathcal{B}$ and the split $0.25 - 0.75$ for two scenarios: $\overline{P} = 100$ W and $\overline{P} = 10$ W, respectively. For this, we include the following two benchmarks: a) sub-optimal EE obtained with the user power split $0.25 - 0.75$, but for an optimal choice of β;

b) the optimal EE obtained over the entire set $\mathcal{P}$. Both figures show a vanishing gap between the above sub-optimal and optimal schemes, showing hence the efficiency of our heuristic $0.25 - 0.75$ power split between the two users. In the large transmit power regime of Figure 4.8(a), the optimality loss of our adaptive NOMA scheme decreases with the number of arms. However, the gap remains large (more than 50% at low $\Gamma_{\min,2}$), highlighting the *tradeoff between EE and available feedback*. On the other hand, in the low power regime of Figure 4.8(b), the optimality gap is negligible for 20 arms.

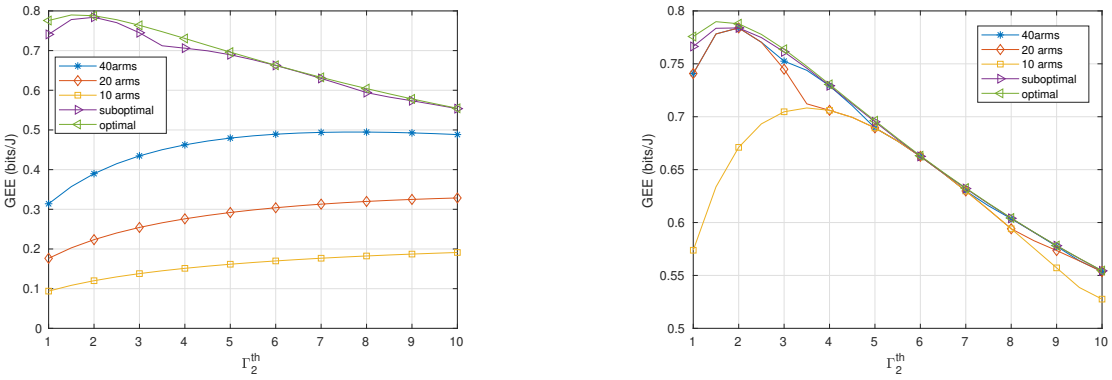

(a) $\overline{P} = 100$ W (b) $\overline{P} = 10$ W

Figure 4.8: Impact of the number of arms on the GEE

In Figure 4.9, we study how the number of arms affects the regret performance of our adaptive NOMA. We focus only on UCB, since it is known to have a better decay rate than EXP3 in the stochastic case, and plot the number of iterations required to reach a regret level of 10%. We see that the larger the number of arms, the more iterations are needed. Hence, even if a better EE performance can be achieved by increasing the number of arms, additional time is needed to explore and exploit all arms. This highlights another fundamental *tradeoff between EE and complexity* and a larger amount of time is required to reach better performance.

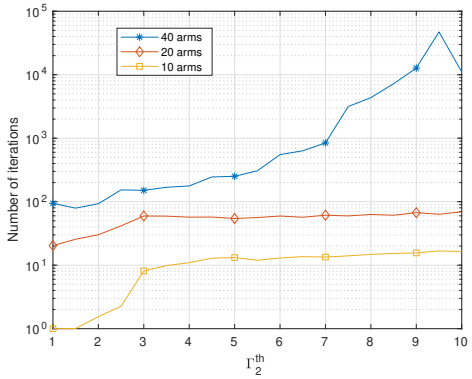

Figure 4.9: Number of iterations required for UCB to achieve 10% regret level: tradeoff performance vs. complexity.

4.5 Conclusions

In this chapter, we analyzed a mutli-user downlink NOMA system aided by an ambient backscatter device. We first derived the information-theoretic achievable rate regions and then formulated the energy efficiency maximization as the tradeoff between the achievable sum rate and the power consumption. Introducing a modification to the problem's constraints allowed to turn our non-convex optimization problem into a convex one and to obtain an analytical solution for the joint optimal reflection coefficient and power allocation policy (up to a line search). Moreover, the ambient backscatter-aided NOMA system was shown to outperform conventional NOMA and OMA (with and without backscattering) as benchmarks. Finally, we investigated the impact of imperfect CSI and highlighted that when the channel estimation is sufficiently high (SNR higher than 10 dB) our solution is still relevant.

Finally, we considered the extreme case of no available CSI at the receiver side. The lack of channel state information was overcome by the use of reinforcement learning, more precisely using the multi-armed bandits framework, under which we proposed a novel adaptive NOMA scheme relying on a single bit of feedback. Although our numerical simulations demonstrated the enormous potential of our adaptive solution, the later was obtained by quantizing the feasible power set with a high enough resolution, implying hence a large amount of time to explore and exploit the set of arms.

In the next chapter, we consider opportunistic rate maximization in cooperative cognitive radio systems. Whereas obtaining the analytical solutions to the non-convex optimization problems considered in this chapter was possible thanks to some modifications in the constraints, the later no longer holds in the presence of a full-duplex operating relay node which performs complex and non-linear operations such as Decode-and-Forward or Compress-and-Forward. Hence, the solutions of the optimization problems considered in Chapter 5 will be obtained with the help of deep learning, which can further be applied in the imperfect CSI case without any feasible set quantization, as opposed to the MAB framework considered in Chapter 4.

Chapter 5

Optimal power allocation maximizing cooperative opportunistic rates

In this chapter, we overview the most relevant contributions [C16], [C19], [J8 prep] of the work performed by the PhD student Yacine Benatia, whom I am co-advising (at 40%) jointly with Romain Negrel (ESIEE, 30%) and E. Veronica Belmega (ETIS lab, 30%, official director); as well as some preliminary studies derived with my collaborator E. Veronica Belmega [J4].

Main contributions

Let us consider a relay-aided cognitive radio network composed of a licensed link and an opportunistic link, which is assisted by a full-duplex operating relay node. The later can perform Decode-and-Forward (DF) or Compress-and-Forward (CF). We propose a machine-learning based opportunistic rate maximization under a primary QoS constraint as well as individual power budget, and further investigate the robustness of our approach under imperfect CSI.
Our main contributions are the following:

- Deriving the achievable rate region under DF and CF.
- Deriving the closed form optimal power allocation policy when the relay performs CF under perfect CSI.
- Proposing an unsupervised deep learning approach when the relay performs DF under perfect CSI.
- Proposing a new robust training enabling the neural network to learn when imperfect CSI is available at its input and to perform much better by avoiding the prohibitive primary QoS violations, even when only poor channel estimations are available.
- Proposing a new machine learning-based relaying scheme selection procedure enabling to chose between CF or DF under imperfect CSI.

5.1 System model

The cooperative cognitive radio network under study is illustrated in Figure 5.1 and consists of one licensed user U_P, also called primary user, and its associated destination D_P; whereas the

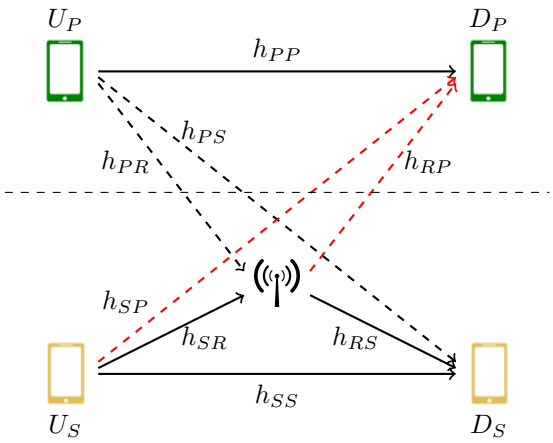

Figure 5.1: Cognitive relay-aided network.

cooperative opportunistic network is composed by a source node U_S, its associated destination D_S and a full-duplex relay R. The opportunistic user has an underlay access mode to the spectrum and cannot perturb the licensed transmission above a tolerated level. This model has been widely studied from an outage point of view, either with a single relay and power allocation [114], or with multiple relay selection and without power allocation [49]–[51], or with a single relay and no power allocation [48], [52], [115].

Let X_P, X_S and X_R, of average power p_P, p_S and p_R, denote the messages sent by the primary, the secondary user and the relay respectively. Further, let Z_R and $Z_i, i \in \{S, P\}$ denote the AWGN of variance N_R and N_i, at the relay and at destination D_i respectively. The received signals at the relay, primary and secondary destination are thus expressed as

$$Y_R = h_{PR}X_P + h_{SR}X_S + Z_R$$
$$Y_i = h_{Ri}X_R + h_{ii}X_i + h_{ji}X_j + Z_j,$$

where $i, j \in \{P, S\}, i \neq j$.

We further assume that the relay only helps the opportunistic transmission. As such, the message from the relay and from the secondary user are treated as additional noise at the primary destination when retrieving its own information X_P. In the same manner, the message from the primary user is considered as additional noise at both the relay and the secondary destination when recovering X_S. Hence, we can consider equivalent correlated additive Gaussian noises at the relay and secondary destination defined as $\widetilde{Z}_R = h_{PR}X_P + Z_R$ and $\widetilde{Z}_S = h_{PS}X_P + Z_S$, of variance $\widetilde{N}_R = h_{PR}^2 p_P + N_R$ and $\widetilde{N}_S = h_{PS}^2 p_P + N_S$ respectively; where the correlation coefficient is given as $\rho_Z = \frac{h_{PR}h_{PS}p_P}{\sqrt{\widetilde{N}_R \widetilde{N}_S}}$.

Let $R_i, i \in \{P, S\}$ denote the achievable rate of the primary and secondary user respectively. Let further $\overline{R_P}$ denote the achievable primary rate in the absence of the opportunistic network, which is expressed as $\overline{R_P} = \frac{1}{2}\log_2\left(1 + \frac{h_{PP}^2 p_P}{N_P}\right)$.

As per usual in cognitive radio setups, as well as in our previous studies [J4], [C16], [C19], the opportunistic network is allowed to communicate over the licensed bands provided that the primary transmission does not degrade too much. Here we consider a minimum QoS

constraint protecting the primary user's rate expressed as $R_P \geq (1-\tau)\overline{R_P}$, $\tau \in [0,1]$: In other words, the primary user can tolerate at most a fractional decrease of $\tau \in [0,1]$ in its achievable rate compared to its maximum rate achieved in the absence of the opportunistic network.

In the following, we assume that the relay performs either DF or CF. We do not consider AF relaying in this study for two main reasons. First, AF is expected to perform poorly in most multi-user interference settings since the relay also amplifies the interference plus noise terms, which enhances the noise variance at the secondary destination compared to DF and CF. Indeed, even in the standard Gaussian relay channel, which is not impaired by multi-user interference, both DF and CF schemes achieve large rates than AF [116]. Second, AF relaying in multi-user networks has been investigated mostly in the multi-hop special case, in which the direct link between the user and its destination is negligible [117]–[125]. When the direct link is taken into account, as in our work, AF turns the channel into a channel with memory [116], under which the achievable rate regions have very complex expressions [PhD], [126] leading to highly non trivial secondary rate maximization problems.

In the next Section, we present the achievable rate regions when the full-duplex relay performs CF or DF.

5.2 Achievable rate regions

5.2.1 Compress-and-Forward

We start our analysis by investigating the achievable rate region when CF relaying is used. Under CF relaying, the relay sends a compressed version of its received signal.

To simplify the presentation, the following notations will be used:

$$K_1 = h_{SR}^2\widetilde{N}_S + h_{SS}^2\widetilde{N}_R - 2h_{SR}h_{SS}\rho_Z\sqrt{\widetilde{N}_S\widetilde{N}_R}, \quad K_2 = (1-\rho_Z^2)\widetilde{N}_R\widetilde{N}_S$$

Below, we provide the achievable rate region, which can be derived by exploiting the results for the Gaussian relay channel with correlated noises [C4].

Proposition 5.2.1. *[J4] Assuming CF at the relay and that all non-intended messages are treated as additional noise, the following rate region is achievable over the cooperative opportunistic network:*

$$R_P \leq C\left(\frac{h_{PP}^2 p_P}{h_{RP}^2 p_R + h_{SP}^2 p_S + N_P}\right)$$
$$R_S \leq C\left(\frac{p_S(K_1 + h_{SS}^2 D)}{K_2 + \widetilde{N}_S D}\right) \text{ with } D = \frac{K_1 p_S + K_2}{h_{RS}^2 p_R}.$$

Proof. At the primary destination, the message from both the relay and the secondary user are considered as additional noise when recovering the primary message, leading to R_P given above. Regarding the opportunistic network, the situation corresponds to the use of CF over a Gaussian relay channel with correlated additive noise at the relay and destination. The achievable secondary rate can thus be obtained from [C4, Prop. 1]. □

5.2.2 Decode-and-Forward

Let us now investigate the achievable rate region of DF relaying. Under this relaying scheme, the relay first decodes the message sent by the opportunistic user and then sends a re-encoded version of this message towards the destinations.

The achievable rates in this case are given in the next proposition, which can be obtained using standard information theoretic arguments.

Proposition 5.2.2. *[J4] Assuming DF scheme at the relay and that all non-intended messages are treated as additional noise, the following rate region is achievable over the cooperative opportunistic network:*

$$R_P \leq C\left(\frac{h_{PP}^2 p_P}{h_{RP}^2 p_R + h_{SP}^2 p_S + 2h_{SP}h_{RP}\alpha\sqrt{p_S p_R} + N_P}\right)$$
$$R_S \leq \min\left\{C(f_{\mathrm{DF},R}(\alpha, p_S, p_R)), C(f_{\mathrm{DF},S}(\alpha, p_S, p_R))\right\},$$

where $\alpha \in [0,1]$ *and*

$$f_{\mathrm{DF},R}(\alpha, p_S, p_R) = \frac{h_{SR}^2(1-\alpha^2)p_S}{\widetilde{N}_R},$$
$$f_{\mathrm{DF},S}(\alpha, p_S, p_R) = \frac{h_{SS}^2 p_S + h_{RS}^2 p_R + 2h_{RS}h_{SS}\alpha\sqrt{p_S p_R}}{\widetilde{N}_S}.$$

Proof. Superposition coding is used at the secondary user in order to coherently combine the message sent by the relay and by the secondary user at the secondary destination. α allows to trade-off between sending a new message and repeating the one from the previous block at the secondary user. At the primary destination, the message from the relay and from the secondary user also coherently combine leading to an increase of the additional noise of $2h_{SP}h_{RP}\alpha\sqrt{p_S p_R}$. The secondary achievable rate follows from perfect decoding at both the relay and the secondary destination. □

In the following Section, we will present the optimal power allocation policy maximizing the opportunistic rate under the QoS protecting the primary transmission when the relay performs CF or DF. The optimal policy under CF can be obtained in closed-form, whereas the one under DF is obtained using deep learning tools.

5.3 Resource allocation for opportunistic rate maximization under perfect CSI

Under both CF and DF, we first assume that perfect CSI is available as commonly considered in the relevant literature [C3], [C4], [C12], [C8], [C6], [51], [55], [56], [58], [116], [127], [128]. The later can be obtained by pilot-based channel estimation prior to any data transmission. Nonetheless, we will relax this assumption in the next Section where we will study the impact of imperfect CSI on the proposed resource allocation policies.

In the remaining, without loss of generality, we assume that all noise processes $Z_i, i \in \{S, P, R\}$ are of unit variance, i.e. $N_S = N_R = N_P = 1$ or equivalently consider channel gains normalized by the receiver noise variance, defined as $g_{ij} = \frac{h_{ij}^2}{N_i}$. To simplify the mathematical expressions and derivations, the following notation will be used

$$A = \frac{g_{PP}p_P}{(1 + g_{PP}p_P)^{(1-\tau)} - 1} - 1.$$

Further, let $\mathbf{h} \triangleq (\sqrt{g_{ij}}, \forall i, \forall j)$ denote the vector collecting all normalized network channels.

5.3.1 Optimization problem under study

In this section, we aim at maximizing the secondary achievable rate under the minimum QoS constraint protecting the primary transmission as well as under individual power constraints within the secondary network expressed as $p_S \leq \overline{P_S}$ and $p_R \leq \overline{P_R}$ as in our studies [C16], [C19]. Note that one could instead consider a total power constraint within the secondary network given as $p_S + p_R \leq \overline{P}$ as considered in [48], [119], [121], [127], [129], [130]. The resulting optimization problems were studied in our previous studies [J4], [C12].

The optimization problem under study in its general form writes as

$$\begin{aligned}
(\mathbf{OP}) \max_{p_R, p_S} \; & R_S(p_S, p_R) \\
\text{s.t. } & R_P \geq (1-\tau)\overline{R_P}, && \text{(QoS)} \\
& 0 \leq p_S \leq \overline{P_S}, \quad 0 \leq p_R \leq \overline{P_R}, && \text{(TP)}
\end{aligned}$$

where the objective, i.e., the achievable rate of the opportunistic user $R_S(p_S, p_R)$ depends on the specific relaying scheme performed. Replacing the achievable rate regions of Propositions 5.2.1 and Proposition 5.2.2 into the considered optimization problem (**OP**) results into optimization problems of the form

$$\begin{aligned}
(\mathbf{OxF}) \max_{p_R, p_S} \; & R_S^{\mathbf{x}F}(\mathbf{h}, p_S, p_R) \\
\text{s.t. } & Q^{\mathbf{x}F}(\mathbf{h}, p_S, p_R) \leq A, && \text{(QoS)} \\
& 0 \leq p_S \leq \overline{P_S}, \quad 0 \leq p_R \leq \overline{P_R}, && \text{(TP)}
\end{aligned}$$

where the objective function and QoS constraint are given under CF and DF respectively as

$$\begin{aligned}
R_S^{CF}(\mathbf{h}, p_S, p_R) &= C\left(\frac{K_1 g_{RS} p_S p_R + g_{SS} p_S (K_1 p_S + K_2)}{K_2 g_{RS} p_R + \widetilde{N}_S (K_1 p_S + K_2)}\right) \\
Q^{CF}(\mathbf{h}, p_S, p_R) &= g_{SP} p_S + g_{RP} p_R \\
R_S^{DF}(\mathbf{h}, p_S, p_R, \alpha) &= \min\left\{C(f_{\mathrm{DF},R}(\alpha, p_S, p_R)), C(f_{\mathrm{DF},S}(\alpha, p_S, p_R))\right\} \\
Q^{DF}(\mathbf{h}, p_S, p_R, \alpha) &= g_{SP} p_S + g_{RP} p_R + 2\alpha\sqrt{g_{SP} g_{RP} p_S p_R}.
\end{aligned}$$

Note that under DF, an additional optimization parameter $\alpha \in [0, 1]$, accounting for the used super-position coding, must also be tuned.

None of the the above optimization problems (**OCF**) nor (**ODF**) is convex. Nonetheless, a closed-form analytical solution can be obtained under CF; whereas a deep neuron network (DNN) based method can be applied to solve (**ODF**).

5.3.2 Closed form expression for CF

To simplify its derivation, we will use the following notations:

$$\begin{aligned}
C_1 &= K_1 g_{RP}(g_{SS}g_{RP} - g_{RS}g_{SP}) \\
C_2 &= K_1 g_{RS}g_{SP}A - 2K_1 g_{SS}A g_{RP} - g_{SS}g_{RP}g_{SP}K_2 \\
C_3 &= g_{SS}A(K_1 A + g_{SP}K_2) \\
C_4 &= K_2 g_{RS}g_{SP}^2 - \widetilde{N}_S K_1 g_{RP}g_{SP} \\
C_5 &= \widetilde{N}_S g_{SP}(K_1 A + K_2 g_{SP})
\end{aligned}$$

The objective function of the optimization problem (**OCF**) can be shown to be monotonically increasing unilaterally w.r.t. p_S for fixed p_R, and w.r.t. p_R for a fixed p_S. This implies that the optimal power allocation lies on the Pareto boundary of the feasible set. Now, regarding the specific shape of the feasible set defining the solution of (**OCF**), five cases can arise as depicted in Figure 5.2, depending on the relative position of the QoS curve and the total power constraints:

[H1] if $\frac{A}{g_{RP}} < \overline{P_R}$ and $\frac{A}{g_{SP}} < \overline{P_S}$, (aside from positivity) only the QoS constraint restricts the feasible set;

[H2] if $\frac{A}{g_{RP}} < \overline{P_R}$ and $\frac{A}{g_{SP}} > \overline{P_S}$, the QoS constraint intersects the secondary user power constraint;

[H3] if $\frac{A}{g_{RP}} > \overline{P_R}$ and $\frac{A}{g_{SP}} < \overline{P_S}$, the QoS constraint intersects the relay's power constraint;

[H4] if $\frac{A}{g_{RP}} > \overline{P_R}$ and $\frac{A}{g_{SP}} > \overline{P_S}$ and $g_{SP}\overline{P_S} + g_{RP}\overline{P_R} < A$, the QoS constraint intersects both total power constraints;

[H5] if $\frac{A}{g_{RP}} > \overline{P_R}$ and $\frac{A}{g_{SP}} > \overline{P_S}$ and $g_{SP}\overline{P_S} + g_{RP}\overline{P_R} \geq A$, only the total power constraints define the feasible set.

A close analysis of these five cases and, since the optimal solution lies on the Pareto boundary of the feasible set, leads us to the following result.

Theorem 5.3.1. *[C19] When the relay employs CF over the cooperative cognitive radio network, the solution to* (**OCF**) *can be found analytically in closed form. Indeed, when **[H5]** is met, the QoS constraint is not restrictive and the solution is simply* $p_R^* = \overline{P_R}, p_S^* = \overline{P_S}$. *In all other cases, **[H1]**–**[H4]**, the solution to* (**OCF**) *lies on the QoS constraint such that* $p_R^* = x^*$, $p_S^* = \frac{A - g_{RP}\, x^*}{g_{SP}}$, *where* x^* *is the closed-form solution to the following single-value optimization problem*

$$\begin{aligned}
(\mathbf{OCF_x}) \quad \max_{x} \quad & f(x) \triangleq \frac{C_1 x^2 + C_2 x + C_3}{C_4 x + C_5}, \\
s.t. \;\; & x \in [x_\ell;\; x_u].
\end{aligned} \tag{5.1}$$

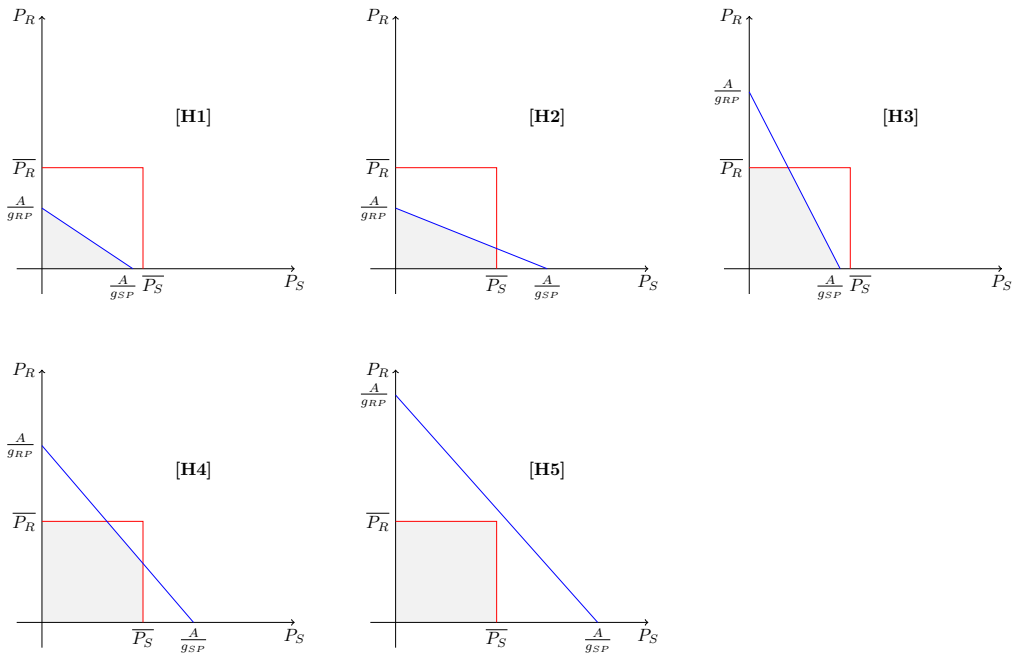

Figure 5.2: Feasible set of (**OCF**).

The values of x_ℓ and x_u defining the box-type constraints depend on the system parameters and the specific case.

If one replaces the individual power constraints in the opportunistic network by an overall power constraint, the optimal power allocation policy maximizing the opportunistic rate can also be obtained in closed form, as proven in [J4].

5.3.3 DNN-based solution for DF

Due to the non-convex nature of the objective function, as well as to the QoS constraint, obtaining the solution of the optimization problems (**ODF**) is very challenging and non-trivial. As such, we proposed to turn to unsupervised learning-based approaches [C16], which exploits a specifically tailored communication loss function.

Solving constrained optimization problems with DNNs is highly non-trivial, unless the constraints are of box-type such as the constraint (TP) and $0 \leq \alpha \leq 1$. This is not the case of the QoS constraint $Q^{DF}(\mathbf{h}, p_S, p_R, \alpha)$ which is a difficult non-convex constraint. Nevertheless, as opposed to the power constraints (TP), the primary QoS constraint is not a physical (hard) constraint but rather a requirement, which can be relaxed and included as a penalty in the objective function below

$$\mathcal{L} = \sum_{\ell=1}^{N} \left(-R_S^{DF}(\mathbf{h}_\ell, p_S, p_R, \alpha) + \lambda [Q^{DF}(\mathbf{h}_\ell, p_S, p_R, \alpha) - A]^+ \right),$$

with $[x]^+ = \max\{0, x\}$ and N denoting the total number of channel realizations $\mathbf{h}_\ell$, $\ell \in \{1, \ldots, N\}$ in the training dataset.

The hyperparameter λ denotes the unit price in bits/Watt of the primary QoS violation. A

small value of λ will result in maximizing the achievable opportunistic rate without taking into account the primary QoS constraint; whereas large values of λ will strictly satisfy the primary QoS constraint but at the cost of opportunistic rate. This tradeoff between opportunistic rate and primary QoS will be further investigated via numerical results.

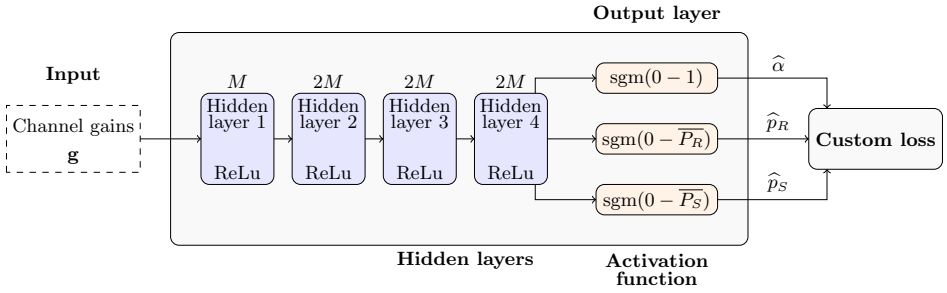

Figure 5.3: Proposed DNN architecture

Our proposed DNN architecture to solve (**ODF**) is composed of four fully connected hidden layers and is depicted in Figure 5.3. The input consists of the channel vector $\mathbf{h}$ which is used to predict the outputs: $(\hat{\alpha}, \hat{P}_R, \hat{P}_S)$, i.e., the solution of (**ODF**). The fully connected architecture is justified because of its generality and given that there is no *a priori* structural or temporal information within the input vector $\mathbf{h}$ to be exploited via more specific architectures such as convolutional or recurrent networks.

The four hidden layers are composed of $M - 2M - 2M - 2M$ neurons with $M = 128$ and are followed by a rectified linear unit (ReLU) activation function due to its low computational complexity. This specific architecture is chosen based on extensive empirical experiments, as discussed in Section 5.3.4.

The final layer is followed by sigmoid activation functions: a standard one $\text{sgm}_\alpha(x) = 1/(1+\text{e}^{-x})$ to map the predicted $\hat{\alpha}$ into its feasible set $[0, 1]$, and two modified ones $\text{sgm}_{p_i}(x) = \overline{p_i}/(1 + \text{e}^{-x})$, $i \in \{S, R\}$, to map the predicted powers $\hat{p}_R$ and $\hat{p}_S$ into $[0, \overline{P_R}]$ and $[0, \overline{P_S}]$ respectively.

5.3.4 DNN-based method: Numerical results

Given the lack of real data available in open access, we will assess the performance of our DNN-based method over simulated data [77], [78], [131], [132]. Unless otherwise specified, we consider a square cell of dimension 10×10 m in which the relay is positioned in the center whereas both primary and secondary user positions are uniformly distributed over the cell. We further assume that the channel gains follow a common fading and path-loss model given as $g_{ij} \sim \frac{\mathcal{N}(0,\sigma_g^2)}{\sqrt{1+d_{ij}^\gamma}}$, where d_{ij} denotes the distance between the nodes i and j and γ is the path loss factor [34]. The path loss factor is set to $\gamma = 3$ and the channel gain standard deviation $\sigma_g = 7$. We assume that $p_P = \overline{P_R} = \overline{P_S} = 10$ W and set the threshold $\tau = 0.25$ for the maximum primary rate degradation.

Dataset In order to train and evaluate our proposed DNN architecture, we use a dataset composed of three disjoint parts:

i) a training set containing 10^6 channel realizations $\mathbf{h}_\ell$;
ii) a validation set containing 2×10^5 channel realizations $\mathbf{h}_\ell$ with the associated ground-truth, i.e., the corresponding optimal resource allocation policies (α^*, p_R^*, p_S^*) obtained by brute force (or exhaustive search) for evaluating the generalization capability and for tuning the hyperparameters of our approach;
iii) a test set containing 2×10^5 channel realizations.

Benchmarks and performance metrics In the following, we propose to compare our DNN-obtained results to the optimal ones obtained by exhaustive search. Thanks to its implementation simplicity, we chose to use exhaustive search to compensate for the lack of closed-form expression under DF. We consider three metrics to validate the performance of our DNN-based method: the relative gap G, the empirical outage Outage and the average primary rate degradation when in outage Δ_{out}.

The relative gap G assesses the relative gap between the predicted achievable rate obtained via our DNN $\hat{R}_{S,\ell}$ and the achievable rate obtained by brute force $R_{S,\ell}^*$ as follows:

$$\mathrm{G} = \frac{\frac{1}{N}\sum_{\ell=1}^{N} \hat{R}_{S,\ell} - R_{S,\ell}^*}{\frac{1}{N}\sum_{\ell=1}^{N} R_{S,\ell}^*} \tag{5.2}$$

The two other considered metrics rely on the degradation of the primary rate defined as $\Delta_\ell = 1 - \hat{R}_{P,\ell}/\overline{R}_{P,\ell}$, where $\hat{R}_{P,\ell}$ corresponds to the primary rate achieved by our proposed DNN. The empirical outage Outage is defined as the proportion of samples in the dataset for which the primary QoS is not satisfied, whereas Δ_{out} denotes the average primary rate degradation when in outage:

$$\text{Outage} = \frac{1}{N}\sum_{\ell=1}^{N} \mathbb{1}\left[\Delta_\ell > \tau\right], \quad \Delta_{\text{out}} = \frac{\sum_{\ell=1}^{N} \mathbb{1}\left[\Delta_\ell > \tau\right] \times \Delta_\ell}{\sum_{\ell=1}^{N} \mathbb{1}\left[\Delta_\ell > \tau\right]}, \tag{5.3}$$

where $\mathbb{1}[x]$ equals 1 when x is true and 0 otherwise.

DNN architecture choice To choose the architecture in Figure 5.3, we have performed extensive simulations over the validation set. In Figure 5.4, we report the most significant results. On the left, we analyze the impact of the number of layers and compare four different architectures composed of one up to four hidden layers as follows: M, $M-2M$, $M-2M-2M$, and $M-2M-2M-2M$, with $M = 128$. We see that there is a significant gain in secondary rate when increasing the number of layers from 1 to 3; moving to 4 layers helps to decrease the outage. Hence, a 4-layer architecture is a good compromise between performance and computational cost. Now, on the right, we compare three different such four-layer DNNs, by varying the number of neurons per layer $M \in \{64, 128, 256\}$. We see that increasing M from 64 to 128 neurons leads to a significant gain in secondary rate; increasing further the number of neurons does not seem justified given the incurred computational cost. For these reasons, we choose $M = 128$ coupled with the 4-layer architecture in Figure 5.3 henceforth.

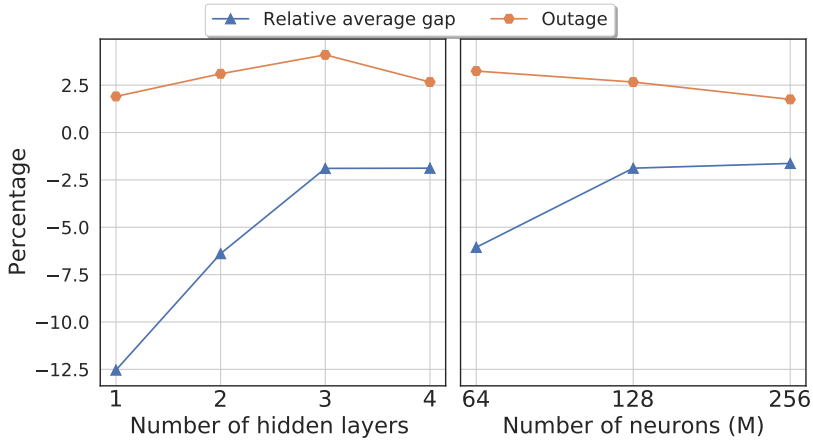

Figure 5.4: Impact of the number of layers and number of neurons on the prediction performance over the validation set.

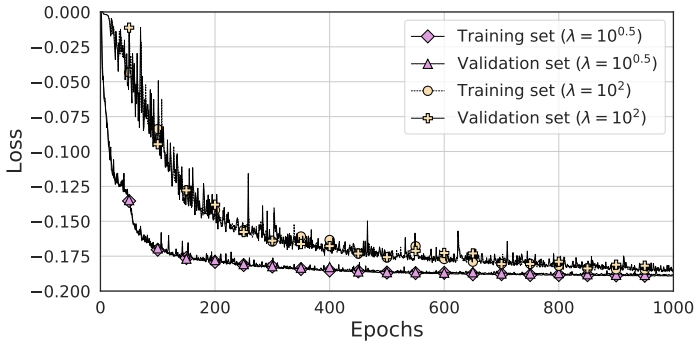

Figure 5.5: Evolution of the loss function evolution over the training epochs over the training and validation sets (no overfitting effects).

No overfitting: performance on train and validation sets In Figure 5.5, we plot the evolution of our custom loss function $\mathcal{L}$ over the number of epochs within the training and validation sets for $\lambda \in \{10^{0.5}, 10^{2}\}$. First, notice that the DNN training converges within 1000 epochs. The superposed performance over the training and validation sets hints towards a good generalization capability of our proposed DNN. More importantly, since the loss function does not increase within the validation set, our approach does not suffer from overfitting. Finally, the decay rate of the loss function is much faster for $\lambda = 10^{0.5}$. Indeed, when λ becomes small, the custom loss is mainly rate-driven and not much emphasis is put on the primary QoS constraint; this leads to a much easier optimization problem to solve. At the opposite, for larger values of λ, the custom loss puts an emphasis on satisfying the primary QoS constraint, which leads to a more difficult problem. Hence, this parameter needs to be tuned carefully as discussed below.

Choice of the hyperparameter λ In Figure 5.6, the relative gap in (5.2) and the outage in (5.3) are depicted as functions of λ over the validation set. For small values of λ (rate-driven custom loss), the relative gap G is positive, which means that the secondary rates obtained via the DNN are larger than the optimal ones via brute force. The reason is that

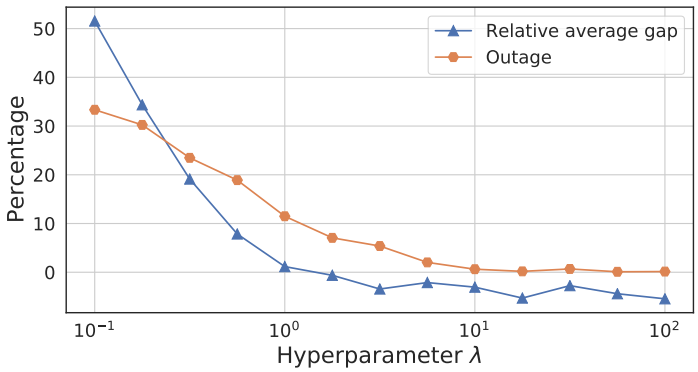

Figure 5.6: Relative average gap G and outage as functions of the hyperparameter λ over the validation set.

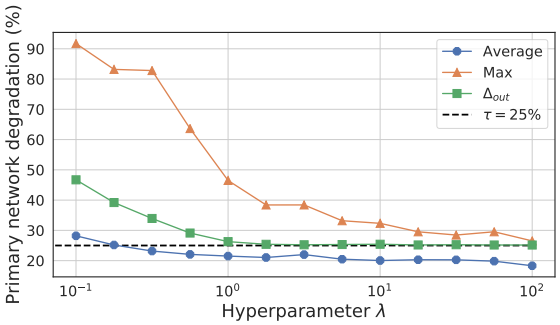

(a) Average and maximum primary rate degradation and average degradation when in outage (Δ_{out}) as functions of λ over the validation set.

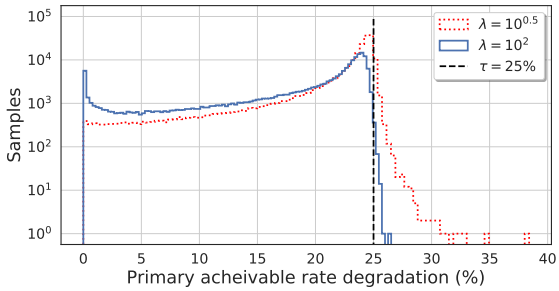

(b) Histogram of the primary rate degradation over the validation set.

Figure 5.7: Impact of the hyperparameter λ.

the primary QoS constraints are not necessarily met by our DNN solutions, as illustrated by the high outage levels. At the opposite, for large values of λ (primary QoS-driven custom loss), the outage goes to zero as expected at a cost in terms of secondary rates. Indeed, our predicted secondary rates are smaller than the optimal ones (negative relative gain G), but this gap is kept below 10 %.

In Figure 5.7, we investigate closer the impact of λ on the primary rate degradation. For this, we plot the average and maximum values of the primary rate degradation as well as the average degradation when in outage Δ_{out} in (5.3) in Figure 5.7(a). Also, in Figure 5.7(b), we illustrate the histogram of the primary rate degradation (Δ) for $\lambda \in \{10^{0.5}, 10^{2}\}$. The mean primary rate degradation falls quickly below the threshold $\tau = 25$ %. For small values of λ, the worst case primary degradation can reach up to 90 %. Nevertheless, such extreme degradation is obtained only for a small number of out-layer data points. This is indicated by the curve Δ_{out} hitting the 25 % threshold reasonably fast as well as by the histogram of the degradation in Figure 5.7(b).

To sum up, the value $\lambda = 10^{0.5}$ achieves a good tradeoff between the achievable secondary rate and the primary QoS degradation in our setting and will be used in the test phase below.

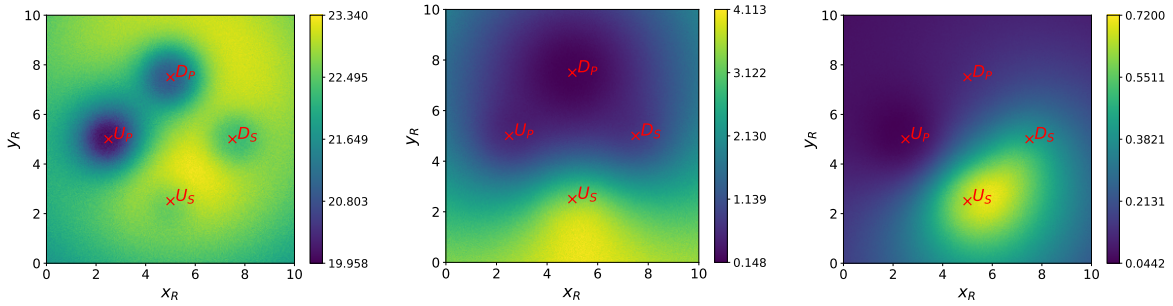

(a) Average primary rate degradation (%).

(b) Average predicted relay power (W).

(c) Average secondary rate (bpcu).

Figure 5.8: Impact of the relay position (x_R, y_R).

Impact of the relay position We will now change the setting and fix the positions of the primary and secondary user/destination nodes: $U_S(5, 2.5)$, $D_S(7.5, 5)$, $U_P(2.5, 5)$, $D_P(5, 7.5)$ as in Figure 5.8; and consider that the relay position (x_R, y_R) varies within the cell. Hence, we generate a second test set composed of 10^4 channel realizations. In Figure 5.8(a), Figure 5.8(b), and Figure 5.8(c), we illustrate the average primary rate degradation, the average predicted relay power $\hat{P}_R$ and the average secondary rate $\hat{R}_S$, respectively as functions of the relay position (x_R, y_R) over this new test set.

In Figure 5.8(a), we notice that the average degradation in the primary rate always falls below the fixed threshold of $\tau = 25$ % irrespective from the relay position. When the relay is very close to the primary nodes, the degradation drops below 20 %, since very little power is allocated to the relay as shown in Figure 5.8(b). The worst case degradation arises when the relay lies between the secondary nodes, since the secondary rate improvement overcomes the damage the relay causes to the primary link. At last, in Figure 5.8(b), we also notice that more power is allocated to the relay when it is close to the secondary user. This is to be expected since DF relaying is known to perform well in terms of achievable rate in these cases, which is indeed confirmed in Figure 5.8(c).

5.4 Relaying scheme selection under imperfect CSI

Let us now assume that the channel gains are impaired by estimation errors. The later, modeled as additive Gaussian noise as in [133], [134], only affect the links from the secondary network to the primary one as we assume that perfect CSI can be obtained by the help of pilot symbols within the secondary network. Since the secondary user transmits in an opportunistic manner, it is unlikely from the primary network to feedback any channel estimation to the secondary user and relay. Hence, $\widehat{h}_{ij} = h_{ij} + \varepsilon_{ij}, \varepsilon_{ij} \sim \mathcal{N}(0, \sigma_{ij}^2)$, $\forall (i,j) \in \{(P,P),(S,P),(R,P),(P,R),$ and $(P,S)\}$ and the normalized estimated channel gains are given as $\widehat{g}_{ij} = \widehat{h}_{ij}^2/N_j$. In the above, the estimation error variance is assumed to be of the form $\sigma_{ij}^2 = \mathrm{Var}[h_{ij}]/\mathrm{SNR}$, where $\mathrm{Var}[h_{ij}]$ denotes the variance of the true channels h_{ij} and $\mathrm{SNR} \in [-10, 20]$ dB represents the SNR of the estimator. The normalized channel gains within the secondary network are on the other hand perfectly known and given as

$\widehat{g}_{ij} = \widehat{h}_{ij}^2/N_j = h_{ij}^2/N_j,\ \forall (i,j) \in \{(S,S),(S,R),\ \text{and}\ (R,S)\}.$

5.4.1 Robust DNN training under imperfect CSI

Note that for CF, our closed-form solution presented in the previous Section highly relies on perfect CSI, which is no longer considered in the remaining of this chapter. As such, we propose to exploit our proposed deep learning approach to solve (**OCF**), using the same neural network architecture as for DF, i.e. depicted in Figure 5.3, with $\lambda = 10^{0.5}$ by simply removing the output α, which is specific to DF, and then retraining the network with the corresponding CF loss function.

Dataset Under imperfect CSI, our train (containing 10^6 samples of both perfect and imperfect channel estimation $\{\widehat{\mathbf{h}}_\ell, \mathbf{h}_\ell\}_\ell$), validation ($2 \times 10^5$ samples of both perfect and imperfect channel estimation $\{\widehat{\mathbf{h}}_\ell, \mathbf{h}_\ell\}_\ell$) and test ($2 \times 10^5$ samples of imperfect channel estimation $\{\widehat{\mathbf{h}}_\ell\}_\ell$) datasets are disjoint.

DNN training In order to make our DNN robust to imperfect CSI, we assume that in the training phase, we have access to pairs of both perfect and imperfect channel estimations $\{\widehat{\mathbf{h}}_\ell, \mathbf{h}_\ell\}_\ell$, where the imperfect ones are obtained by adding Gaussian noise to the initial ones. The perfect channel estimations are fed to our loss function $\mathcal{L}$, whereas the imperfect channel estimations are given as the input of our DNN and the training process is restarted for each value of the considered channel estimated SNR. In addition, we use early stopping with a patience parameter of 20 epochs under both DF and CF to avoid any overfitting effect.

Benchmarks and performance metrics In the following, we propose to compare our DNN-based predictions under imperfect CSI to the optimal power allocation policies under perfect CSI. The latter are obtained either in closed form under CF [C19] or by brute force (exhaustive/grid search) under DF. Thanks to its implementation simplicity, we chose to use brute force to compensate for the lack of closed-form expression under DF. We consider the three same metrics as in the previous Section to validate the performance of our DNN-based method under imperfect CSI, namely the relative gap G, the empirical outage Outage and the average primary rate degradation when in outage Δ_{out}.

Here, the relative gap G assesses the gap between the predicted rate $\hat{R}_{S,\ell}$, achieved by either the DNN or the benchmark under imperfect CSI, and the ideal optimal rate $R^*_{S,\ell}$ obtained with the benchmark under perfect CSI for each sample in the dataset:

$$\mathrm{G} = \frac{\frac{1}{N}\sum_{\ell=1}^{N} \hat{R}_{S,\ell} - R^*_{S,\ell}}{\frac{1}{N}\sum_{\ell=1}^{N} R^*_{S,\ell}} \tag{5.4}$$

Figure 5.9 and Figure 5.10 present the robustness to imperfect CSI in terms of relative secondary gap, outage and average primary rate degradation as a function of the SNR of the channel estimation under CF and DF respectively. Under both CF and DF, we compare the performance achieved by the benchmark under imperfect CSI (either closed-form expression

under CF or bruteforce under DF), the one achieved by our DNN trained only with perfect CSI labeled as 'DNN', and the one achieved with our new proposed robust training labeled as 'N-DNN', i.e. when both perfect and imperfect CSI are used in the training phase. First, note that although designed initially for DF, our proposed DNN is able to generalize to CF relaying as well with almost no architecture change beside removing one of the predicted output, as can be seen from the almost zero gap between the performance achieved by the benchmark and by the DNN. Second, for all relaying schemes, both the benchmark and the DNN trained with only perfect CSI harm the primary communication in almost $20-50\%$ of cases with an average primary rate degradation when in outage between 35 and 65%, highly above the defined threshold $\tau = 25\%$. On the other hand, our DNN with robust training achieves lower secondary rate compared to the benchmark or to the DNN trained only with perfect CSI (loss in terms of relative gap of the order of $20-40\%$) but satisfies almost always the QoS constraint with an outage of only 5%, which is crucial in cognitive radio setups. Furthermore, when in outage, the primary rate degradation is kept below 45%. One can also note that the outage under CF is less than that under DF, which is to be expected since the optimization problem under DF is more difficult to solve due to the non-convex objective function and QoS constraint.

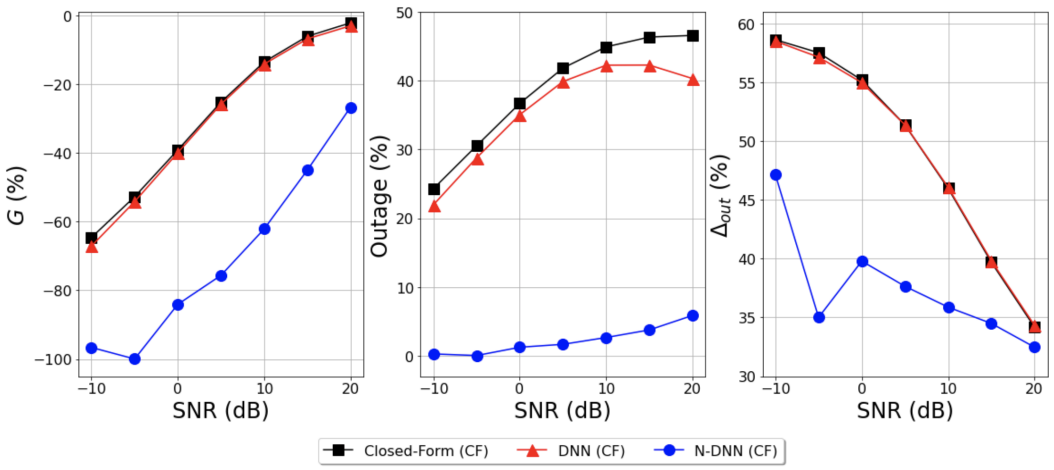

Figure 5.9: Impact of imperfect CSI on our proposed solutions for CF over the test set.

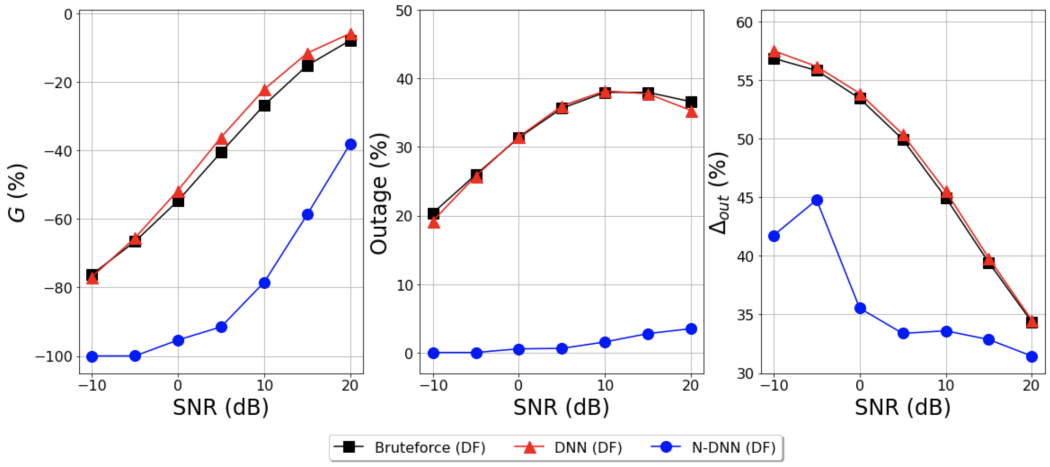

Figure 5.10: Impact of imperfect CSI on our proposed solutions for DF over the test set.

Once our proposed robust training has been validated, one can focus on the comparison of the two relaying schemes as a function of the nodes spatial positions within the considered square cell. More specifically, we now assume that the position of the primary and secondary user/destination pairs is fixed as $U_S(5, 2.5)$, $D_S(7.5, 5)$, $U_P(2.5, 5)$, $D_P(5, 7.5)$, whereas the relay can be placed anywhere within the cell.

Figure 5.11 and Figure 5.12 depict the average power transmitted by the secondary network, the average secondary rate as well as the average primary rate degradation for four different channel estimation SNR under CF and DF respectively, where each simulation result is averaged over 10^4 channel realizations. Under poor channel estimation (SNR $\in \{-10, 0\}$dB), the secondary network barely transmits leading to almost no primary rate degradation and almost zero secondary rate. As the quality of the CSI increases, one can note that CF performs best when the relay is close to the secondary destination, whereas DF performs well when the relay is close to the secondary user, as for the standard relay channel. Furthermore, in all cases, one can see that the average primary rate degradation stays below the fixed threshold value of $\tau = 25\%$.

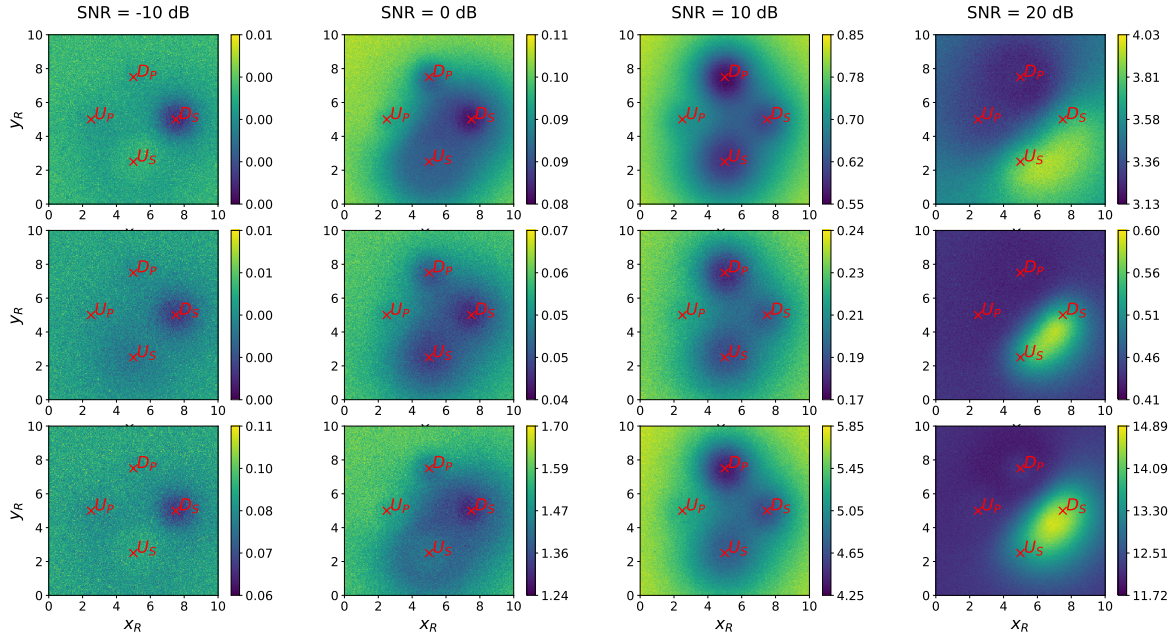

Figure 5.11: Impact of the relay position for CF relaying.
Top plots: average total power (W); middle: average secondary rate (bpcu); bottom: average primary rate degradation (%).

Since none of the two relaying schemes performs best for all network configurations, as expected from an information point of view, we now investigate the problem of relaying scheme selection and we propose two different approaches to choose among CF and DF. In our cognitive radio setting, we focus here the relay scheme selection on protecting the primary network, which of course may be at the cost of secondary achievable rate.

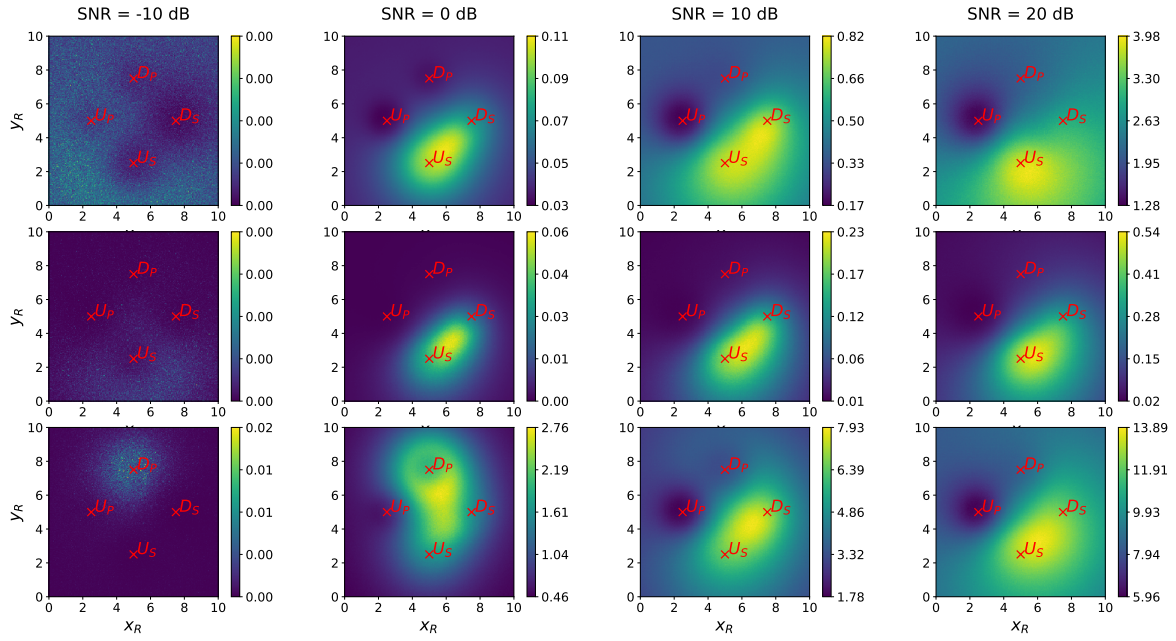

Figure 5.12: Impact of the relay position for DF relaying.
Top plots: average total power (W); middle: average secondary rate (bpcu); bottom: average primary rate degradation (%).

5.4.2 Two DNN-based method

Usually, relaying scheme selection consists in choosing the relaying scheme achieving the largest SNR [85], [135]. Such a criterion is well-suited for many communication setups but not for cognitive radio where one should protect the primary transmission. To simplify the presentation, let Δ_ℓ^{CF} and Δ_ℓ^{DF} denote the degradation of the primary rate caused by the opportunistic transmission under CF and DF respectively obtained by our proposed DNNs presented in Section 5.4.1 for the ℓ-th data sample. In the following, we propose to explicitly incorporate the primary rate degradation within our selection criterion.

In order to choose between CF and DF, we compare the two degradation of the primary rate Δ_ℓ^{CF} and Δ_ℓ^{DF}. If both relaying schemes meet the QoS constraint, i.e. $\Delta_\ell^{CF}, \Delta_\ell^{DF} \leq \tau$, then we choose the relaying scheme yielding the largest secondary rate. If only one of the relaying scheme meets the QoS constraint, then we choose this scheme; otherwise we choose the relaying scheme exhibiting the smallest primary rate degradation. Hence, we put more emphasis on meeting the primary QoS constraint, at the cost of the secondary rate.

5.4.3 Extra DNN-based method

We now introduce a novel supervised DNN-based relaying scheme selection, where a DNN takes as inputs the imperfect channel estimations as well as the corresponding optimal powers under both DF and CF computed by the DNNs presented in Section 5.4.1 and outputs the best relaying scheme. Our intuition is that, whereas the previously presented heuristic approach only exploits DNNs specifically trained for either DF or CF, an additional DNN could improve the two aforementioned DNNs by learning some correlation between the channel gains and

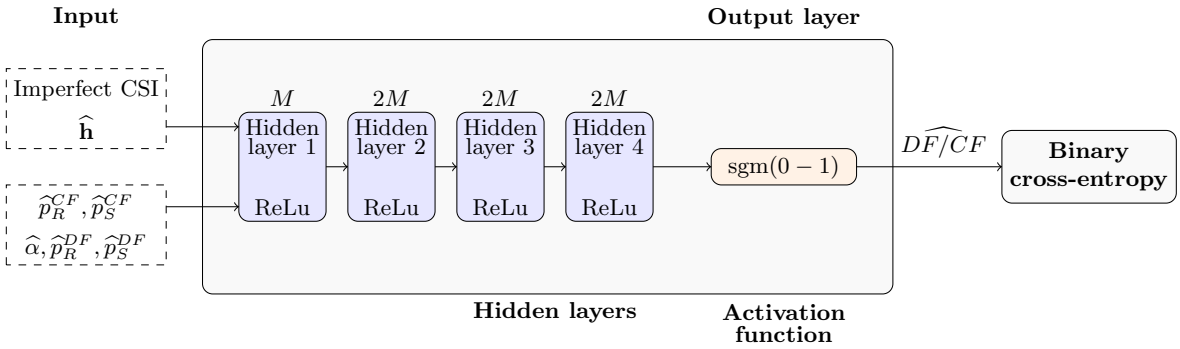

Figure 5.13: Proposed DNN architecture to choose among CF and DF which relaying scheme should be performed.

the best relaying scheme.

We hence consider a binary classification problem, for which the binary cross-entropy, given below, is usually used as loss function:

$$\mathcal{L} = -\frac{1}{L}\sum_{i=1}^{L} y_i \log \hat{y}_i + (1 - y_i)\log(1 - \hat{y}_i), \tag{5.5}$$

where L is the number of available training data, y_i corresponds to the ground-truth best relaying scheme (0 stands for CF and 1 for DF) obtained by the naive approach, and $\hat{y}_i$ is the probability of selecting DF computed and outputted by the DNN under perfect CSI. The architecture of the considered DNN for relaying selection, depicted in Figure 5.13, is the same as previously for solving the power allocation problem, but we here increase the number of neurons M to $M = 256$ as we found this value to achieve good performance throughout extensive numerical simulations. Also, the final layer consists here in a sigmoid activation function outputting the probability $\hat{y}_i$ of selecting DF; the later is then compared to a threshold, set either to 0.5 or to a cognitive radio-tailored one allowing to minimize the average primary degradation when in outage Δ_{out}, to decide whether DF or CF should be selected.

5.4.4 Numerical results

Dataset The training set contains 10^7 samples of imperfect channel estimation $\widehat{\mathbf{h}}_\ell$, the associated optimal powers obtained via the DNN under our proposed robust training presented in Section 5.4.1, as well as the corresponding best relaying scheme obtained via our two DNN-based method. The validation set contains 2×10^5 samples of imperfect channel estimation $\widehat{\mathbf{h}}_\ell$ as well as the associated optimal powers; and our test set contains 2×10^6 samples of imperfect channel estimation with the corresponding optimal powers and best relaying scheme as ground truth, enabling to assess the performance of our proposed DNN-based relaying scheme selection approach.

DNN training In the training phase, the optimal relaying scheme computed via our two DNN-based method is fed to the loss function $\mathcal{L}$ given in (5.5), whereas the imperfect channel

estimations and the corresponding optimal powers under both DF and CF are given as input to our DNN. Note that the training process is restarted for each value of the considered SNR of the CSI estimator. Here, we use early stopping with a patience parameter of 10 epochs for both DF and CF to avoid any overfitting effect.

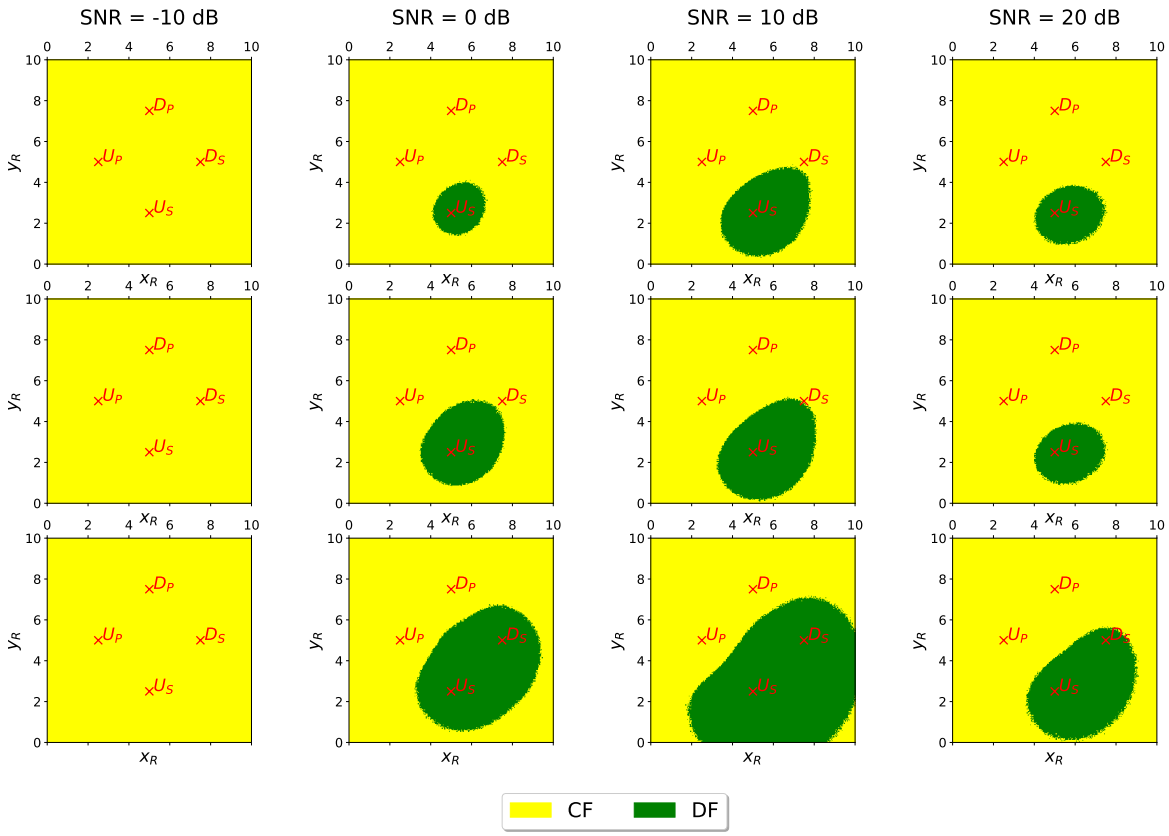

Figure 5.14: Chosen relaying scheme when the relay position ranges all over the cell under the two DNN-based method (top), the extra DNN-based one with fixed threshold of 0.5 (middle) and the extra DNN-based one with radio cognitive-tailored threshold (bottom)

Figure 5.14 shows the chosen relaying scheme as a function of the relay position under the two DNN-based method, the 0.5 fixed-threshold extra DNN-based one, denoted as 'Extra DNN', as well as the cognitive-radio tailored threshold extra DNN-based one, denoted as 'Extra DNN-S', for different levels of CSI estimation respectively. Here we assume that the position of the primary and secondary users and destinations are fixed, whereas the relay can be placed anywhere within the square cell. First, we can note that, regardless of the quality of the CSI estimation, CF is selected more often than DF under all approaches. Furthermore, as expected from a cooperative communications point of view, DF is more efficient when the relay is close to the secondary user, which can be observed for all CSI estimation between $[0 - 20]$dB under both the fixed-threshold extra DNN and the two DNN-based methods. Note that under the cognitive radio tailored threshold extra-DNN method, the set of relay positions where DF is chosen also contains positions where the relay is close to the secondary destination, for which the achievable data rate under DF is not expected to be large. The intuition is that, under this method, we choose the relaying scheme which degrades the less

the primary transmission. Indeed, for these relay positions, CF achieves higher rates than DF by also consuming more power, leading hence to larger primary degradation. Finally, under all approaches, CF is almost always chosen in very poor CSI estimation conditions, irrespective from the position of the relay. DF seems indeed to be more sensitive to imperfect CSI, since the relay needs to correctly decode the secondary message; when it only quantizes the received signal under CF.

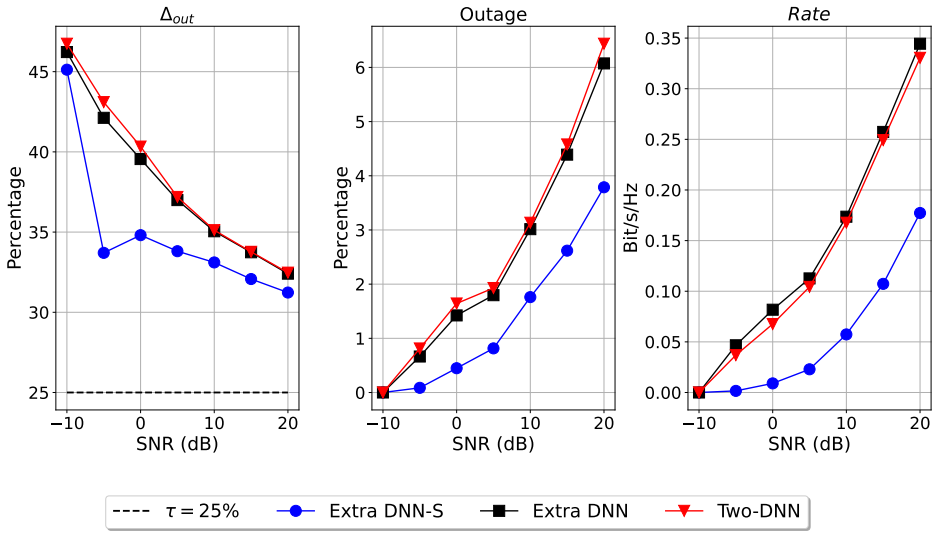

Figure 5.15: Average degradation when in outage, outage and secondary rate as functions of SNR over the test set

In Figure 5.15, we compare the two DNN-based method to the two extra DNN-based ones, with either the threshold set to 0.5, denoted as 'Extra DNN' or to the cognitive radio-tailored one denoted as 'Extra DNN-S', in terms of primary rate degradation when in outage Δ_{out}, percentage of outage and secondary rate for different CSI estimations SNR. First, the proposed two DNN-based method and the fixed threshold extra DNN-based one achieve more or less the same performance, meaning that there was little additional relation to be learned between the channel gains and the best relaying scheme. This highlights the strength of our proposed robust DNN-based power allocation scheme for a fixed relaying scheme. The almost zero-gap between the two DNN-based method and the fixed-threshold extra DNN-based one follows also from the fact that each of the two relaying schemes performs best for disjoint positions of the relay with respect to all other nodes. Nonetheless, choosing for each CSI quality the threshold minimizing the primary rate degradation when in outage significantly increases the performance from a cognitive radio point of view: the number of outage is divided by a factor of almost 2 for all values of SNR $\in [-10, 20]$dB, whereas the primary degradation when in average is decreased by up to 8% especially under poor channel estimation. This increase in terms of primary communication protection comes of course at the cost of the secondary rate, which in decreased by half, as shown in Figure 5.15. Further, using a third DNN allows to generalize over which criterion the relaying scheme should be selected: we here presented the extreme case where the decision was solely based on the minimization of the primary rate degradation when in outage, but one could instead consider

any tradeoff weighting between the secondary rate and primary protection instead, which is not feasible under the two DNN-based method.

5.5 Conclusions and perspectives

In this chapter we studied a full-duplex cooperative cognitive network under two relaying schemes, namely Decode-and-Forward and Compress-and-Forward. We first derived the achievable rate regions and then the optimal power allocation policies under both individual power constraints and a QoS constraint protecting the primary transmission.

Under CF and perfect CSI, the optimal power allocation policy was provided in closed-form, whereas under DF, due to the resulting non-linear and non-convex optimization problem, we proposed an unsupervised deep learning based solution. The later was further rendered robust to errors in channel estimation, and also used for CF under imperfect CSI. Finally, we proposed a new DNN-based relaying selection method exploiting a cognitive radio tailored threshold at the classifier output allowing to minimize the average primary rate degradation when in outage.

While all system parameters such as the maximum allowed primary rate degradation τ, as well as the power budget within the secondary network $\overline{P_R}$ and $\overline{P_S}$ were fixed and known by our proposed DNN, it would be an interesting research direction to relax this assumption and consider some DNN-based approaches able to generalize over variation of the later within a given range.

The next and final chapter of this HDR manuscript presents an overall discussion of interesting open issues and prospective research directions.

Chapter 6

Open issues and perspectives

In this chapter, we discuss some open research directions, starting with some short- to mid-term perspectives and ending with long-term ones regarding beyond 5G wireless networks.

In the recent years, the concepts of Internet of Things and Internet of Everything are gaining momentum [136]. Currently, million of sensors and communicating devices are already deployed in cities, homes, wearables, etc. and this number is expected to experience an explosive growth, reaching several billion by 2030 [137]. Exploiting these widely deployed sensors, smart homes, smart cities, e-health, e-commerce, etc. are becoming reality. Hence, high-data rate with reliable communications, both in terms of latency and security are required. Although the 5-th generation (5G) of wireless networks brought improvement in terms of user connectivity and network throughput, it is expected not to be able to fulfill the demands of future intelligent and autonomous wireless networks [138], [139], paving hence the road to the 6-th generation (6G) of wireless networks. Beside the requirements already considered in 5G, such as network densification, increased throughput, massive user connectivity, high reliability and energy efficiency, 6G will lead to the emergence of new requirements, such as handling massive volumes of data, artificial intelligence (AI) integrated communication, enhanced security, etc. Furthermore, compared to 5G, 6G has stricter requirement in terms of energy-efficiency, latency, reliability, security [140]. Various candidate technologies have thus already been proposed to overcome the bottleneck of 5G to meet the bold 6G requirements, such as artificial intelligence, full-duplex, intelligent reflecting surfaces (IRS), sub-THz and visible light communication, simultaneous wireless information and power transfer (SWIPT), physical layer security and blockchains, etc. [140].

Intelligent Reflecting Surfaces (IRS), backscattering

Intelligent Reflecting Surfaces (IRS) is a very promising technology capable of enhancing the network energy-efficiency while improving the achievable data rates. IRS are two dimensional arrays of low-cost passive elements that do not require a specific energy source to operate and which are able to reflect the ambient RF signals in a full-duplex manner without any self-interference. By carefully adjusting the reflection coefficients, the reflected signals coherently add at the destination without additional noise [141], [142], enhancing hence the network throughput. For instance, we showed in Chapter 4 that including one backscattering

device, which is a special case of IRS, enhances the energy-efficiency of the network compared to the case without backscattering.

Simultaneous wireless information and power transfer (SWIPT)

One of the bottleneck of the future autonomous wireless networks, in which a large number of smart devices need to communicate at anytime, is the lifetime of batteries, especially if the later can hardly be replaced. SWIPT is among the most promising techniques to improve the lifetime of energy-constrained networks by exploiting the RF waves for both wireless power transfer and information transfer. Using this approach, some energy can be harvested through the received RF signals and then used to fulfill some power efficiency requirements.

SWIPT can be implemented in different manners, the two more common being time-switching and power splitting [140]. Under time-switching, the system harvests energy for a given fraction of the time-slot, whereas the remaining part is used for information transfer. Under the power splitting mode, a fraction of the received signal is used for energy harvested during the entire time-slot. Of course, the fraction in time or in power that is used for harvesting should be optimized, enabling the system to best perform both in terms of system throughput and energy efficiency.

Artificial intelligence (AI)

Due to the blend of various technologies deployed to reach the requirements of 6G, as well as to the large number of communicating devices, it is very unlikely to obtain closed-form network optimization [139]. Machine learning techniques are hence expected to play a vital role in future wireless communication networks, especially when the later is too complicated to be optimized by humans as for instance for joint optimization in network design, resource allocation and management, etc. For instance, we showed in Chapter 5, that even for a simple cooperative cognitive radio network composed only by one primary and secondary communication link and a full-duplex operating relay node, maximizing the opportunistic rate under some QoS and power budget constraints is not-convex and we turned to deep learning techniques to solve it. Since 6G networks are expected to be more complicated ones, considering for instance many nodes, AI is among the most important characteristic of 6G networks.

Whereas most of the current AI deployed in wireless networks is based on centralized computations, it is expected that the intelligence within future wireless networks will be implemented at the users end. As such, unsupervised learning or reinforcement learning, which do not require labeling could be used to operate the network in an autonomous manner [139]; and federated learning, where users can train the models with only local data without sending them to a central server [140] could also be deployed.

Physical layer security

Since smart homes, smart cities, e-health, e-commerce etc. are gaining momentum within 6G applications, security, secrecy and privacy are vital features of future wireless networks.

The broadcast nature of wireless medium makes it vulnerable to several security threats,

such as eavesdropping or jamming. Both passive and active attacks threaten the physical layer: under passive attacks, the eavesdropper damages data confidentiality by monitoring the legitimate communication without affecting the data transmission, while under active attacks, the attacker directly harms the legitimate communication by either affecting the data availability, integrity or authenticity [140].

Although conventional cryptography-based security techniques are implemented in higher layers, they are becoming more vulnerable in the age of Big Data and AI. Physical layer security, on the other hand, is a promising solution exploiting some physical properties such as the noise, fading and interference to ensure secure communications [143]. The main idea is to distinguish the quality of the signal received by the legitimate users and by the eavesdropper. As long as the eavesdropper's channel quality is worse than the one of the legitimate users, secret communication can be achieved [143]. In this framework, the secrecy rate R^s is defined as the gap between the rate R_u achieved by the legitimate user and the rate R_e achieved by the eavesdropper: $R^s = \max\{R_u - R_e, 0\}$. Hence, as long as the legitimate users are closer to the base station, or the access point, than the eavesdropper, a non-zero secrecy rate can be achieved.

Let us now consider the blending of some of the above presented technologies, as well as some 5G enabling techniques such as NOMA, to simultaneously optimize various aspects of future wireless networks.

The first short- to mid-term perspective consists in combining physical layer security, NOMA, IRS, SWIPT and AI in order to maximize the secrecy energy efficiency of such a system.

6.1 Secrecy energy efficiency maximization for multi-user NOMA systems

While both energy efficiency and secrecy sum rate maximization under a total power budget and minimum QoS constraints have been studied for downlink multi-user NOMA [C11], [144], very few works can be found on secrecy energy efficiency maximization in the literature. To the best of our knowledge, [145] is the first work considering secrecy energy efficiency optimization in a downlink multi-user NOMA network, where the ratio between the secrecy sum rate and the power consumption is maximized. The optimal solution was not given in closed-form but relies on a numerical dichotomy-based method. Since studying efficiencies defined as a ratio can be more involved than considering scalarized one, we intend to first study the scalarized tradeoff between the achievable secrecy sum rate and the power consumption. Note that if the scalarized optimization problem is convex, the obtained solution can be used in Dinkelbach's algorithm to also optimize the ratio.

6.1.1 Secrecy energy efficiency maximization

Let us first consider a network composed of one base station or access point, K legitimate users and one passive eavesdropper. To cope with the possible large number of users to be served, NOMA is employed. Hence, the source sends the message X_i intended for each receiver $i \in \{1, \ldots, K\}$ with power p_i via superposition coding and broadcasts $X = \sum_{i=1}^{K} X_i$. We further denote by $\overline{P}$ the total power budget of the BS, such that $\sum_i p_i \leq \overline{P}$. Also, each user k is required to meet a QoS constraint expressed in terms of a minimum achievable rate of $R_{\min,k}$. At the receiver side, as well as at the eavesdropper side, SIC is employed to recover the messages. The received signal at user k and at the eavesdropper are respectively given as $Y_k = h_k X + Z_k$ and $Y_e = h_e X + Z_e$, where the additive noises are assumed to be Gaussian ones of variance σ_k^2 and σ_e^2 respectively. Without loss of generality, let us further assume that $M-1$ users out of the K served within the network experience poorer channel condition compared to the eavesdropper and that the channel gains are ordered as: $\frac{h_1^2}{\sigma_1^2} \leq ... \leq \frac{h_{M-1}^2}{\sigma_{M-1}^2} \leq \frac{h_e^2}{\sigma_e^2} < \frac{h_M^2}{\sigma_M^2} \leq ... \leq \frac{h_K^2}{\sigma_K^2}$. The achievable secrecy sum rate $SSR(\mathbf{p})$ is hence given as

$$SSR(\mathbf{p}) = \sum_{k=M}^{K} C\left(\frac{h_k^2 p_k}{h_k^2(p_{k+1}+\ldots+p_K)+\sigma_k^2}\right) - C\left(\frac{h_e^2 p_k}{h_e^2(p_{k+1}+\ldots+p_K)+\sigma_e^2}\right).$$

Let us consider the secrecy energy efficiency defined as the scalarized tradeoff between the achievable secrecy sum rate and the power consumption, which can be seen as an extension of the scalarized energy-efficiency metric without taking into account physical layer security: $SEE(\mathbf{p}) = SSR(\mathbf{p}) - \alpha\left(\sum_{k=1}^{K} p_k + P_c\right)$.

The optimization under study is hence given as

$$\begin{aligned}
&\max_{\mathbf{p}} \; SSR(\mathbf{p}) - \alpha\left(\sum_{k=1}^{K} p_k + P_c\right) \\
&\text{s.t.} \;\; \sum_{k=1}^{K} p_K \leq \overline{P}, && (TP) \\
&\qquad C\left(\frac{h_k^2 p_k}{h_k^2(p_{k+1}+\ldots+p_K)+\sigma_k^2}\right) \geq \; R_{\min,k}, \forall 1 \leq k \leq K && (QoS)
\end{aligned}$$

Solving this optimization problem will be the first objective of Miled Alam, a PhD student I am currently co-advising (40%) jointly with Giulia Cervia (50%), Laurent Clavier (5%, official co-director) and Sylvain Lecomte (5%, official co-director) within the project Beyond5G.

6.1.2 Backscattering enhanced communications and energy harvesting perspectives

In Chapter 4, we showed that including an ambient backscatter device increases the energy efficiency of a multi-user downlink NOMA transmission even when the backscatter device has its own data to transmit.

A mid-term objective within the project Beyond5G is to study the impact of backscattering in terms of secrecy energy efficiency and energy harvesting. Hence, the achievable secrecy rate region of such networks needs first to be investigated. Then, in a first step, the reflection coefficient and the power allocation could be jointly optimized without taking into account any energy harvesting consideration. Nonetheless, jointly optimizing the secrecy energy efficiency, the reflection coefficient and the amount of harvested energy is a very interesting problem allowing to move one step further towards networks autonomy. Note that SWIPT could also be considered instead of or jointly with backscattering to enhance the network autonomy [146], [147]. The resulting optimization problems, even without any consideration on the harvested part, are expected to be complex and non-convex, and as such may lead to the use of machine learning in their solving.

Another mid-term perspective within the PEPR 5G project is to consider IRS-enhanced multi-user NOMA networks. By carefully tuning the IRS, sufficient difference between the users' effective channel gains can be achieved, leading to cases where NOMA is known to outperform OMA [148]. Furthermore, in traditional NOMA systems, a large QoS minimum rate for a weak user usually leads to a network outage, whereas with IRS-enhanced NOMA, the users' effective channel gains can be modified and arranged such that users with large QoS requirements experience large effective channel gains, decreasing hence the probability of outage [149]. As such, we intend to first derive the achievable rate regions of such networks and then to develop efficient algorithms that jointly tune the transmit strategy (power allocation, assignment of users over carriers) and the backscattering/IRS strategy (reflection coefficients, energy harvesting).

Another mid-term perspective relies in blending AI and security to jointly detect and localize some security attacks in indoor and outdoor setups.

6.2 Artificial intelligence for security attack detection and localization

Due to the broadcast nature of the wireless medium, beside passive attacks such as eavesdropping, many active attacks, such as jamming, spoofing, man-in-the-middle or denial of service (DoS), threaten the wireless networks [150]–[152]. For instance, under jamming, legitimate transmissions get overwhelmed by artificial radio signal, preventing legitimate receivers from decoding their intended signals. On the other hand, under spoofing, instead of degrading the quality of legitimate signals, the adversary mimics the transmissions from a legitimate user at the physical layer for instance to emulate a primary user in cognitive setups, or to intrude some private network. Under man-in-the-middle, the adversary expropriates the legitimate transmitted signals in order to modify or delete them prior to forwarding them to the legitimate receivers; whereas under DoS attacks, the legitimate users are denied access to networks resources. Hence, it is of most importance to detect such attacks and if possible to localize the attackers to enable the networks to correctly operate. The project DEPOSIA tackles such security threats by using AI to detect 'non-usual' situations which are expected

to be attacks. The goals of this project are three-fold: the first objective is to detect an illicit RF source by developing new network monitoring architecture, the second one is to develop an AI able to detect the presence of an attack, whereas the last one is to develop an AI able to geo-localize the attacker. In the later two objectives, the attacker denotes any illicit source, as for instance a drone in outdoor environments or any non-authorized device within a given area. This study will take place both in indoor and outdoor environments, each of these cases leading to specific monitoring architectures and AI solutions.

The next Section presents a long term perspective investigating the interaction between distributed learning, and more specifically federated learning, and information theory in multi-user cooperative networks.

6.3 Interplay between federated learning and information theory in multi-user cooperative networks

Moving toward distributed learning to solve resource allocation problems in future multi-user networks seems a rather natural move. Due to the current and future user densification, as well as to spectrum scarcity, simple cooperative cognitive radio networks composed of one primary and secondary communication link as well as only one relay node as studied in Chapter 5 are expected to grow, by including multiple primary, secondary and helping relay nodes. Although the optimal solution can be obtained in a centralized manner, gathering all required data at a single server or node will become very time- and resource-consuming, especially in larger networks. Hence, distributed deep learning, such as federated learning [153], where each of the users and relay computes locally its own transmission parameters (both the optimal relaying scheme to be performed and the optimal power allocation) seems to be an interesting solution provided that the considered optimization problem can be decoupled into several local optimization problems.

In contrast to traditional machine learning, federated learning does not require users to send their data to a centralized server for training: under federated learning, each end-device learns a local model given its own learning data, after which it sends its local learning model parameters, i.e. weight and gradient parameters, to the server for global model aggregation. Finally, the global model parameters are sent back to each end-device [137].

Nonetheless, considering distributed approaches poses severe challenges in terms of privacy and security. Although raw data are not forwarded to some central node, and hence stay at the device end, sharing learning model parameters such as gradients leads to information leakage, since it can be used to reconstruct users' training data [154], [155]. Differential privacy recently attracted attention in federated learning to guarantee users' privacy [156] since it allows to analyze a dataset without reveling individual private information by adding some noise to either statistical queries or the original data itself. Of course, the larger the amount of added noise, the better the privacy but the lower the accuracy. Hence questions such as finding the optimal privacy budget to achieve both good accuracy and strong privacy protection or finding other variants of differential privacy are very interesting future

research paths that could benefit from information theory. The former seems somehow related to covert communications, where from an information theory point of view, the aim is to find the largest data rate achieving reliable communication in the sense of vanishing error probability and covertness, defined in terms of bounded Kullback-Leibler divergence or total variation, hence statistical metrics.

Bibliography

Our contributions

[C1] A. Savard and C. Weidmann, "Improved decoding for binary source coding with coded side information," in *IEEE ITW, Sevilla, Spain*, 2013.

[C2] A. Savard and C. Weidmann, "Optimized codes for the binary coded side-information problem," in *IEEE ISTC, Bremen, Germany*, 2014.

[C3] A. Savard and C. Weidmann, "On the multiway relay channel with direct links," in *IEEE ITW, Hobart, Australia*, 2014.

[C4] A. Savard and C. Weidmann, "Lattice coding for the Gaussian one- and two-way relay channels with correlated noises," in *IEEE ISIT, Hong-Kong*, 2015.

[J1] A. Savard and C. Weidmann, "On the Gaussian multiway relay channel with intra-cluster links," *EURASIP Journal on Wireless Communications and Networking*, vol. 52, pp. 1–17, 2016.

[J3] Y. Mestrah, A. Savard, A. Goupil, G. Gellé, and L. Clavier, "An unsupervised LLR estimation with unknown noise distribution," *EURASIP Journal on Wireless Communications and Networking*, no. 26, pp. 1–11, 2020.

[C5] M. Egan, L. Clavier, M. de Freitas, L. Dorville, J. M. Gorce, and A. Savard, "Wireless communication in dynamic interference," in *IEEE Globecom, Singapour*, 2017.

[C7] Y. Mestrah, A. Savard, A. Goupil, L Clavier, and G. Gellé, "Blind estimation of an approximated likelihood ratio in impulsive environment," in *IEEE PIMRC, Bologna, Italy*, 2018.

[C9] Y. Mestrah, A. Savard, A. Goupil, G. Gellé, and L. Clavier, "Robust and simple log-likelihood approximation for receiver design," in *IEEE WCNC, Marrakech, Morocco*, 2019.

[C10] M. de Freitas, M. Egan, L. Clavier, A. Savard, and J. M. Gorce, "Power control in parallel symmetric α-stable noise channels," in *IEEE SPAWC, Cannes, France*, 2019.

[C15] Y. Mestrah, D. Anade, A. Savard, A. Goupil, M. Egan, P. Mary, J. M. Gorce, and L. Clavier, "Unsupervised log-likelihood ratio parameter estimation for short LDPC packets in impulsive noise," in *IEEE WCNC, Austin, USA*, 2022.

[J7 sub] S. Gelincik, P. Mary, A. Savard, and J. Baudais, "A pre-transformation method to increase the minimum distance of polar-like codes," *sub. to IEEE Trans. Commun.*, 2022.

[C17] S. Gelincik, P. Mary, J. Baudais, and A. Savard, "Achieving PAC code performance with SCL decoding without extra computational complexity," in *IEEE ICC, Seoul, South Korea*, 2022.

[C18] S. Gelincik, P. Mary, A. Savard, and J. Baudais, "Preserving the minimum distance of polar-like codes while increasing the information length," in *IEEE ISIT, Espoo, Finland*, 2022.

[J2] M. Tahmasbi, A. Savard, and M. R. Bloch, "Covert capacity of non-coherent rayleigh-fading channels," *IEEE Trans. Inf. Theory*, vol. 66, no. 4, pp. 1979–2005, 2020.

[J5] H. El Hassani, A. Savard, and E. V. Belmega, "Adaptive NOMA in time-varying wireless networks with no CSIT/CDIT relying on a 1-bit feedback," *IEEE Wireless Commun. Lett.*, vol. 10, no. 4, pp. 750–754, 2021.

[J6] H. El Hassani, A. Savard, E. V. Belmega, and R. de Lamare, "Multi-user downlink NOMA systems aided by an ambient backscatter device: Achievable rate region and energy-efficiency maximization," *IEEE Trans. on Grenn. Commun. Netw.*, 2022.

[C11] H. El Hassani, A. Savard, and E. V. Belmega, "A closed-form solution for energy-efficiency optimization in multi-user downlink NOMA," in *IEEE PIMRC, London, UK*, 2020.

[C13] H. El Hassani, A. Savard, and E. V. Belmega, "Energy-efficient 1-bit feedback noma in wireless networks with no CSIT/CDIT," in *IEEE SSP Workshop, Rio de Janeiro, Brazil*, 2021.

[C14] H. El Hassani, A. Savard, E. V. Belmega, and R. de Lamare, "Energy-efficient cooperative backscattering closed-form solution for NOMA," in *IEEE Globecom, Madrid, Spain*, 2021.

[C20] H. El Hassani, A. Savard, E. V. Belmega, and R. de Lamare, "Energy-efficient solutions in two-user downlink NOMA systems aided by ambient backscattering," in *IEEE Globecom, Rio de Janeiro, Brazil*, 2022.

[J4] A. Savard and E. V. Belmega, "Full-duplex relaying for opportunistic spectrum access under an overall power constraint," *IEEE Access*, vol. 8, pp. 168262 –168 272, 2020.

[C16] Y. Benatia, A. Savard, R. Negrel, and E. V. Belmega, "Unsupervised deep learning to solve power allocation problems in cognitive relay networks," in *IEEE ICC, Workshop, Seoul, South Korea*, 2022.

[C19] Y. Benatia, R. Negrel, A. Savard, and E. V. Belmega, "Robustness to imperfect CSI of power allocation policies in cognitive relay networks," in *IEEE SPAWC, Oulu, Finland*, 2022.

[C12] A. Savard and E. V. Belmega, "Optimal power allocation policies in multi-hop cognitive radio networks," in *IEEE PIMRC, London, UK*, 2020.

[C8] A. Savard and E. V. Belmega, "Optimal power allocation in a relay-aided cognitive network," in *ACM EAI ValueTools, Palma de Mallorca, Spain*, 2019.

[C6] A. Savard and L. Clavier, "On the two-way diamond relay channel with lattice-based Compress-and-Forward," in *IEEE WCNC, Barcelona, Spain*, 2018.

[NC10] A. Savard and E. V. Belmega, "Achievable rate regions for cooperative cognitive radio networks with complex channels and circular normal additive noises," in *GRETSI, Nancy, France*, 2022.

[J8 prep] Y. Benatia, A. Savard, R. Negrel, and E. V. Belmega, "Robust DNN for power allocation problems in cognitive relay networks," *in preparation*, 2023.

[PhD] A. Savard, "Coding for cooperative communications: Topics in distributed source coding and relay channels," Ph.D. dissertation, University of Cergy-Pontoise, France, 2015.

Other references

[1] P. C. Pinto and M. Z. Win, "Communication in a Poisson field of interferers-part II: Channel capacity and interference spectrum," *IEEE Trans. Wireless Commun.*, vol. 9, no. 7, pp. 2187–2195, 2010.

[2] P. Cardieri, "Modeling interference in wireless ad hoc networks," *IEEE Commun. Surveys Tuts.*, vol. 12, no. 4, pp. 551–572, 2010.

[3] D. Middleton, I. of Electrical, and E. Engineers, *An introduction to statistical communication theory*. McGraw-Hill New York, 1960, vol. 960.

[4] D. Middleton, "Statistical-physical models of urban radio-noise environments-part I: Foundations," *IEEE Trans. Electromagn. Compat.*, no. 2, pp. 38–56, 1972.

[5] D. Middleton, "Statistical-physical models of electromagnetic interference," *IEEE Trans. Electromagn. Compat.*, no. 3, pp. 106–127, 1977.

[6] D Middleton, "Performance of telecommunications systems in the spectral-use environment. part 7: Interference scenarios and the canonical and quasi-canonical (first-order) probability models of class A interference," *NASA STI/Recon Technical Report N*, vol. 83, p. 13 353, 1982.

[7] N. Andreadou and F.-N. Pavlidou, "Modeling the noise on the OFDM power-line communications system," *IEEE Trans. Power Del.*, vol. 25, no. 1, pp. 150–157, 2009.

[8] H. Ishikawa, M. Itami, and K. Itoh, "A study on adaptive modulation of OFDM under middleton's class-A impulsive noise model," in *2007 Digest of Technical Papers International Conference on Consumer Electronics*, IEEE, 2007, pp. 1–2.

[9] M. Z. Win, P. C. Pinto, and L. A. Shepp, "A mathematical theory of network interference and its applications," *Proceedings of the IEEE*, vol. 97, no. 2, pp. 205–230, Feb 2009.

[10] M. Egan, L. Clavier, C. Zheng, M. de Freitas, and J. M. Gorce, "Dynamic interference for uplink SCMA in large-scale wireless networks without coordination," *EURASIP JWCN*, vol. 1, p. 213, 2018.

[11] L. Clavier, T. Pedersen, I. Larrad, M. Lauridsen, and M. Egan, "Experimental evidence for heavy tailed interference in the IoT," *IEEE Commun. Lett.*, vol. 25, no. 3, pp. 692–695, 2020.

[12] R. Gallager, "Low-density parity-check codes," *IRE Trans. on Inf. theory*, vol. 8, no. 1, pp. 21–28, 1962.

[13] D. J. MacKay and R. M. Neal, "Near shannon limit performance of low density parity check codes," *Electronics letters*, vol. 33, no. 6, pp. 457–458, 1997.

[14] D. J. MacKay, D. J. Mac Kay, *et al.*, *Information theory, inference and learning algorithms*. Cambridge university press, 2003.

[15] F. R. Kschischang, B. J. Frey, and H.-A. Loeliger, "Factor graphs and the sum-product algorithm," *IEEE Trans. Inf. Theory*, vol. 47, no. 2, pp. 498–519, 2001.

[16] R Tanner, "A recursive approach to low complexity codes," *IEEE Trans. Inf. Theory*, vol. 27, no. 5, pp. 533–547, 1981.

[17] S.-Y. Chung, G. D. Forney, T. J. Richardson, and R. Urbanke, "On the design of low-density parity-check codes within 0.0045 dB of the shannon limit," *IEEE Commun. Lett.*, vol. 5, no. 2, pp. 58–60, 2001.

[18] T. J. Richardson, M. A. Shokrollahi, and R. L. Urbanke, "Design of capacity-approaching irregular low-density parity-check codes," *IEEE Trans. Inf. Theory*, vol. 47, no. 2, pp. 619–637, 2001.

[19] Y. Fang, Y. Bu, P. Chen, F. C. Lau, and S. Al Otaibi, "Irregular-mapped protograph LDPC-coded modulation: A bandwidth-efficient solution for 6G-enabled mobile networks," *IEEE Trans. Intell. Transp. Syst.*, 2021.

[20] C. Tarver, M. Tonnemacher, H. Chen, J. Zhang, and J. R. Cavallaro, "GPU-based, LDPC decoding for 5G and beyond," *IEEE Open Journal of Circuits and Systems*, vol. 2, pp. 278–290, 2021.

[21] S. Ambike, J. Ilow, and D. Hatzinakos, "Detection for binary transmission in a mixture of Gaussian noise and impulsive noise modeled as an alpha-stable process," *IEEE Signal Process. Lett.*, vol. 1, no. 3, pp. 55–57, 1994.

[22] H. B. Mâad, A. Goupil, L. Clavier, and G. Gellé, "Clipping demapper for LDPC decoding in impulsive channel," *IEEE Commun. Lett.*, vol. 17, no. 5, pp. 968–971, 2013.

[23] V. Dimanche, A. Goupil, L. Clavier, and G. Gellé, "On detection method for soft iterative decoding in the presence of impulsive interference," *IEEE Commun. Lett.*, vol. 18, no. 6, pp. 945–948, 2014.

[24] I. A. Koutrouvelis, "An iterative procedure for the estimation of the parameters of stable laws: An iterative procedure for the estimation," *Communications in Statistics-Simulation and Computation*, vol. 10, no. 1, pp. 17–28, 1981.

[25] J. H. McCulloch, "Simple consistent estimators of stable distribution parameters," *Communications in Statistics-Simulation and Computation*, vol. 15, no. 4, pp. 1109–1136, 1986.

[26] V. Dimanche, A. Goupil, L. Clavier, and G. Gellé, "Estimation of an approximated likelihood ratio for iterative decoding in impulsive environment," in *2016 IEEE WCNC*, IEEE, 2016, pp. 1–6.

[27] R. Yazdani and M. Ardakani, "Linear LLR approximation for iterative decoding on wireless channels," *IEEE Trans. Commun.*, vol. 57, no. 11, pp. 3278–3287, Nov. 2009.

[28] T. J. Richardson and R. Urbkane, *Modern Coding Theory*. Cambridge University Press, 2008.

[29] Y. Polyanskiy, H. Poor, and S. Verdu, "Channel coding rate in the finiteblocklength regime," *IEEE Trans. Inf. Theory*, vol. 56, pp. 2307–2359, Dec. 2010.

[30] D. Anade, J.-M. Gorce, P. Mary, and S. M. Perlaza, "An upper bound on the error induced by saddlepoint approximations - applications to information theory," *Entropy*, vol. 22, no. 6, p. 690, 2020.

[31] *5G-PPP*, https://5g-ppp.eu/.

[32] F. Tariq, M. R. A. Khandaker, K. Wong, M. Imran, M. Bennis, and M. Debbah, "Speculative study on 6G," *arXiv preprint arXiv:1902.06700*, 2019.

[33] Z. Ding, X. Lei, G. K. Karagiannidis, R. Schober, J. Yuan, and V. K. Bhargava, "A survey on non-orthogonal multiple access for 5G networks: Research challenges and future trends," *IEEE J. Sel. Areas Commun.*, vol. 35, no. 10, pp. 2181–2195, 2017.

[34] Z. Ding, Z. Yang, P. Fan, and H. V. Poor, "On the performance of non-orthogonal multiple access in 5G systems with randomly deployed users," *IEEE Signal Process. Lett.*, vol. 21, no. 12, pp. 1501–1505, 2014.

[35] J. Choi, "Power allocation for max-sum rate and max-min rate proportional fairness in NOMA," *IEEE Commun. Lett.*, vol. 20, no. 10, pp. 2055–2058, 2016.

[36] Q. Wu, W. Chen, D. W. K. Ng, and R. Schober, "Spectral and energy-efficient wireless powered IoT networks: NOMA or TDMA?" *IEEE Trans. Veh. Technol.*, vol. 67, no. 7, pp. 6663–6667, 2018.

[37] D. Tse and P. Viswanath, *Fundamentals of wireless communication*. Cambridge university press, 2005.

[38] L. Dai, B. Wang, Y. Yuan, S. Han, I Chih-Lin, and Z. Wang, "Non-orthogonal multiple access for 5G: Solutions, challenges, opportunities, and future research trends," *IEEE Commun. Mag.*, vol. 53, no. 9, pp. 74–81, 2015.

[39] T. M. Cover and J. A. Thomas, *Elements of information theory*. John Wiley & Sons, 2012.

[40] A. El Gamal and Y.-H. Kim, *Network information theory*. Cambridge university press, 2011.

[41] V. Liu, A. Parks, V. Talla, S. Gollakota, D. Wetherall, and J. R. Smith, "Ambient backscatter: Wireless communication out of thin air," *ACM SIGCOMM Computer Communication Review*, vol. 43, no. 4, pp. 39–50, 2013.

[42] N. Van Huynh, D. T. Hoang, X. Lu, D. Niyato, P. Wang, and D. I. Kim, "Ambient backscatter communications: A contemporary survey," *IEEE Commun. Surveys Tuts.*, vol. 20, no. 4, pp. 2889–2922, 2018.

[43] G. Wang, F. Gao, R. Fan, and C. Tellambura, "Ambient backscatter communication systems: Detection and performance analysis," *IEEE Trans. Commun.*, vol. 64, no. 11, pp. 4836–4846, 2016.

[44] C. Boyer and S. Roy, "Backscatter communication and RFID: Coding, energy, and MIMO analysis," *IEEE Trans. Commun.*, vol. 62, no. 3, pp. 770–785, 2014.

[45] Y. Kokar, D.-T. Phan-Huy, R. Fara, K. Rachedi, A. Ourir, J. de Rosny, M. Di Renzo, J.-C. Prévotet, and M. Helard, "First experimental ambient backscatter communication using a compact reconfigurable tag antenna," in *IEEE Globecom Workshops*, 2019, pp. 1–6.

[46] C. Song, Y. Ding, A. Eid, J. G. Hester, X. He, R. Bahr, A. Georgiadis, G. Goussetis, and M. M. Tentzeris, "Advances in wirelessly powered backscatter communications: From antenna/RF circuitry design to printed flexible electronics," *Proceedings of the IEEE*, vol. 110, no. 1, pp. 171–192, 2021.

[47] Z. Ma, Z. Zhang, Z. Ding, P. Fan, and H. Li, "Key techniques for 5G wireless communications: Network architecture, physical layer, and MAC layer perspectives," *Science China Information Sciences*, vol. 58, no. 4, pp. 1–20, 2015.

[48] E. E. B. Olivo, D. P. M. Osorio, H. Alves, J. C. S. Santos Filho, and M. Latva-Aho, "Cognitive full-duplex Decode-and-Forward relaying networks with usable direct link and transmit-power constraints," *IEEE Access*, vol. 6, pp. 24 983–24 995, 2018.

[49] B. Zhong, Z. Zhang, X. Chai, Z. Pan, K. Long, and H. Cao, "Performance analysis for opportunistic full-duplex relay selection in underlay cognitive networks," *IEEE Trans. Veh. Technol.*, vol. 64, no. 10, pp. 4905–4910, 2015.

[50] Y. Deng, K. J. Kim, T. Q. Duong, M. Elkashlan, G. K. Karagiannidis, and A. Nallanathan, "Full-duplex spectrum sharing in cooperative single carrier systems," *IEEE Trans. on Cogn. Commun. Netw.*, vol. 2, no. 1, pp. 68–82, 2016.

[51] X.-T. Doan, N.-P. Nguyen, C. Yin, D. B. Da Costa, and T. Q. Duong, "Cognitive full-duplex relay networks under the peak interference power constraint of multiple primary users," *EURASIP JWCN*, vol. 2017, no. 1, pp. 1–10, 2017.

[52] E. E. B. Olivo, D. P. M. Osorio, H. Alves, J. C. S. Santos Filho, and M. Latva-aho, "An adaptive transmission scheme for cognitive Decode-and-Forward relaying networks: Half duplex, full duplex, or no cooperation," *IEEE Trans. Wireless Commun.*, vol. 15, no. 8, pp. 5586–5602, 2016.

[53] E. C. van der Meulen, "Three-terminal communication channels," *Adv. Appl. Prob.*, vol. 3, pp. 120–154, 1971.

[54] E. V. Belmega, S. Lasaulce, and M. Debbah, "Capacity of cooperative channels: Three terminals case study," *Book Chapter in "Cooperative Wireless Communications"*, 2009.

[55] T. M. Cover and A. E. El Gamal, "Capacity theorems for the relay channel," *IEEE Trans. Inf. Theory*, vol. 25, no. 5, pp. 572–584, Sept. 1979.

[56] B. Rankov and A. Wittneben, "Achievable rate regions for the two-way relay channel," *IEEE ISIT*, 2006.

[57] E. V. Belmega, B. Djeumou, and S. Lasaulce, "Power allocation games in interference relay channels: Existence analysis of Nash equilibria," *EURASIP JWCN*, 2010.

[58] O. Sahin and E. Erkip, "Achievable rates for the gaussian interference relay channel," in *IEEE GLOBECOM*, 2007.

[59] M. Di Renzo, K. Ntontin, J. Song, F. H. Danufane, X. Qian, F. Lazarakis, J. De Rosny, D.-T. Phan-Huy, O. Simeone, R. Zhang, *et al.*, "Reconfigurable intelligent surfaces vs. relaying: Differences, similarities, and performance comparison," *IEEE Open J. Commun. Soc.*, vol. 1, pp. 798–807, 2020.

[60] A. Goldsmith, S. A. Jafar, I. Maric, and S. Srinivasa, "Breaking spectrum gridlock with cognitive radios: An information theoretic perspective," *Proceedings of the IEEE*, vol. 97, no. 5, pp. 894–914, 2009.

[61] F. Zhou, Y. Wu, Y.-C. Liang, Z. Li, Y. Wang, and K.-K. Wong, "State of the art, taxonomy, and open issues on cognitive radio networks with NOMA," *IEEE Wireless Commun.*, vol. 25, no. 2, pp. 100–108, 2018.

[62] R. Masmoudi, E. V. Belmega, and I. Fijalkow, "Efficient spectrum scheduling and power management for opportunistic users," *EURASIP JWCN*, 2016.

[63] R. Masmoudi, E. V. Belmega, I. Fijalkow, and N. Sellami, "A unifying view on energy-efficiency metrics in cognitive radio channels," in *IEEE EUSIPCO*, 2014, pp. 171–175.

[64] C. Isheden, Z. Chong, E. Jorswieck, and G. Fettweis, "Framework for link-level energy efficiency optimization with informed transmitter," *IEEE Trans. Wireless Commun.*, vol. 11, no. 8, pp. 2946–2957, 2012.

[65] S. Boyd and L. Vandenberghe, *Convex optimization*. Cambridge university press, 2004.

[66] A. Zappone and E. Jorswieck, "Energy efficiency in wireless networks via fractional programming theory," *Foundations and Trends in Commun. and Inf. Theory*, vol. 11, no. 3-4, pp. 185–396, 2015.

[67] R. S. Prabhu and B. Daneshrad, "An energy-efficient water-filling algorithm for OFDM systems," in *2010 IEEE International Conference on Communications*, IEEE, 2010, pp. 1–5.

[68] W. Dinkelbach, "On nonlinear fractional programming," *Management science*, vol. 13, no. 7, pp. 492–498, 1967.

[69] R. Jagannathan, "On some properties of programming problems in parametric form pertaining to fractional programming," *Management Science*, vol. 12, no. 7, pp. 609–615, 1966.

[70] R. S. Sutton and A. G. Barto, *Reinforcement learning: An introduction*. MIT press, 2018.

[71] E. V. Belmega, P. Mertikopoulos, and R. Negrel, "Online convex optimization in wireless networks and beyond: The feedback-performance trade-off," in *RAWNET 2022-International Workshop on Resource Allocation and Cooperation in Wireless Networks*, 2022, pp. 1–8.

[72] S. Bubeck and N. Cesa-Bianchi, "Regret analysis of stochastic and nonstochastic multi-armed bandit problems," *arXiv preprint arXiv:1204.5721*, 2012.

[73] T. L. Lai and H. Robbins, "Asymptotically efficient adaptive allocation rules," *Advances in applied mathematics*, vol. 6, no. 1, pp. 4–22, 1985.

[74] P. Auer, N. Cesa-Bianchi, Y. Freund, and R. E. Schapire, "Gambling in a rigged casino: The adversarial multi-armed bandit problem," in *Proc. of IEEE 36th Annual Foundations of Computer Science*, 1995, pp. 322–331.

[75] S. Pouyanfar, S. Sadiq, Y. Yan, H. Tian, Y. Tao, M. P. Reyes, M.-L. Shyu, S.-C. Chen, and S. S. Iyengar, "A survey on deep learning: Algorithms, techniques, and applications," *ACM Computing Surveys (CSUR)*, vol. 51, no. 5, pp. 1–36, 2018.

[76] A. Zappone, M. Di Renzo, and M. Debbah, "Wireless networks design in the era of deep learning: Model-based, ai-based, or both?" *IEEE Transactions on Communications*, vol. 67, no. 10, pp. 7331–7376, 2019.

[77] F. Zhou, X. Zhang, R. Q. Hu, A. Papathanassiou, and W. Meng, "Resource allocation based on deep neural networks for cognitive radio networks," in *IEEE ICCC*, 2018, pp. 40–45.

[78] W. Lee, "Resource allocation for multi-channel underlay cognitive radio network based on deep neural network," *IEEE Commun. Lett.*, vol. 22, no. 9, pp. 1942–1945, 2018.

[79] W. Lee, "Resource allocation for multi-channel underlay cognitive radio network based on deep neural network," *IEEE Commun. Lett.*, vol. 22, no. 9, pp. 1942–1945, 2018.

[80] W. Lee and K. Lee, "Deep learning-aided distributed transmit power control for underlay cognitive radio network," *IEEE Trans. Veh. Technol.*, vol. 70, no. 4, pp. 3990–3994, 2021.

[81] Y.-y. Guo, J. Yang, X.-l. Tan, and Q. Liu, "An energy-efficiency multi-relay selection and power allocation based on deep neural network for Amplify-and-Forward cooperative transmission," *IEEE Wireless Commun. Lett.*, 2021.

[82] A. Abdelreheem, O. A. Omer, H. Esmaiel, and U. S. Mohamed, "Deep learning-based relay selection in d2d millimeter wave communications," in *2019 International Conference on Computer and Information Sciences (ICCIS)*, IEEE, 2019, pp. 1–5.

[83] S. Aldossari and K.-C. Chen, "Relay selection for 5g new radio via artificial neural networks," in *2019 22nd International Symposium on Wireless Personal Multimedia Communications (WPMC)*, IEEE, 2019, pp. 1–5.

[84] T.-V. Nguyen, T. Huynh-The, and B. An, "A deep cnn-based relay selection in eh full-duplex iot networks with short-packet communications," in *ICC 2021 - IEEE International Conference on Communications*, 2021, pp. 1–6. DOI: 10.1109/ICC42927.2021.9500787.

[85] T. T. Duy and H. Y. Kong, "Performance analysis of mixed Amplify-and-Forward and Decode-and-Forward protocol in underlay cognitive networks," *China Communications*, vol. 13, no. 3, pp. 115–126, 2016.

[86] D. P. Setiawan and H.-A. Zhao, "Performance analysis of hybrid af and df protocol for relay networks," in *2017 International Conference on Control, Electronics, Renewable Energy and Communications (ICCREC)*, IEEE, 2017, pp. 207–211.

[87] M. Vaezi, Z. Ding, and H. V. Poor, *Multiple access techniques for 5G wireless networks and beyond*. Springer, 2019, vol. 159.

[88] Y. Saito, Y. Kishiyama, A. Benjebbour, T. Nakamura, A. Li, and K. Higuchi, "Non-orthogonal multiple access (NOMA) for cellular future radio access," in *IEEE VTC Spring*, 2013, pp. 1–5.

[89] P. Li, R. C. De Lamare, and R. Fa, "Multiple feedback successive interference cancellation detection for multiuser MIMO systems," *IEEE Trans. Wireless Commun.*, vol. 10, no. 8, pp. 2434–2439, 2011.

[90] W. U. Khan, X. Li, M. Zeng, and O. A. Dobre, "Backscatter-enabled NOMA for future 6G systems: A new optimization framework under imperfect SIC," *IEEE Commun. Lett.*, vol. 25, no. 5, pp. 1669–1672, 2021.

[91] Y. Xu, Z. Qin, G. Gui, H. Gacanin, H. Sari, and F. Adachi, "Energy efficiency maximization in NOMA enabled backscatter communications with QoS guarantee," *IEEE Wireless Commun. Lett.*, vol. 10, no. 2, pp. 353–357, 2020.

[92] S. Zhou, W. Xu, K. Wang, C. Pan, M.-S. Alouini, and A. Nallanathan, "Ergodic rate analysis of cooperative ambient backscatter communication," *IEEE Wireless Commun. Lett.*, vol. 8, no. 6, pp. 1679–1682, 2019.

[93] B. Lyu, C. You, Z. Yang, and G. Gui, "The optimal control policy for RF-powered backscatter communication networks," *IEEE Trans. Veh. Technol.*, vol. 67, no. 3, pp. 2804–2808, 2017.

[94] Y. Ye, L. Shi, R. Qingyang Hu, and G. Lu, "Energy-efficient resource allocation for wirelessly powered backscatter communications," *IEEE Commun. Lett.*, vol. 23, no. 8, pp. 1418–1422, 2019.

[95] X. Kang, Y.-C. Liang, and J. Yang, "Riding on the primary: A new spectrum sharing paradigm for wireless-powered iot devices," *IEEE Trans. Wireless Commun.*, vol. 17, no. 9, pp. 6335–6347, 2018.

[96] S. Gong, X. Huang, J. Xu, W. Liu, P. Wang, and D. Niyato, "Backscatter relay communications powered by wireless energy beamforming," *IEEE Trans. Commun.*, vol. 66, no. 7, pp. 3187–3200, 2018.

[97] W. U. Khan, M. A. Javed, T. N. Nguyen, S. Khan, and B. M. Elhalawany, "Energy-efficient resource allocation for 6G backscatter-enabled NOMA IoV networks," *IEEE Trans. Intell. Transp. Syst.*, 2021.

[98] J. K. Devineni and H. S. Dhillon, "Ambient backscatter systems: Exact average bit error rate under fading channels," *IEEE Trans. Green Commun. Netw.*, vol. 3, no. 1, pp. 11–25, 2018.

[99] X. Jia and X. Zhou, "Performance characterization of relaying using backscatter devices," *IEEE Open J. Commun. Soc.*, vol. 1, pp. 819–834, 2020.

[100] J. Qian, F. Gao, G. Wang, S. Jin, and H. Zhu, "Noncoherent detections for ambient backscatter system," *IEEE Trans. Wireless Commun.*, vol. 16, no. 3, pp. 1412–1422, 2016.

[101] W. Liu, Y.-C. Liang, Y. Li, and B. Vucetic, "Backscatter multiplicative multiple-access systems: Fundamental limits and practical design," *IEEE Trans. Wireless Commun.*, vol. 17, no. 9, pp. 5713–5728, 2018.

[102] W. U. Khan, F. Jameel, T. Ristaniemi, S. Khan, G. A. S. Sidhu, and J. Liu, "Joint spectral and energy efficiency optimization for downlink NOMA networks," *IEEE Trans. on Cogn. Commun. Netw.*, vol. 6, no. 2, pp. 645–656, 2019.

[103] Z. Ding, R. Schober, and H. V. Poor, "Unveiling the importance of SIC in NOMA systems—part II: New results and future directions," *IEEE Commun. Lett.*, vol. 24, no. 11, pp. 2378–2382, 2020.

[104] B. Makki, K. Chitti, A. Behravan, and M.-S. Alouini, "A survey of NOMA: Current status and open research challenges," *IEEE Open J. Commun. Soc.*, vol. 1, pp. 179–189, 2020.

[105] J. Tang, J. Luo, M. Liu, D. K. So, E. Alsusa, G. Chen, K.-K. Wong, and J. A. Chambers, "Energy efficiency optimization for NOMA with SWIPT," *IEEE J. Sel. Topics Signal Process.*, vol. 13, no. 3, pp. 452–466, 2019.

[106] W. Chen, H. Ding, S. Wang, D. B. da Costa, F. Gong, and P. H. J. Nardelli, "Backscatter cooperation in NOMA communications systems," *IEEE Trans. Wireless Commun.*, vol. 20, no. 6, pp. 3458–3474, 2021.

[107] S. Zeb, Q. Abbas, S. A. Hassan, A. Mahmood, R. Mumtaz, S. M. Hassan Zaidi, S. Ali Raza Zaidi, and M. Gidlund, "NOMA Enhanced Backscatter Communication for Green IoT Networks," in *ISWCS*, 2019, pp. 640–644.

[108] A. W. Nazar, S. A. Hassan, and H. Jung, "BER analysis of a NOMA Enhanced Backscatter Communication System," in *IEEE GLOBECOM*, 2020, pp. 1–6.

[109] A. W. Nazar, S. A. Hassan, H. Jung, A. Mahmood, and M. Gidlund, "BER analysis of a backscatter communication system with non-orthogonal multiple access," *IEEE Trans. Green Commun. Netw.*, vol. 5, no. 2, pp. 574–586, 2021.

[110] G. Lee, M. Jung, A. T. Z. Kasgari, W. Saad, and M. Bennis, "Deep reinforcement learning for energy-efficient networking with reconfigurable intelligent surfaces," in *IEEE ICC 2020*, IEEE, 2020, pp. 1–6.

[111] H. Zhang, J. Zhang, and K. Long, "Energy efficiency optimization for NOMA UAV network with imperfect CSI," *IEEE J. Sel. Areas Commun.*, vol. 38, no. 12, pp. 2798–2809, 2020.

[112] D. Ghosh, M. K. Hanawal, and N. Zlatanov, "Learning to optimize energy efficiency in energy harvesting wireless sensor networks," *arXiv preprint arXiv:2012.15203*, 2020.

[113] E. V. Belmega, P. Mertikopoulos, R. Negrel, and L. Sanguinetti, "Online convex optimization and no-regret learning: Algorithms, guarantees and applications," 2018.

[114] S. B. Mafra, H. Alves, D. B. Costa, R. D. Souza, E. M. Fernandez, and M. Latva-aho, "On the performance of cognitive full-duplex relaying under spectrum sharing constraints," *EURASIP JWCN*, vol. 2015, no. 1, p. 169, 2015.

[115] M. G. Khafagy, M.-S. Alouini, and S. Aissa, "Full-duplex opportunistic relay selection in future spectrum-sharing networks," in *2015 IEEE International Conference on Communication Workshop (ICCW)*, 2015.

[116] G. Kramer, M. Gastpar, and P. Gupta, "Cooperative strategies and capacity theorems for relay networks," *IEEE Trans. Inf. Theory*, vol. 51, no. 9, pp. 3037–3063, 2005.

[117] L. T. Tan, L. Ying, and D. W. Bliss, "Power allocation for full-duplex relay selection in underlay cognitive radio networks: Coherent versus non-coherent scenarios," *arXiv preprint arXiv:1703.01527*, 2017.

[118] Y. Shi, L. Zhang, Z. Chen, Y. Gong, and G. Wu, "Optimal power allocation for AF full-duplex relay in cognitive radio network," in *IEEE GLOBECOM*, 2013.

[119] D. W. K. Ng, E. S. Lo, and R. Schober, "Dynamic resource allocation in MIMO-OFDMA systems with full-duplex and hybrid relaying," *IEEE Trans. Commun.*, vol. 60, no. 5, pp. 1291–1304, May 2012.

[120] M. Moradikia, H. Bastami, A. Kuhestani, H. Behroozi, and L. Hanzo, "Cooperative secure transmission relying on optimal power allocation in the presence of untrusted relays, a passive eavesdropper and hardware impairments," *IEEE Access*, vol. 7, pp. 116 942–116 964, 2019.

[121] K. P. Roshandeh, A. Kuhestani, M. Ardakani, and C. Tellambura, "Ergodic sum rate analysis and efficient power allocation for a massive MIMO two-way relay network," *IET Communications*, vol. 11, no. 2, pp. 211–217, 2017.

[122] L. Fan, N. Zhao, X. Lei, Q. Chen, N. Yang, and G. K. Karagiannidis, "Outage probability and optimal cache placement for multiple Amplify-and-Forward relay networks," *IEEE Trans. Veh. Technol.*, vol. 67, no. 12, pp. 12 373–12 378, 2018.

[123] C. Xue, Q. Zhang, Q. Li, and J. Qin, "Joint power allocation and relay beamforming in nonorthogonal multiple access Amplify-and-Forward relay networks," *IEEE Trans. Veh. Technol.*, vol. 66, no. 8, pp. 7558–7562, 2017.

[124] K. Singh, M.-L. Ku, J.-C. Lin, and T. Ratnarajah, "Toward optimal power control and transfer for energy harvesting Amplify-and-Forward relay networks," *IEEE Trans. Wireless Commun.*, vol. 17, no. 8, pp. 4971–4986, 2018.

[125] S. Li, K. Yang, M. Zhou, J. Wu, L. Song, Y. Li, and H. Li, "Full-duplex Amplify-and-Forward relaying: Power and location optimization," *IEEE Trans. Veh. Technol.*, vol. 66, no. 9, pp. 8458–8468, 2017.

[126] W. Chang, S.-Y. Chung, and Y. Lee, "Gaussian relay channel capacity to within a fixed number of bits," *ArXiv*, vol. abs/1011.5065, 2010.

[127] L. Li, X. Zhou, H. Xu, G. Y. Li, D. Wang, and A. Soong, "Simplified relay selection and power allocation in cooperative cognitive radio systems," *IEEE Trans. Wireless Commun.*, vol. 10, no. 1, pp. 33–36, 2011.

[128] H. Chour, E. A. Jorswieck, F. Bader, Y. Nasser, and O. Bazzi, "Global optimal resource allocation for efficient FD-D2D enabled cellular network," *IEEE Access*, vol. 7, pp. 59690 –59 707, 2019.

[129] C. T. Ng and A. J. Goldsmith, "The impact of CSI and power allocation on relay channel capacity and cooperation strategies," *IEEE Trans. Wireless Commun.*, vol. 7, no. 12, pp. 5380–5389, 2008.

[130] H. Thampy and A. V. Babu, "Outage probability analysis and optimization of cognitive full-duplex relay networks," *Springer Wireless Personal Comm.*, vol. 105, no. 2, pp. 1329–1352, Feb. 2019.

[131] H. Sun, X. Chen, Q. Shi, M. Hong, X. Fu, and N. D. Sidiropoulos, "Learning to optimize: Training deep neural networks for wireless resource management," in *IEEE SPAWC*, 2017, pp. 1–6.

[132] F. Liang, C. Shen, W. Yu, and F. Wu, "Towards optimal power control via ensembling deep neural networks," *IEEE Trans. Commun.*, vol. 68, no. 3, pp. 1760–1776, 2019.

[133] X. Zong, X. Zhu, A. Zhu, and J. O. Byrne, "Optimization and transmit power control based on deep learning with inaccurate channel information in underlay cognitive radio network," in *Journal of Physics: Conference Series*, IOP Publishing, vol. 1746, 2021, p. 012 090.

[134] V. Rizzello and W. Utschick, "Learning the CSI denoising and feedback without supervision," in *IEEE SPAWC*, 2021, pp. 16–20.

[135] S. S. Ikki and M. H. Ahmed, "Performance analysis of adaptive Decode-and-Forward cooperative diversity networks with best-relay selection," *IEEE Trans. Commun.*, vol. 58, no. 1, pp. 68–72, 2010.

[136] Z. Zhang, Y. Xiao, Z. Ma, M. Xiao, Z. Ding, X. Lei, G. K. Karagiannidis, and P. Fan, "6G wireless networks: Vision, requirements, architecture, and key technologies," *IEEE Veh. Technol. Mag.*, vol. 14, no. 3, pp. 28–41, 2019.

[137] L. U. Khan, W. Saad, Z. Han, E. Hossain, and C. S. Hong, "Federated learning for internet of things: Recent advances, taxonomy, and open challenges," *IEEE Commun. Surveys Tuts.*, vol. 23, no. 3, pp. 1759–1799, 2021.

[138] M. Z. Chowdhury, M. Shahjalal, S. Ahmed, and Y. M. Jang, "6G wireless communication systems: Applications, requirements, technologies, challenges, and research directions," *IEEE Open J. Commun. Soc.*, vol. 1, pp. 957–975, 2020.

[139] M. Giordani, M. Polese, M. Mezzavilla, S. Rangan, and M. Zorzi, "Toward 6G networks: Use cases and technologies," *IEEE Commun. Mag.*, vol. 58, no. 3, pp. 55–61, 2020.

[140] Y. Zhao, W. Zhai, J. Zhao, T. Zhang, S. Sun, D. Niyato, and K.-Y. Lam, "A comprehensive survey of 6G wireless communications," *arXiv preprint arXiv:2101.03889*, 2021.

[141] A. Faisal, H. Sarieddeen, H. Dahrouj, T. Y. Al-Naffouri, and M.-S. Alouini, "Ultramassive MIMO systems at terahertz bands: Prospects and challenges," *IEEE Veh. Technol. Mag.*, vol. 15, no. 4, pp. 33–42, 2020.

[142] Y.-C. Liang, R. Long, Q. Zhang, J. Chen, H. V. Cheng, and H. Guo, "Large intelligent surface/antennas (LISA): Making reflective radios smart," *Journal of Communications and Information Networks*, vol. 4, no. 2, pp. 40–50, 2019.

[143] A. D. Wyner, "The wire-tap channel," *Bell system technical journal*, vol. 54, no. 8, pp. 1355–1387, 1975.

[144] Y. Zhang, H.-M. Wang, Q. Yang, and Z. Ding, "Secrecy sum rate maximization in non-orthogonal multiple access," *IEEE Commun. Lett.*, vol. 20, no. 5, pp. 930–933, 2016.

[145] R. Yao, L. Yao, X. Zuo, N. Qi, Y. Liu, and J. Xu, "Secrecy energy efficiency maximization in a NOMA system," in *2019 IEEE 11th International Conference on Communication Software and Networks (ICCSN)*, IEEE, 2019, pp. 106–110.

[146] J. Tang, J. Luo, M. Liu, D. K. So, E. Alsusa, G. Chen, K.-K. Wong, and J. A. Chambers, "Energy efficiency optimization for noma with swipt," *IEEE J. Sel. Topics Signal Process.*, vol. 13, no. 3, pp. 452–466, 2019.

[147] A. Sirojuddin, V. Nzima, K. Singh, S. Biswas, and W.-J. Huang, "Backscatter-aided relaying for next-generation wireless communications with swipt," *IEEE Access*, vol. 9, pp. 159 093–159 104, 2021.

[148] Z. Ding, L. Lv, F. Fang, O. A. Dobre, G. K. Karagiannidis, N. Al-Dhahir, R. Schober, and H. V. Poor, "A state-of-the-art survey on reconfigurable intelligent surface-assisted non-orthogonal multiple access networks," *Proceedings of the IEEE*, vol. 110, no. 9, pp. 1358–1379, 2022.

[149] Y. Liu, S. Zhang, X. Mu, Z. Ding, R. Schober, N. Al-Dhahir, E. Hossain, and X. Shen, "Evolution of NOMA toward next generation multiple access (NGMA) for 6G," *IEEE J. Sel. Areas Commun.*, vol. 40, no. 4, pp. 1037–1071, 2022.

[150] H. Pirayesh and H. Zeng, "Jamming attacks and anti-jamming strategies in wireless networks: A comprehensive survey," *IEEE Commun. Surveys Tuts.*, 2022.

[151] Y. Shi, K. Davaslioglu, and Y. E. Sagduyu, "Generative adversarial network in the air: Deep adversarial learning for wireless signal spoofing," *IEEE Trans. on Cogn. Commun. Netw.*, vol. 7, no. 1, pp. 294–303, 2020.

[152] M. Wazid, A. K. Das, S. Shetty, P. Gope, and J. J. Rodrigues, "Security in 5G-enabled internet of things communication: issues, challenges, and future research roadmap," *IEEE Access*, vol. 9, pp. 4466–4489, 2020.

[153] W. Saad, M. Bennis, and M. Chen, "A vision of 6g wireless systems: Applications, trends, technologies, and open research problems," *IEEE Netw.*, vol. 34, no. 3, pp. 134–142, 2019.

[154] S. Chen, D. Yu, Y. Zou, J. Yu, and X. Cheng, "Decentralized wireless federated learning with differential privacy," *IEEE Trans. Ind. Informat.*, vol. 18, no. 9, pp. 6273–6282, 2022.

[155] A. Wainakh, F. Ventola, T. Müßig, J. Keim, C. G. Cordero, E. Zimmer, T. Grube, K. Kersting, and M. Mühlhäuser, "User-level label leakage from gradients in federated learning," *Proceedings on Privacy Enhancing Technologies*, vol. 2022, no. 2, pp. 227–244, 2022.

[156] A. El Ouadrhiri and A. Abdelhadi, "Differential privacy for deep and federated learning: A survey," *IEEE Access*, vol. 10, pp. 22 359–22 380, 2022.